Introduction

Iran and its neighbouring areas are considered as a complex puzzle, in which continental fragments of various origins were assembled and are now separated by discontinuous ophiolitic belts within the Alpine–Himalayan orogenic system. The formation and evolution of such a large orogenic system have been controlled by the opening and closure of the Tethyan Oceans (the Paleotethys in the north and the Neotethys in the south) (Stampfli, 2000; Stampfli and Kozur, 2007). Metamorphic rocks, which are scarcely exposed in different units (Huckriede et al., 1962; Stöcklin, 1968, 1974, 1977; Nabavi, 1976; Berberian, 1976a, b), were interpreted as Late Precambrian basement (Stöcklin, 1968, 1974, 1977; Haghipour, 1974, 1977). Similar to other high-grade metamorphic rocks in Central Iran, the Shotur Kuh Complex has been assumed to represent a Pre-Cambrian metamorphic basement. New geological mapping in the northeastern part of the Central Iranian Zone (Rahmati Ilkhchi et al., 2002) showed that the basement rocks are covered by Triassic sequence and that there are no data to confirm a Precambrian age for this complex.

This thesis focuses on tectonics and on the magmatic, and metamorphic petrology of the Shotur Kuh complex. In order to understand and seek mechanisms of metamorphism and deformation in relation to geotectonic processes during geological history, a brief summary of the regional geology and age dating from different basement units in Iran is presented. The thesis consists of four chapters. The first chapter is a compilation of available data from the literature about metamorphism and geochronology data of metamorphic rocks and their protoliths. Chapters 2 and 3 include results of my research work that are accepted for publication and submitted for publication, respectively. In general, these two chapters provide an interdisciplinary approach to the metamorphism and tectono-metamorphic evolution of the Shotur Kuh complex and emphasize the related links between geochronology, metamorphic petrology, micro-structural and macro-structural analyses, and tectonics. The last chapter (4) is a summary of the achieved results with their possible interpretation and some future directions of research in basement units of Iran.

CHAPTER 1

Summary of Geology and Metamorphism in Iran

1.1. Geology and Tectonics of Iran

Iran represents a mosaic of continental blocks separated from each other by fold-and-thrust belts formed during the opening closure of the Tethyan oceanic basins (Gansser et al., 1981; Stampfli, 2000; Stampfli and Kozur, 2007). The Paleotethys Ocean separated the Variscan domain from the Gondwana-derived Cimmerian blocks. This ocean closed in the Late Triassic by northward subduction under the southern Laurasian (Turan) margin. Rifting in the Late Palaeozoic to Early Mesozoic resulted in growth of the Neotethys (Berberian and King, 1981; Talbot and Alavi, 1996; Stampfli and Borel, 2002). Based on the presence of basement units and fold-thrust belts, some with ophiolite, three major structural units can be distinguished in Iran (e.g., Berberian and King, 1981). They include the Zagros fold and thrust belt (southern unit), the central unit (Cimmerian block) and the northern unit (Fig. 1). Further subdivision of these units is based on structural style, the age and nature of magmatism, and the age and intensity of deformation and metamorphism.

Fig.1. Simplified structural unit of Iran with the Arabian Plate in the South and the Turan Plate in the North (after Berberian and King, 1981).

1.1.1 The Zagros Fold and Thrust Belt (southern unit)

The Zagros fold and thrust belt with Precambrian basement and platform–type sediments developed during the Palaeozoic. It is subdivided into three subzones (subunits): the Zagros fold belt, the Zagros thrust zone, and the Makran, Zabol-Baluch zone, including the Eastern Iranian Ranges.
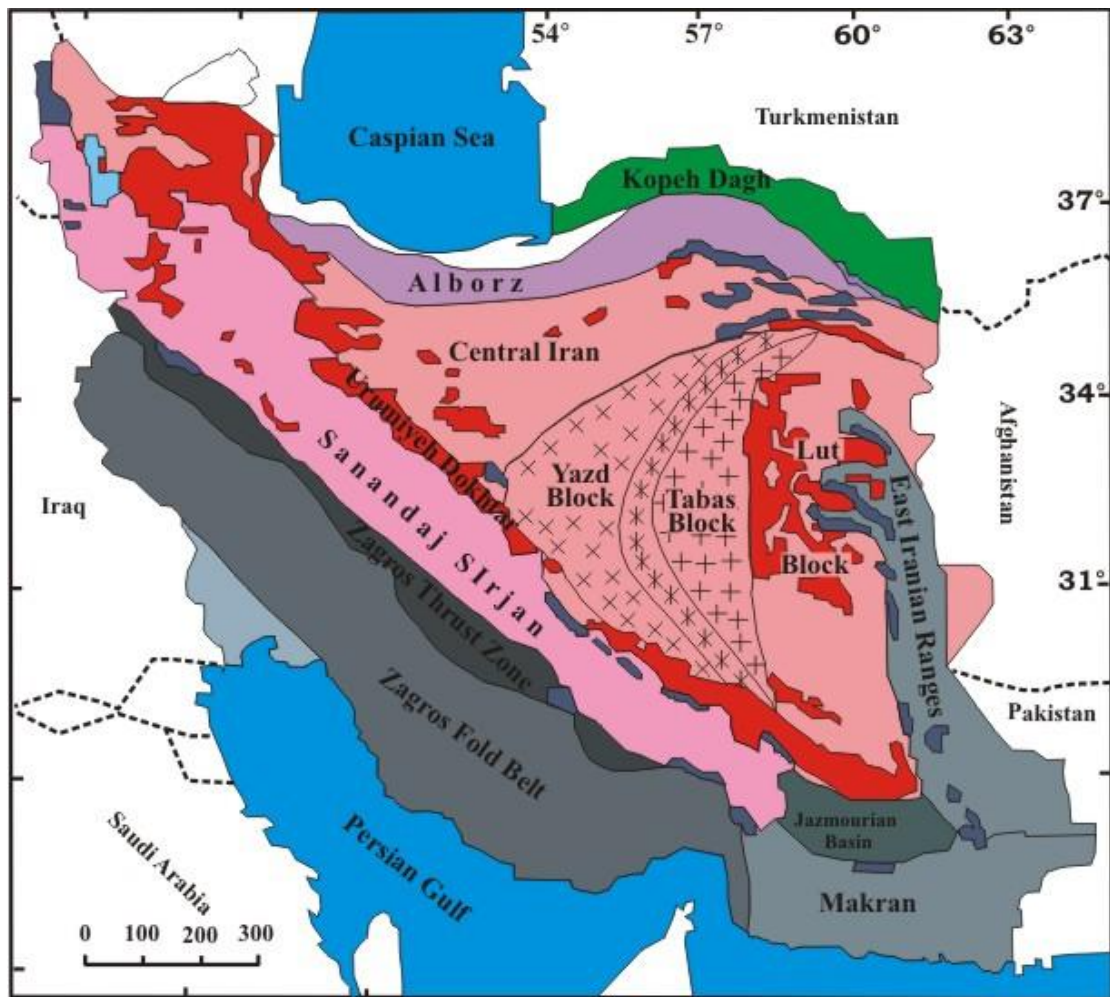

Fig. 2. Geological sketch map showing the main Iranian geological zones (after Berberian, et al., 1981).

1.1.1.1. The Zagros fold belt

The Zagros belt (Falcon, 1969) occurs in the southwest of Iran and bounds the northern margin of the stable platform of Arabia (Fig. 2). It is an approximately 200–300-km wide zone with a thick sedimentary sequence of Precambrian to Pliocene age. The Zagros folded belt is characterized by NW-SE-trending, doubly plunging, parallel anticlines and synclines, which are generally formed by a flexural slip

mechanism (Colman-Sadd, 1978). The basal evaporate-dolomite in the basis sedimentary sequences has played an important role in controlling the style of deformation and detachment mechanism (Kent, 1958; Falcon, 1974; Talbot and Jarvis, 1984).The evaporates also cut throughout the overlying sedimentary rocks and appear on the surface as salt diapirs. Within these diapirs, numerous "exotic" blocks of various rock types are present, which contain fragments of both the overlying rocks and the metamorphic (schist and gneiss) blocks of the underlying basement. This zone, formed in the late Cenozoic, is still tectonically active with shortening and thickening due to the collision of the Arabian Peninsula with Central Iran (Berberian, 1995). The precise timing of the Arabia–Eurasia collision recorded in the Zagros Mountains, with estimates ranging from Late Cretaceous to late Miocene time, remains controversial (Dewey et al., 1973; Hempton, 1987; Alavi, 1994; McQuarrie et al., 2003; Mohajjel et al., 2003; Alavi, 2004).

1.1.1.2. The Zagros Thrust zone

This is a narrow zone that occurs along the northern border of the Zagros fold belt. Most of the rocks present here are deep-sea sediments of the Zagros Mesozoic and early Tertiary basin. The Mesozoic and Paleozoic rock sequences are thrust southwest in several schuppen-like slices on younger Mesozoic and Tertiary rocks of the folded belt. Thrusting of Central Iranian substance above the Zagros was followed by dextral wrench faulting along a Zagros fault zone (Ricou, 1976; Ricou et al., 1977). The wrench faulting is still going on.

1.1.1.3. The Makran, Zabol–Baluch Zone and the Eastern Iranian Ranges

The Makran and Zabol–Baluch zone occurs south of the Lut block (Fig. 1). It is a belt of post–Cretaceous flysch–molasse in Iran that continues to the Pakistan Baluchistan Range Makran, Zabol–Baluch zone, where it consists of Eocene to Miocene turbidites and Pliocene to recent silts, sandstones, and conglomerates (Falcon, 1974). The Makran Range corresponds to Cenozoic accreting margin, bounding the northern, oceanic part of the Arabian–African plate (Gulf of Oman). The Eastern Iranian Ranges are in a north-south direction and occur east of the Lut block.

1.1.2. The Central Units (Cimmerian Block)

These units are assumed to represent marginal fragments detached from Gondwana and attached to Eurasia during the Mesozoic period and finally rejoined to the Gondwanic Afro–Arabian plate in the Late Cretaceous. Their crystalline basement consolidated during the Precambrian (Pan–African) orogeny, and it is covered by Late Proterozoic to Paleozoic platform–type sediments. Alpine tectonics occurred during the Cimmerian phase. The central unit includes Sanandaj-Sirjan, Urumiyeh-Dokhtar Magmatic Arc, parts of Central Iran, Alborz, and Central and Southern Afghanistan. Here, only tectonic units in Iran are discussed.

1.1.2.1. The Sanandaj Sirjan metamorphic zone

The Sanandaj Sirjan zone is a continuation of the Taurus orogenic belt in Turkey and reaches length of about 1500 km in the territory of Iran. It is often considered a hinterland that has been folded and metamorphosed during the Early Cimmerian orogeny (Upper Triassic), tectonized again in the Upper Cretaceous, and finally deformed with the Zagros Main Thrust. The Sanandaj Sirjan zone is subdivided into an outer belt of imbricate thrust slices that includes the Zagros suture and an inner belt of mainly Mesozoic metamorphic rocks. This zone is characterized by the presence of metamorphic rocks with abundant deformed and undeformed plutons. The rocks of this zone are mostly of Mesozoic age, but Paleozoic rocks are also present, and they are common in the southeast part (Berberian, 1977).

1.1.2.2. The Urumiyeh Dokhtar (Urumiyeh Bazman) Magmatic Arc

The Urumiyeh Dokhtar Magmatic Arc (or "Urmia-Dokhtar zone" of Schröder, 1944) runs parallel to the Sanandaj Sirjan zone along its northeast side. It contains intrusive and extrusive rocks of Eocene–Quaternary ages that form about a 50-km-wide zone (Berberian and Berberian, 1981). The arc is assumed to have resulted due to the collision of the Arabian and Central Iranian continental plate margins. The apparent thickness of the continental crust along this zone is 45-50 km. This increase in thickness is presumably due to magmatic activity and northeastward thrust faulting (Alavi, 1994). Seismic data suggest the possibility of the existence of a segment of the oceanic crust beneath the southeastern part of the Urumiyeh-Dokhtar Magmatic Arc (Kadinsky-Cade and Barazangi, 1982).

5

1.1.2.3. The Central Iranian Zone

The Central Iranian zone occurs between the Alborz and Kopeh Dagh ranges in the north and the Zagros and Makran ranges in the west to south and east of Iran. The Central Iranian crust has been a decoupled part of Africa before becoming part of Eurasia after the opening of the Neotethys in Triassic times. This microplate, which formed in pre-Paleozoic times, shows no indication of any Variscan orogeny (Delaloye et al., 1981). It is fragmented by crustal faults (the Great Kavir, Nain–Baft, and Harirud faults) into several blocks. The blocks are partly bounded by the Upper Cretaceous-to-Lower Eocene ophiolite and ophiolitic mélange (Takin 1972). From east to west, three major crustal blocks can be distinguished (Fig. 2): the Lut Block, the Tabas Block, and the Yazd Block (Berberian, et al., 1981). The Tabas and Yazd blocks are separated by a 600-km-long and relatively narrow belt (the Kashmar-Kerman tectonic zone). The Lut block, which is composed of Paleozoic to Mesozoic rocks has different lithology from those of Central Iran (Crawford, 1972; Stöcklin, 1974) and may therefore be related to the microplate of Afghanistan-Pamir (Krumsiek, 1976; Gealey, 1977). It probably collided with Central Iran (Eurasia) during the Paleogene. The northern part of the Lut Block is covered by Neogene andesitic, dacitic, and rhyolitic lava flows. According to Alavi (1991a), Central Iran (Fig. 2) comprises the Sabzevar block and the Tabriz Qom belt (Fig. 3). The Sabzevar block is characterized by the presence of ophiolitic mélange, which tapers out toward the east and continues to the transitional Binalud zone. This block is limited by the Doruneh and Nain Faults from south and east, respectively. Its northern boundary is not always clear, but in most cases is followed by the Mayamey- Attari fault.

1.1.2.4. The Alborz Zone

The Alborz Mountains, forming a gently sinuous east–west range in the north of Iran is bounded to the north and northeast by the Paleotethys collision suture zone (Arabia–Eurasia collision from the Cimmerian orogeny), which is overprinted by the later Alpine structures. The strong positive gravity anomaly in the southern Caspian Sea area testifies perhaps to its being a remnant of Paleotethys. The suture zone is characterized by the presence of metamorphosed Cimmerian ophiolites and deep-sea sediments. It is affected by Pre-Jurassic structural deformations, which produced

intense multiple fold and thrust faults (Alavi, 1979, 1991b). According to Stampfli et al. (1991), the Alborz zone separated from Gondwanaland in the Ordovician–Silurian and collided with Eurasia in the Late Triassic (Sengör, et al., 1988). Metamorphic relics of Palaeotethyan collision are preserved in discontinuous outcrops along the northern margin, such as the Gorgan Schists in the northeast.
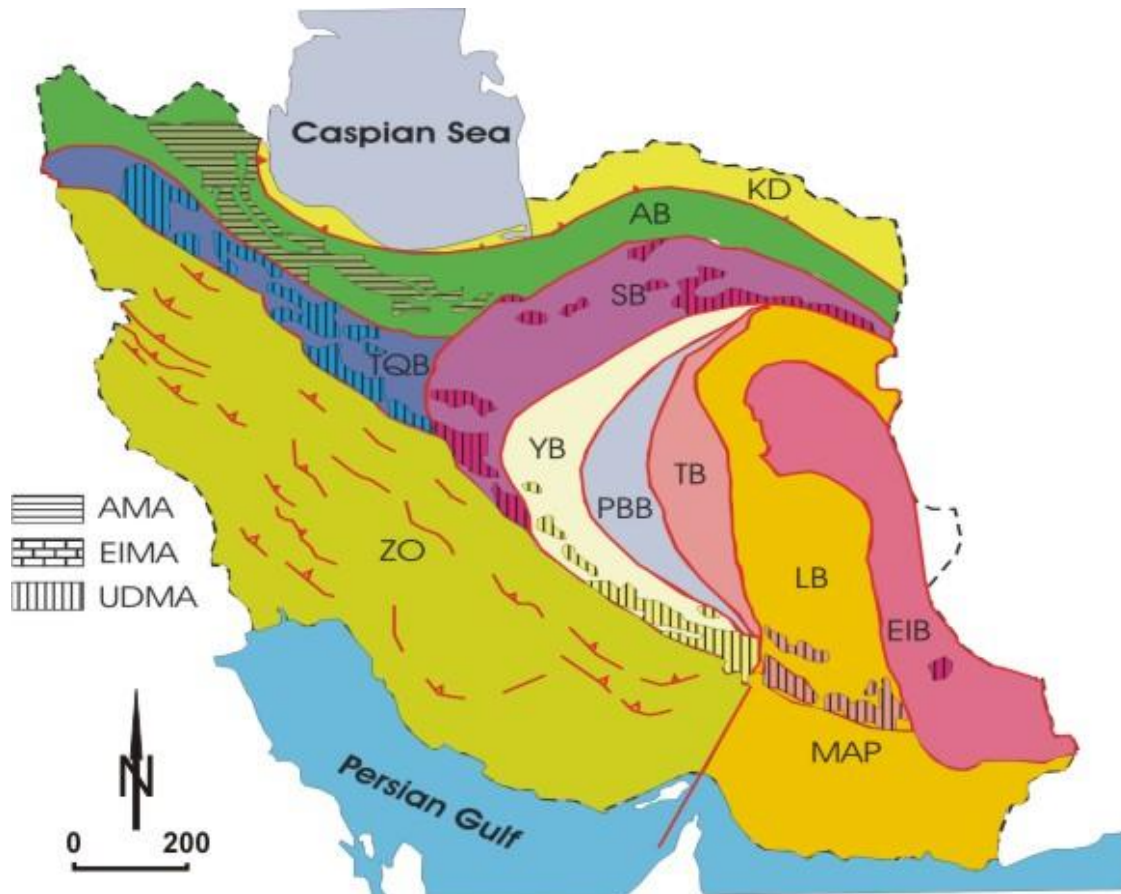

Fig.3. Index map showing the main tectonic elements of Iran (after Alavi, 1991a). Abbreviations: AB = Alborz belt, AMA = Alborz magmatic assemblage, EIB = East Iranian block, EIMA = East Iran magmatic assemblage, KD = Kopeh Dagh, LU = Lut block, MAP = Makran accretionary prism, PBB = Posht Badam block, SB = Sabzevar block, TB = Tabas block, TQB = Tabriz Qom belt, UDMA = Urumiyeh Dokhtar magmatic assemblage, YB = Yazd block, ZO = Zagros orogen.

1.1.3. The northern unit

The northern unit includes remnants of the Paleotethys and marginal band of the Variscan realm of Central Asia, mainly overlapped by the Alpine realm. This unit is sharply separated from the central unit by the north Iran suture. It is identified by continental crust, including fragments of more or less cratonized former (Paleozoic)

7

oceanic crust. It was deformed and largely consolidated during the early Cimmerian and late Alpine movements (Stöcklin, 1977). The northern unit includes mainly (1) the South Caspian depression, (2) the northern part of the Iranian suture zone, (3) the Kopeh Dagh range, (4) the Paropamisus and (5) the Western Hindu Kush ranges. Here, only the Kopeh Dagh range is discussed.

The Kopeh Dagh range in northeast Iran is a fold zone marginal to the Turan. It is formed by Variscan metamorphosed basement with platform sediments in the southwest. Similar to that in Zagros, this belt is composed of about 10 km of Mesozoic and Tertiary sediments (mostly carbonates) and was folded during Plio–Pleistocene.

1.2. Distribution of Basement Rocks in Iran

Consolidation of the Iranian basement units is assumed to occur during "Baikalian" or Pan–African orogeny with post–Pan–African magmatism (e.g., Berberian and King, 1981). The basement rocks include both metamorphosed and unmetamorphosed sedimentary (slightly metamorphosed) and igneous (mostly granitic) rocks. Metamorphic PT conditions of these rocks range from very-low-grade to amphibolite (locally granulite) facies.

1.2.1. The Southern Unit

Basement rocks are not exposed on the surface in the southern unit. Only numerous "exotic" blocks of igneous and metamorphic rocks are present within the salt diapirs. Low-grade metamorphosed Upper Cretaceous flysch-like sediments with ophiolitic mélange occur in the Ratuk complex in the eastern Iranian Range (Fig. 4. A, Geological Survey of Iran, 1990a,b), The mélange with talc–schist, chlorite–schist, mica–schist with greenschist matrix contain lenses of eclogites, blueschists, and metacherts (Fotoohi Rad 2005). Considering Tirrul et al., (1983), metamorphism of these rocks occurred before the Maastrichtian.

1.2.2. TheCentral Units (Cimmerian Block)

Metamorphism and age relations of basement rocks in the Central unit have not been properly studied, and only a little data are available based on stratigraphical

sequences. In addition to metamorphic rocks and age relations of their sedimentary protoliths, we describe here magmatic rocks occurring in the basement units.
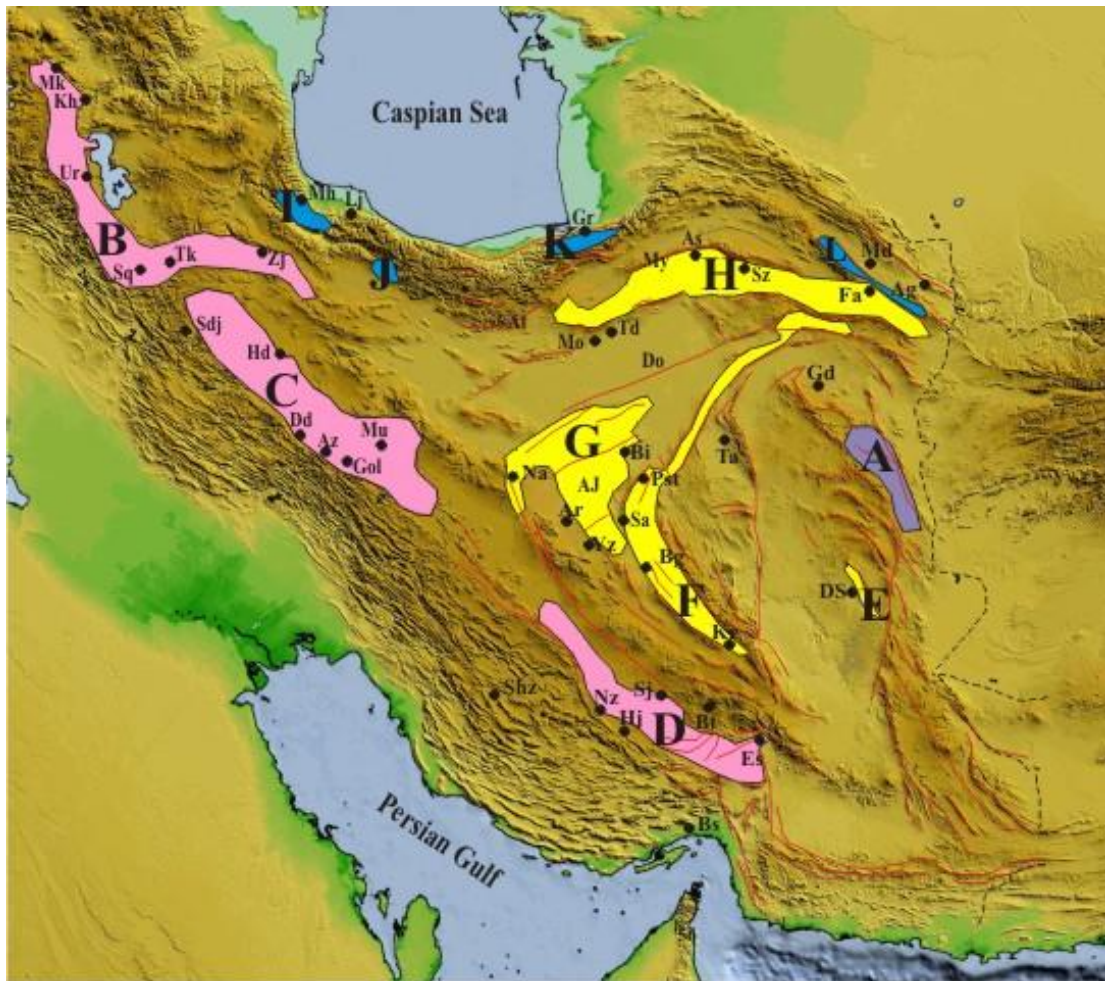

Fig.4. Distribution of metamorphic rocks in southern unit (A), central unit (B-L) and north unit. Abbreviations: Ag = Aghdarband, AJ =Anarak-Jandagh , Ar = Ardakan, As =Abass Abad, At = Attari Fault, Az = Azna, Bg = Bafgh, Bi = Biabanak, Bs =Bandar Abass , Bt =Baft, Dd = Dorud, Do =Doruneh Fault, Ds = Deh Salm, Fa = Fariman, Es = Esphandagheh, Gd =Gonabad, Gol = Golpaygan, Gr = Gorgan, Hd = Hamadan, Hj = Haji Abad , Kh = Khoy, Kr =Kerman, Lj = Lahijan, Md = Mashhad, Mh =Masuleh, Mk = Maku, Mo =Moalleman, Mu = Muteh, My =Mayamey Fault, Na = Nakhlak, Ni = Nain, Nz = Neyriz, Pst = Poshteh Badam, Sa = Saghand, Sdj = Sanandaj, Shz = Shiraz, Sj = Sirjan, Sq = Saqqez, Sz = Sabzevar, Ta = Tabas, Td = Torud, Tk = Takab, Ur =Urumiyeh, Yz = Yazd, ZJ = Zanjan.

1.2.2.1. The Sanandaj Sirjan Metamorphic Zone

Metamorphic rocks are exposed in three regions (for simplification marked as B, C, and D in Fig. 4) along the Sanandaj Sirjan zone.

Region B

In the Maku area (Fig. 4. B), slightly metamorphosed Ordovician shales and sandstones with volcanic rocks are present (Berberian1976, Berberian and Hamdi, 1977). Numerous granitoids, exposed within lower greenschist facies metamorphic rocks west of the Saqqez region, were previously mapped as Precambrian (e.g., Eftekhar-Nezhad, 1973). However, Omrani and Khabbaznia (2003) assumed a Cretaceous or even younger age for these rocks. U-Pb data from zircon yielded an age of 551 ± 25 Ma for the Sheikh Chupan granodiorite and 544 ± 19 Ma for the Bubaktan foliated granite (Hassanzadeh, et al., 2008).

In addition to greenschist-amphibolite facies rocks, the Khoy area (Fig. 4. B) contains poly-metamorphic ophiolite (lherzolitic, harzburgite and ultramafic meta-cumulate) with blueschist (Khalatbari-Jafari 2003). Medium-pressure metamorphic rocks correspond to green schists, metavolcanics, micaschists, amphibolites, and gneisses. K-Ar age data for amphiboles, biotites, and muscovites in high-pressure metamorphic rocks yielded 197 Ma to 160 Ma, but Middle Juriassic ages of 158.6 ± 1.4 Ma and 154.9 ±1.0 Ma were obtained for using Ar-Ar data for amphibolite facies rocks (Ghazi et al. 2001). According to Khalatbari-Jafari (2003), at least four metamorphic episodes can be based on age data distinguished: Lower Jurassic (197–181 Ma), Middle Jurassic (160–155 Ma), Lower Cretaceous (121.2 ± 6.2 – 102.1± 5.4 Ma) and Upper Cretaceous (81.2 ± 1.2 – 69.4 ± 1.6Ma). U-Pb data of zircon from the Moghanlou granitic orthogneiss (between Zanjan and Takab, Fig. 4. B) yielded ages of 548 ± 27 Ma and 568 ± 44 Ma (Hassanzadeh, et al., 2008).

The very-low-grade sedimentary rocks (shale and siltstone) of the Soltanieh Mountains in the Zanjan area (Fig. 4. B) are intruded by granite (Alavi-Naini, 1994; Stöcklin et al., 1965; Stöcklin and Eftekhar-Nezhad, 1969; Babakhani and Sadeghi, 2005). The whole-rock Rb-Sr age of 645 Ma, (Crawford, 1977) and U-Pb zircon ages of 544 ± 29 Ma and 599 ± 42 Ma were obtained for this granite (Hassanzadeh, et al., 2008). The granite is foliated, and Rb-Sr data from biotite indicate a Lower- to Middle- Jurassic age of 175 ± 5 Ma for its metamorphism (McDougall and Harrison, 1999). Younger ages of 53.4 ± 0.4 Ma and 2.8 ± 0.1 Ma were obtained using U-Pb zircon age for equi-granular biotite granite and leucogranite, respectively (Hassanzadeh, et al., 2008).

Region C

In the central part of the Sanandaj Sirjan zone in the Hamadan area (Fig. 4. C), metamorphic rocks are derived both from sedimentary and magmatic rocks (the Alvand granitoid complex). The metasedimentary rocks range from very-low-grade slate through phyllite, garnet-staurolite schists to andalusite/sillimanite gneisses. Similar to other units protoliths of metamorphic rocks were assumed to be Precambrian in age (Furon, 1941), but based on the new geological map (1:100,000 geological map of Hamadan), they are assigned to Midle-Jurassic. K-Ar data from amphiboles, muscovites, and biotites in these rocks gave ages between 114 Ma to 60 Ma, and granite emplacement occurred during the Late Cretaceous (ca. 82 Ma, Baharifar et al., 2004).

The area north of Dorud and Azna (Fig. 4. C) contains metamorphosed Late Paleozoic to Mesozoic succession dominated by metacarbonate, schist, and amphibolite. They contain andesitic lavas and pyroclastic rocks that are conformably overlain by Aptian-Albian limestone.

Metamorphic rocks in the Muteh area (Golpaygan, Fig. 4. C) are represented by gneiss, marble, amphibolite, mica schist, phyllite, and quartzite. The supposed Precambrian age of this basement unit (Thiele, 1966; Thiele et al., 1968) was doubted by Rachidnejad-Omran et al. (2002), who assumed a Paleozoic age for volcano-sedimentary protoliths and a Mesozoic age for their metamorphism. The Muteh leucogranite occurring in this basement unit yielded an age of 578 ± 22 Ma and 596 ± 24 Ma using the U-Pb method on zircon. Younger K-Ar ages on biotite (128.3 ± 4.7, 68.9 ± 1.0, and 67.5 ± 1.0 Ma) and whole rock (124.4 ± 4.4 Ma) rocks are attributed to metamorphic overprint in granite (Rachidnejad-Omran et al., 2002). Moritz et al., (2006) obtained two Ar-Ar plateau ages of 109.65 ± 2.04 Ma and 86.55± 1.00 Ma for these rocks.

A large dome of high-grade metamorphic rocks with biotite granite orthogneisses is exposed in the Haji Qara mountain (Varzaneh near Muteh, Golpaygan area). U-Pb zircon data yielded an age of 588 ± 23 Ma for granite formation (Hassanzadeh, et al., 2008). The Middle Jurassic age (174.5 ± 2.9 Ma) of metamorphism of these rocks is confirmed by K-Ar data on amphibole (Rachidnejad-Omran et al., 2002). A younger Ar-Ar age of Eocene times is interpreted as the cooling age of this unit (Rachidnejad-Omran et al., 2002; Moritz et al., 2006).

Region D

The Tutak gneiss dome (300 km northeast of Shiraz, Fig. 4. D), in the southeastern part of the Sanandaj Sirjan zone, consists of metagranite and marble from Kuh-e-Sefid (Alizadeh, 2008) that come from a Devonian-Carboniferous sequence (Hushmandzadeh et al., 1990). Ar-Ar ages of 179.5±1.7Ma and 76.8±0.2 Ma (Sarkarinejad et al., 2009) are attributed to deformation and metamorphism of these rocks, respectively.

The Quri-Kor-e-Sefid (Neyriz area, Fig. 4. D) is comprised of low- to high-grade metamorphic rocks that are thrust over the Neyriz ophiolites (Ricou, 1974). These metamorphic rocks consist of orthogneiss with some amphibolite lenses in the base with 520 Ma age (based on U-Pb zircon). In addition to orthogneisses and amphibolites, migmatites, minor micaschist, marble, metamorphic mafic, and ultramafic rocks are also present. Based on coral and Palynomorphs, Devonian to Early Carboniferous ages are assumed for protoliths of meta-sedimentary rocks (Roshan Ravan et al., 1995; Eshraghi et al., 1999). K-Ar age on amphiboles and micas are clustered in four groups between 300 and 60 Ma (Sheikholeslami et al., 2003). These low- to high-grade metamorphic rocks are unconformably overlain by Upper Triassic rocks (Sheikholeslami et al., 2008).

The Seh-Ghalatoun HP-LT metamorphic with ophiolite mélange is exposed near the village of Deh Chah in the eastern part of the Neyriz (Fig. 4. D). The predominant rocks in the area are amphibolite, garnet amphibolite, quartzo feldspathic gneiss, kyanite gniess, biotite gneiss, muscovite-garnet schist and phyllite with numerous intercalations of eclogite facies rocks. A Lower Jurassic age of 187 ± 2.6 Ma (based on zircon SHRIMP U-Pb) and 180 ± 21 Ma (based on monazite CHIME U-Th-total Pb) is assumed for metamorphism of the Chah-Sabz and Seghalaton rocks (Fazlnia et al., 2007).

Blueschist facies rocks are 12 km west of Neyriz. The blueschist facies consists of marble, amphibolite, serpentinized harzburgite and gabbros. K-Ar data on amphibole yielded Cretaceous age 89.09 ± 1.34, 90.18 ± 0.88 Ma and 91.23 ± 0.89 Ma (Sarkarinejad et al., 2009) for the blueschist facies metamorphism. A relatively older age of 119.95 ± 0.88 Ma and 112.58 ± 0.66 Ma for these rocks was obtained using the Ar-Ar method on biotite. These Late Aptian ages are related to early thrusting and peak high-pressure metamorphism of the Neyriz ophiolite. Biotite and hornblende

from biotite schist and garnet amphibolite yielded ~ 87 ± 7 Ma and 96 ±1.3 Ma (Hynes and Reynolds, 1980).

The Sikhoran complex (Fig. 4. D) in the Esphandagheh area is bounded, by a blueschist metamorphic belt that gave an age of 80.7 Ma (K-Ar on phengite; Ghasemi et al, 2002). In the northern part of this complex, various metamorphic rocks of Paleozoic age, including gneisses, amphibolites, marbles and skarn are present. The Sikhoran complex (mafic-ultramafic) is tectonically overlain, by amphibolites, marbles, micaschists and green schists of Devonian age (Sabzehei 1974). In the neighbor region of Baft, black schists and cherts, belonging to the same series, contain remains of Achritarchs and Chitinozoaires of Lower Paleozoic age (Cambrian to Ordovician, Sabzehei, 1977). According to Ghasemi et al, (2002) the K–Ar ages of the amphibolites from the south of the Sikhoran complex, are 164 to 161 Ma (amphibole). The gneisses at the southwestern margin of this complex yield 301± 7 Ma (biotite), and the anatectic granite linked to these gneisses give an age of 330 ±8 Ma (Muscovite). Agard et al, (2006) reported Ar-Ar ages from phengite for three areas: they are in the range of 82.38 ± 1-102.26 ± 4 and 89.23 ± 1-109.27 ± 3 Ma for Ashin, 95.81 ± 6-126.51 ± 2 Ma for Seghina, and 87.48 ± 1-102.66 ± 2 and 116.57 ± 9-118.09 ± 1 Ma for samples from Sheikh Ali.

1.2.2.2. The Central Iranian Zone

Metamorphic rocks exposed in Central Iran occur in four regions (E, F, G and H, Fig. 4).

Region E

The Deh Salm Metamorphic Complex is divided two major lithostratigraphic groups. The lower group consists of an alternation of marble, schists, and amphibolites. The upper group consists of phyllites, mica schists and schists. The whole metamorphic complex is considered to be Upper Triassic- Jurassic and together with some older rocks they are metamorphosed during the Post- Jurassic (or at least Post-Middle Jurassic) (Stöcklin et al., 1972).

Region F

Metamorphic rocks from the Saghand area are assumed to represent the oldest lithostratigraphic formations (Nadimi, 2005; Nadimi, 2007). From bottom to top, they include the Chapedony, Poshte Badam, Boneh Shurow, and Tashk formations (Fig. 5).

The Chapedony Formation (Fig. 4. E) is assumed to represent a Paleoproterozoic complex (Hushmandzadeh, 1969; Haghipour and Pelissier, 1977). This age for the source rocks is assumed also by U-P data from detrital zircon of 2140.9 Ma (Ramezani and Tucker, 2003) and by Rb/Sr whole rock ages of 2382 Ma (Haghipour, 1974). Metamorphic rocks of this formation are schist, amphibolite, marble, quartzite, gneiss, ribbon gneiss and migmatite (Haghipour, 1974). Their PT conditions range from greenschist, through amphibolite, to granulite facies. An Eocene age of 48.2 Ma has been obtained for metamorphic zircon in metagranite (Ramezani and Tucker, 2003).
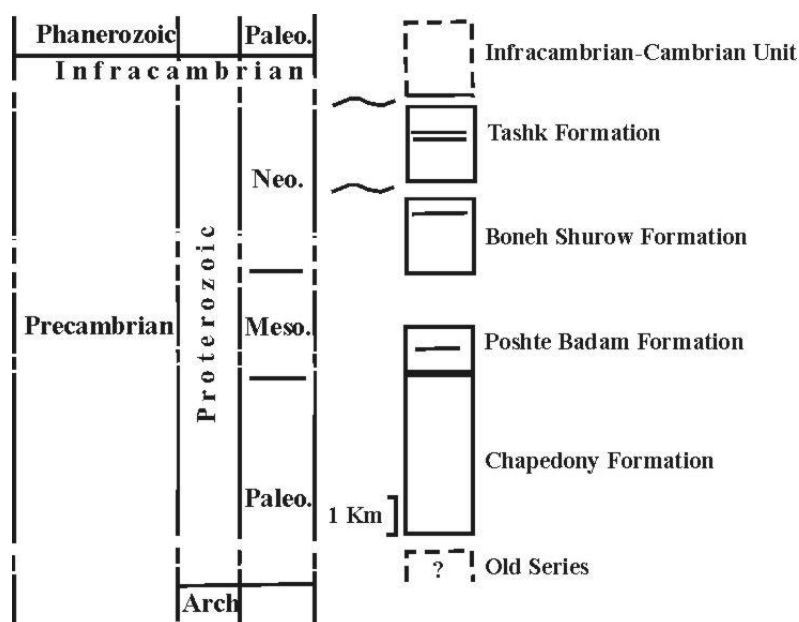

Fig.5. Generalized stratigraphic section of the basement complexes in the Saghand region (after Nadimi 2007).

Metamorphic rocks of the Poshte Badam Formation (Fig. 4. F) involve greenstones, schists, meta-greywacke, marble, gneisses, amphibolites, pyroxenites, serpentinite, meta-basalt and meta-conglomerate (Haghipour and Pelissier, 1977). The Boneh Shurow Formation (Fig. 4. E) is a widely exposed metamorphic unit that forms ridge-

shaped outcrops directly next to the Poshte Badam fault (Haghipour and Pelissier, 1977; Ramezani and Tucker, 2003). It exhibits a distinct metamorphic layering composed of an alternation of pink quartzofeldspathic gneisses, greenish-gray mica schists, and dark-colored amphibolites. The crystallization age of the granitic protolith(s) of the Boneh-Shurow gneiss (U-Pb zircon) is in the range from 617 Ma to 602 Ma (Ramezani and Tucker, 2003) and an age of 547.6 ± 2.5 Ma is assumed to date the lower-amphibolite facies metamorphism.

The Tashk Formation (Fig. 4. F) consists of dark greenish-gray greywackes, schist, quartzitic schist, quartzite, marble, amphibolite, gneiss, slaty shale, sandstone locally interbedded with arkosic arenites, argillites, and tuffaceous deposits that occur sub-parallel to the Boneh–Shurow Formation (Haghipour and Pelissier, 1977). U-Pb zircon ages from the Tashk Formation range between 627 Ma and 533 Ma (Ramezani and Tucker, 2003).

According to Samani (1994), the Chapedony, Boneh Shurow and Tashk (Natak) Formations are of Proterozoic age 874-750 Ma, and they underwent a Mesozoic (180-220 Ma) dynamothermal and a Cenozoic (52 Ma) hydrothermal metamorphism. An Rb-Sr model age of 540 Ma was obtained for the Bornavard granite (Fig3. F) (Crawford 1977).

Region G

The Anarak Metamorphic Complex, south of Nakhlak (Fig. 4. G), is subdivided into several subunits (Sharkovski et al. 1984). It consists of phyllites, mica schists, greenschists, marble, calcareous schists, and blueschists (Sharkovski et al. 1984). A few remnants of archaeocyathids in marble (Geological Survey of Iran, 1984a) give an Early to Middle-Cambrian age, whereas crinoids and gastropods dubitatively suggest a younger age (Sharkovski et al. 1984). Reyre & Mohafez (1970) obtained a 203 ± 13 Ma Rb–Sr mineral age and a Precambrian (845 Ma) whole rock Rb–Sr age for protoliths of the rocks. Variscan ages of 315 ± 5 Ma (Rb-Sr) and 333–320 Ma (Ar-Ar) for metamorphism of the Anarak Metamorphic Complex were obtained by Crawford (1977) and (Bagheri & Stampfli 2008), respectively.

The Doshakh and the Bayazeh units were previously interpreted as a greenschists-facies Precambrian or Lower Paleozoic metamorphic basement of the Yazd block (Sharkovski et al., 1984). Middle Permian–Middle Triassic age for some of these rocks was obtained based on conodonts (Bagheri and Stampfli, 2008), but Sharkovski

et al. (1984) reported a wider range of K-Ar ages (400–180 Ma from metamorphic rocks in this area. The younger ages are assumed to be related to later retrograde events (Romanko and Morozov, 1983; Almasian, 1997). K-Ar ages of 270–183 Ma were obtained by Sharkovski et al. (1984). Two set of Ar-Ar data were obtained by Bagheri et al. (2007), and most Ar-Ar data from muscovite yielded 333–318 Ma cooling ages that are related to the first metamorphic event. Two samples of muscovite and hornblende data gave Middle Jurassic age of 163.86 ± 1.76 Ma and 156.56 ± 33.15 Ma, respectively, for metamorphism of the basement rocks (Bagheri et al., 2007).

Region H

This region is a part of Central Iranian Block after Stöcklin (1974) and Berberian and King (1981), and the Sabzevar Block according to Alavi (1991a, Fig. 3). Similar to other high-grade metamorphic rocks in Central Iran, the rocks exposed in this block were mapped as a Precambrian basement (geological map, 1: 250,000 scale, the Geological Survey of Iran). The metamorphic complex in the Khar Turan area (Fig. 4. H) consists of amphibolite-grade gneisses and schists (Hassanzadeh, et al 2008). Neoproterozoic ages (554 ± 40, 534 ± 31, 522 ± 23 Ma and 551 ± 20 Ma) were obtained for granite and protoliths of the orthogneiss, using U-Pb dating on zircon (Hassanzadeh, et al 2008). The orthogneisses of Band-e Hezar Chāh (Fig. 4. H) yielded relatively older ages of 581 ± 21 Ma, and 601 ± 22 Ma (Hassanzadeh, et al., 2008). A sample of biotite-rich granite gneiss in Torud area yielded 566 ± 31 Ma (Hassanzadeh, et al 2008).

Paleozoic sedimentary and metasedimentary rocks are exposed in the Torud area (Hushmandzadeh et al., 1978). Based the geological map in the Kalateh-Reshm, the polymetamorphic and polydeformed rocks with some mafic and ultramafic rocks near Kuh Siah Poshteh are assumed to be Paleozoic in age (Jafariyan, 2000). Some small remnants of ophiolitic rocks are exposed near the Khondar anticline in the Meyamey (Amini Chehragh, 1999), but they are interpreted as Pre-Cretaceous (?) in age. Pre-Jurassic (Khalatbari Jafari et al., 2008) and Post-Jurassic to Pre-Cretaceous (Navai, 1987) metamorphic rocks are exposed in the Abass Abad and Biarjmand areas.

The Shotur Kuh metamorphic complex was assumed as Precambrian metamorphic basement (Hushmandzadeh et al 1978). Geological mapping in the Shotur Kuh area (Rahmati Ilkhchi et al., 2002) as well new petrological and geochrnologicala data

show that the orthogneisses are derived from Neoproterzoic granites that were metamorphosed during the Middle Jurassic.

The western belt of Fariman is a continuation of the Sabzevar ophiolitic belt that runs parallel to the Mayamey fault and separates central Iran from the Alborz-Binalud structural zone (Khalatbari Jafari et al., 2009). The Cretaceous Fariman belt discontinuously runs parallel with the Doruneh fault and joins to the Nain ophiolite.

1.2.2.3. The Alborz Zone

Metamorphic rocks are exposed in three regions (I, J and K) along the southern border of the Caspian Sea (Fig. 4) and one in the Bilalud area (L).

Region I

The Shanderman Complex (Fig. 4. I) is formed mainly by metabasites and mica schists, with minor calcschists, quartzites, phyllites and patches of serpentinized peridotite (Davies et al., 1972; Clark et al., 1975). The whole-rock Rb-Sr data from phyllite yielded a Middle–Late Devonian age of 382 ± 48 and 375 ± 12 Ma (Crawford, 1977). However, a Neoproterozoic age of 551 ± 9 Ma was obtained for the Lahijan biotite granite using the U-Pb data on zircon (Hassanzadeh, et al., 2008; Lam, 2002). An Ar-Ar age of 315 ± 9 Ma from paragonitic white micas in phyllite suggests a Late Carboniferous metamorphism of these rocks (Zanchetta et al., 2009). Lam (2002) obtained, using Th/He data on zircon, three ages of 133 ± 7.98 Ma, 152 ± 9.12 Ma and 162 ± 9.72 Ma that are interpreted to represent Middle Jurassic to Early Cretaceous cooling of these rocks.

Region J

The Kahar Formation (Fig. 4. J) is assumed to be Neoproterozoic in age (e.g., Gansser and Huber, 1962; Stocklin et al., 1969; Stocklin, 1974, 1977; Jenny, 1977). However, Upper Riphean to Middle-Upper Vendian or Paleozoic age for formation was assumed based on fossils (Sabouri, 2003., Golshani, 1990).

Region K

The Gorgan metamorphic rocks (Fig. 4. K) involve mainly phyllites, sericite-chlorite-schists, and quartzite. They show low-grade metamorphic conditions with

prehnite-pumpellyite and have been considered Precambrian in age (Afshar-harb, 1979; Delaloye, et al., 1981; Gansser, 1951; Hubber, 1957; Salehi-Rad, 1979; Stahl, 1911; Stampfli, 1978; Stöcklin, 1971; Tietze, 1877). A Late Ordovician (Caradoc-Ashgill) age for these rocks is based on fossils (Ghavidel Syooki 2007).

Region L

Metamorphosed Late Paleozoic-Devonian rocks are exposed in the Binalud area (Fig. 4. K, Majidi, 1978). According to Davoudzadeh et al. (1975), metamorphism of the Rhaetic-Liassic sediments of the Binalud area occurred during Middle Jurassic (around 176 Ma). Four main deformation stages are determined in this area. Deformation D1 and D_2 correspond to progressive stage of metamorphism that occurred in greenschist to amphibolite facies conditions. D_3 deformation is related to retrogression, and D_4 occurred in relatively brittle condition and relates to younger metamorphic process (Koohpeyma, 2007).

1.2.3. The Northern Unit

Metamorphosed Late Paleozoic-Devonian rocks are exposed at Aghdarband in the Kopeh Dagh (Majidi, 1978).

1.2.4. Summary of Geochronological Data of Metamorphism in Basement Rocks in Iran

Consolidation of the Iranian basement units by metamorphism with partial granitization and partly intense folding occurred during Late Precambrian. This process continued during several major orogenic phases that were accompanied by syntectonic metamorphism and magmatic events (Aghanabati, 2004). The most important orogenic events were during the Paleozoic, Middle Triassic, Middle Jurassic, Late Jurassic and late Cretaceous periods (Fig. 6). Some authors (e.g., Hushmandzadeh el al., 1973) assume only epeirogenic movements during Paleozoic time. However, available geologic and age data (Fig. 7, Table. 1) suggest the occurrence of Variscan (300 -333Ma) or/and Caledonian (375-400Ma) deformation with questionable regional metamorphism, although several orogenic events accompanied with metamorphism have now been established during the Mesozoic.

The earliest Alpine events were apparently vigorous in some parts of Iran, and they were accompanied by metamorphism (Hushmandzadeh et al., 1973).
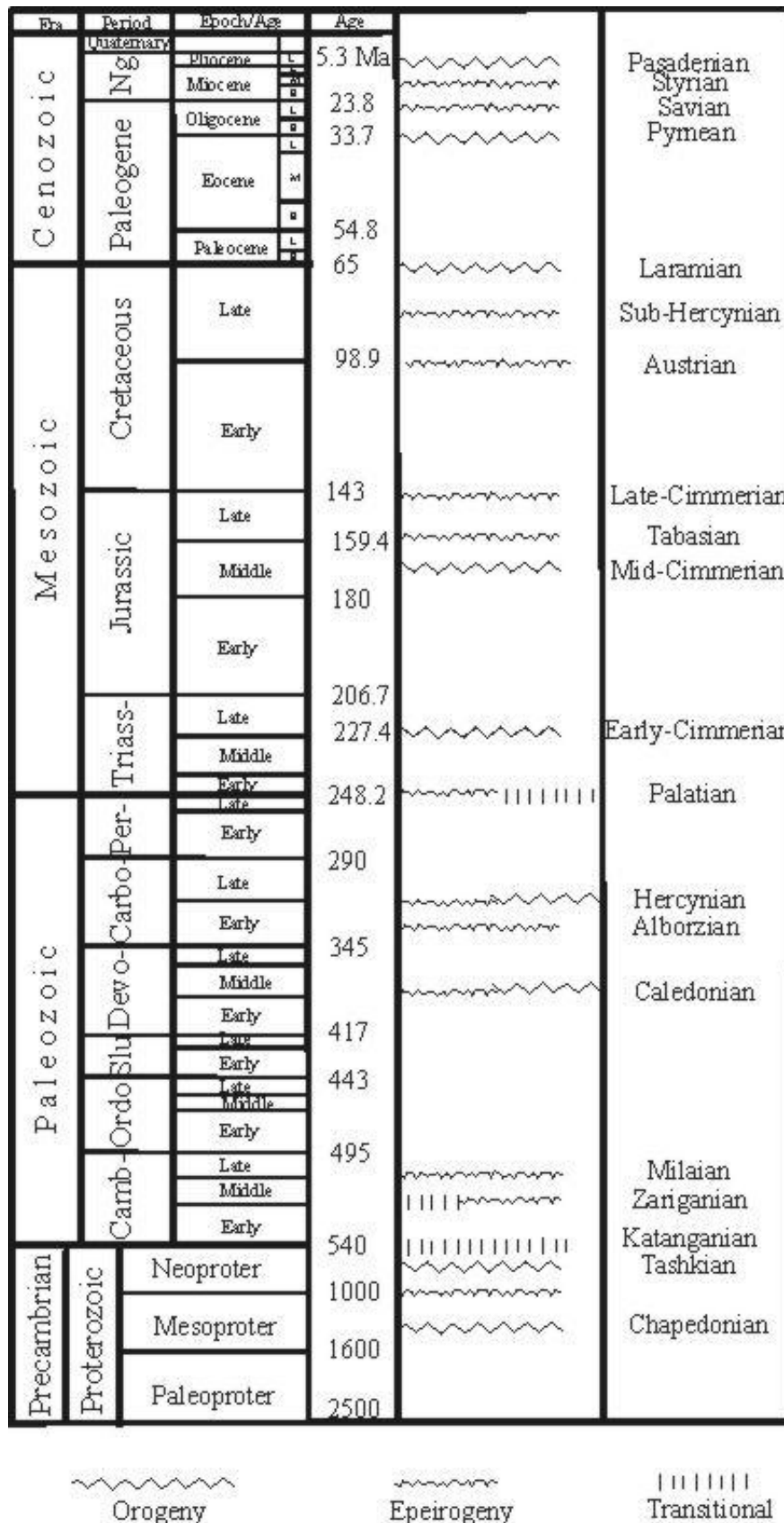
Era	Period	Epoch/Age		Age		
Cenozoic	Ng	Quaternary				
		Pliocene	L	5.3 Ma		Pasadenian
		Miocene	M/U			Styrian
				23.8		Savian
	Paleogene	Oligocene	L/U	33.7		Pyrnean
		Eocene	M			
			U	54.8		
		Paleocene	L/U	65		Laramian
Mesozoic	Cretaceous	Late				Sub-Hercynian
				98.9		Austrian
		Early				
	Jurassic	Late		143		Late-Cimmerian
				159.4		Tabasian
		Middle		180		Mid-Cimmerian
		Early				
	Triass-	Late		206.7		
				227.4		Early-Cimmerian
		Middle				
		Early				
		Late		248.2		Palatian
Paleozoic	Per-	Early		290		
	Carbo-	Late				Hercynian
		Early		345		Alborzian
	Devo-	Late				
		Middle				Caledonian
		Early		417		
	Silu-	Late				
		Early		443		
	Ordo-	Late				
		Middle				
		Early		495		
	Camb-	Late				Milaian
		Middle				Zariganian
		Early		540		Katanganian Tashkian
Precambrian	Proterozoic	Neoproter		1000		
		Mesoproter		1600		Chapedonian
		Paleoproter		2500		

Orogeny   Epeirogeny   Transitional

Fig.6. Classifications of orogeny and epeirogeny activity, which affected the geology of Iran in different times (after Aghanabati, 2004)

The Cimmerian events occurred between 200 Ma and ca. 65Ma and correspond well to the closure of the Neo-Tethyan basin. The Early Cimmerian event occurred during the Middle Triassic; causing the paleogeographical changes, accompanied by folding, magmatic intrusions, and metamorphism in the Paleozoic platform cover and in Early Mesozoic sediments (Hushmandzadeh, el al. 1973). The Late Cimmerian orogeny occurred at the Jurassic-Cretaceous boundary, and it was previously thought that this orogeny was accompanied by folding, paraconformity, magma emplacement, and metamorphism, but it is now believed that all of these orogenic phenomena must be associated with the Mid-Cimmerian (Bathonian/intra Bajocian, Aghanabati, 1992). Evidence for a Mid-Cimmerian movement (~154.9-176 Ma) in many parts of Iran includes tectonic uplift accompanied by denudational interval, paraconformity, igneous activates (Shirkuh granite, Kolaghazi granite, Shahkuh granite and Charfarsakh granite, Aghanabati, 1992), and metamorphism. Successive Early Tertiary movements accompanied a weak regional metamorphism in this period. The latest orogenic episode with metamorphic overprint occurred between the Eocene and Oligocene time.

Geochronological data summarized in Table 1 and Fig. 7 show two maxima with a high number of Cretaceous (60-130 Ma) and fewer frequent Upper- to Middle-Jurassic (155-165 Ma) ages of metamorphism for the Sanandaj Sirjan zone, In contrast, the Central Iran basement suffered mainly by Jurassic metamorphism. There are only a few Jurassic-to-lower Cretaceous metamorphic ages in Albroz. The concentration of Jurassic ages in Central Iran and partly in Sanandaj Sirjan and Albroz suggests that this metamorphism was significant for the entire regions. Generally, the data show youngering of metamorphic recrystallization and mineral formation age from north to the south.
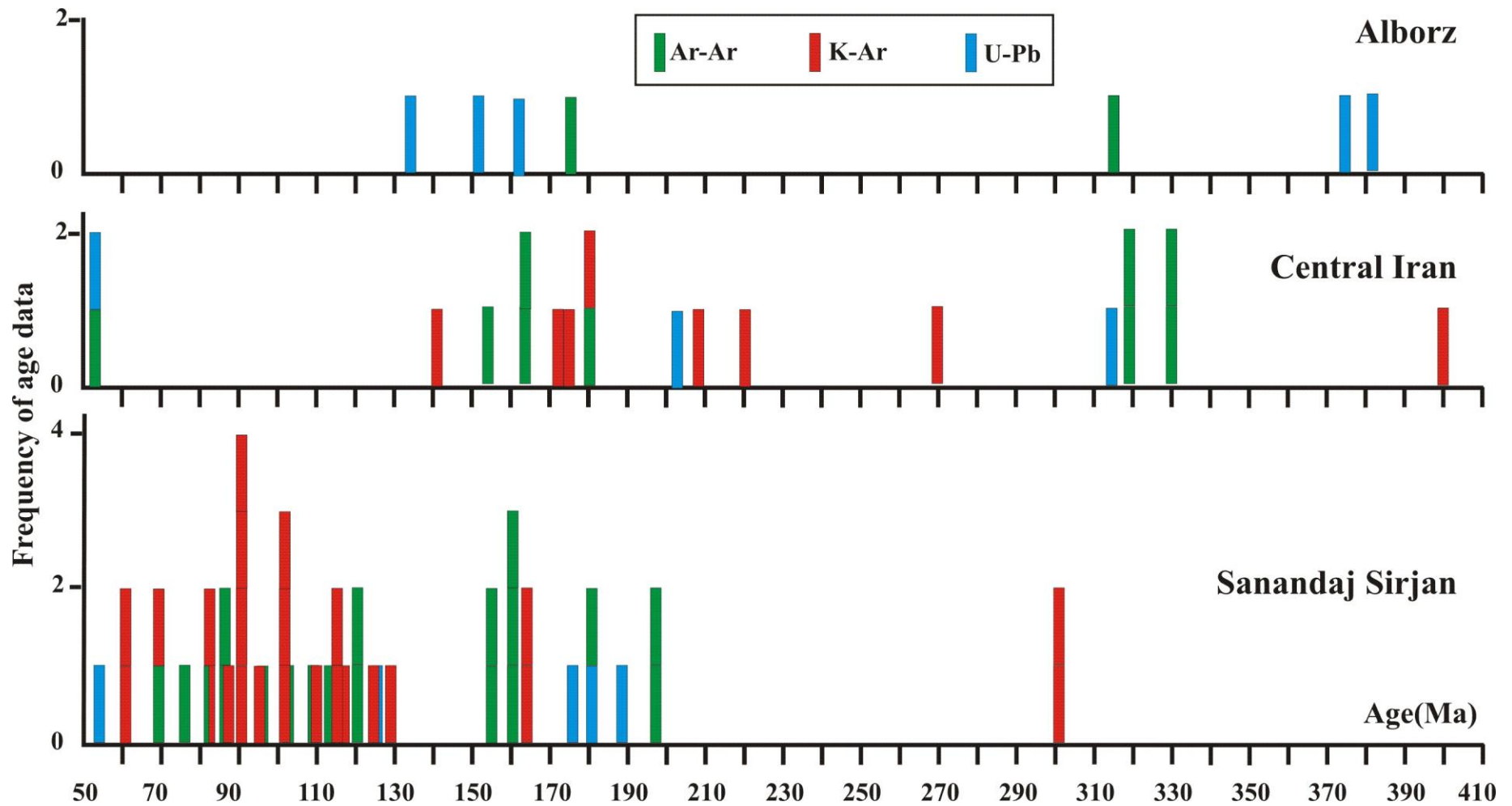
Fig.7. Histogram of available radiometric ages of metamorphic minerals from Alborz, Central Iran and Sanandaj Sirjan. The age data and location of the samples are in Figure 4, and Table 1.

Table 1. Summary of Available Geochronological Data from Metamorphic Basement Rocks in Central Iran, Including the Sanadaj Sirjan zone, Albroz and Shotur Kuh

----

Subunit	rock	Protolith age	Age of metamorphism			
		Fossil/*U-Pb*	U-Pb	K-Ar	Ar-Ar	reference
Sanandaj Sirjan zone						
Region B	granitoids	551 ± 25 Ma				(17)
	granitoids	544 ± 19				
	Micaschist, Amphibolite Gneiss, meta-ophiolite				197 Ma	(20)
					160 Ma	
					158.6± 1.4 Ma	(14)
					154.9 ±1.0	
					197Ma	(20)
					181 Ma	(20)
					160Ma	(20)
					155 Ma	(20)
					121.2 ± 6.2 Ma	(20)
					102.1± 5.4 Ma	(20)
					81.2 ± 1.2 Ma	(20)
					69.4 ± 1.6Ma	(20)
	granitic orthogneiss	548 ± 27 Ma				(17)
		568 ± 44 Ma				(17)
	granite	645 Ma*				(6)
	granite	544 ± 29 Ma				(17)
		599 ± 42 Ma				(17)
	foliated granite		175 ± 5 Ma*			(23)
	biotite granite		53.4 ± 0.4 Ma			(17)

	leucogranite		2.8 ± 0.1			(17)
Region C						(17)
	metasedimentary	Precambrian		114 Ma		(5)
		L-M Jurassic		60 Ma		(5)
				82 Ma		(5)
	Gneiss,marble,Amphibolite	Precambrian				(37)
		Paleozoic		128.3 ± 4.7 Ma		(25)
	leucogranite	578 ± 22 Ma		68.9 ± 1.0 Ma	109.65 ± 2.04 Ma	(17), (25), (24)
		596 ± 24 Ma	124.4 ± 4.4 Ma*	67.5 ± 1.0 Ma)	86.55± 1.00 Ma	(17), (25), (25), (24)
	granite	588 ± 23 Ma		174.5 ± 2.9 Ma		(17), (25)
Region D						(25)
	metagranite, marble	Devonian-Carboniferous			179.5±1.7Ma	(19), (33)
					76.8±0.2Ma	(33)
	orthogneiss amphibolite	520 Ma				(35)
	meta-sedimentary	Devonian to early Carboniferous		300 Ma		(29), (8), (35)
				60 Ma		(35)
	HP-LT metamorphic rock		187±2.6 Ma	89.09 ±1.34 Ma	119.95 ±0.88 Ma	(9), (33)
			180±21 Ma	90.18 ±0.88 Ma	112.58 ±0.66 Ma	(9), (33)
				91.23 ±0.89	87 ±7 Ma	(33), (18)
					96 ±1.3 Ma	(18)
	marbles, micaschists	Cambrian to Ordovician		164 to 161 Ma		(31), (13)
	gneisses			301± 7 Ma		(13)
	anatectic granite			330 ±8 Ma		(13)
	HP-LT metamorphic rock				82.38±1 Ma	(2)
					102.26±4 Ma	(2)

					89.23±1 Ma	(2)
					109.27±3 Ma	(2)
					95.81±6 Ma	(2)
					126.51±2 Ma	(2)
					87.48±1 Ma	(2)
					102.66±2 Ma	(2)
					116.57±9 Ma	(2)
					118.09±1 Ma	(2)
Central Iran						
Region E	meta-sedimentary	Upper Triassic-Jurassic				(36)
Region F	schist,amphibolite, marble	2382 Ma* 2140.9 Ma	48.2 Ma			(16), (27)
	granite	617 Ma	547.6 ± 2.5 Ma			(27)
		602 Ma				(27)
	schist, quartzite, marble, amphibolite, gneiss	627 Ma				(27)
		533 Ma				(27)
		874 Ma			220 Ma	(32)
		750 Ma			180Ma	(32)
					52 Ma	(32)
	Granite	540 Ma*				(6)
Region G	phyllites, mica schists, greenschists, blueschists	Early–? Middle Cambrian age				
		845 Ma*	203 ± 13 Ma*		333–320 Ma	(28), (28), (4)
			315 ± 5 Ma*			(6)
	meta-sedimentary	Middle Permian–			333–318 Ma	(6)

		Middle Triassic				
				400 Ma.		(34)
				180 Ma.	163.86±1.76 Ma	(34), (3)
					156.56 ± 33 Ma	(3)
				270 Ma		(34)
				183 Ma		(34)
Region H	gneisses and schists	554 ± 40 Ma				(17)
		534 ± 31 Ma				(17)
		522 ± 23 Ma				(17)
		551 ± 20 Ma				(17)
		581 ± 21 Ma				(17)
		601 ± 22 Ma				(17)
	granite gneiss	566 ± 31 Ma				(17)
Alborz						
Region I	metabasites , micaschists, peridotite		375±12 Ma*			(6)
			382±48 Ma*		315+9 Ma	(6), (38)
	granite	551 ± 9 Ma	133 + 7.98 Ma			(17), (21)
			152 + 9.12 Ma			(21)
			162 +9.72 Ma			(21)
Region J	phyllites, schists	Neoproterozoic				(10)
		U- Riphean to M-U- Vendian				(30)
		Paleozoic				(15)
Region K	phyllites, sericite-chlorite-schists	Precambrian				(1)
		Late Ordovician				(12)

Region L	meta-sedimentary	Late Paleozoic-Devonian		176 Ma		(22), (7)
Shotur-Kuh						
	orthogneiss	547 ± 7 Ma		141.2 ± 2.2	166 Ma	(26)
		566 ± 31 Ma		208.7 ± 3.2		(17), (26)
				171.8 ± 2.7		(26)

(1) Afshar-harb (1979), (2) Agard et al (2006), (3) Bagheri et al (2007), (4) Bagheri & Stampfli (2008), (5) Baharifar et al (2004), (6) Crawford (1977), (7) Davoudzadeh et al (1975). (8) Eshraghi et al (1999), (9) Fazlnia et al (2007), (10) Gansser and Huber (1962), (11) Geological Survey of Iran (a,1984), (12) Ghavidel Syooki (2007), (13) Ghasemi et al (2002), (14) Ghazi et al (2001), (15) Golshani (1990), (16) Haghipour (1974), (17) Hassanzadeh, et al (2008), (18) Hynes and Reynolds (1980), (19) (Hushmandzadeh et al 1990), (20) Khalatbari-Jafari, et al (2003), (21) Lam (2002), (22) Majidi (1978), (23) McDougall and Harrison (1999), (24) Moritz et al (2006), (25) Rachidnejad-Omran et al (2002), (26) Rahmati Ilkhchi et al (submitted for publication), (27) Ramezani and Tucker (2003), (28) Reyre & Mohafez (1970), (29) Roshan Ravan et al (1995), (30) Sabouri (2003), (31) Sabzehei (1977), (32) Samani (1994), (33) Sarkarinejad et al (submitted for publication, 2009), (34) Sharkovski et al (1984), (35) Sheikholeslami et al (2003), (36) Stöcklin et al (1972), (37) Thiele (1966), (38) Zanchetta et al (2009).

540 Ma* = whole rock (Rb-Sr)

1.3. References:

Afshar-Harb, A., 1979. The stratigraphy, tectonic and petroleum geology of Kopet-Dagh region, northern Iran. Ph.D. thesis. Petrolium Geology Section of Royal School of Mine, Imperial College London, 315p.

Agard, P., Monie´, P., Gerber, W., Omrani, J., Molinaro, M., Meyer, B., Labrousse, L., Vrielynck, B., Jolivet, L.and Yamato P., 2006. Transient, synobduction exhumation of Zagros blueschists inferred from P-T, deformation, time, and kinematic constraints: Implications for Neotethyan wedge dynamics Journal of Geophysical Reserch, V. 111, B11401.

Aghanabati, A., 1992. Representing the Mid-Cimmerian tectonic event in Iran. Scientific Quarterly Journal, Geosciences, Vol. 6. Geological Survey of Iran.

Aghanabati, A., 2004. Geology of Iran. Geological Survey of Iran, book, pp 586.

Aistov, L., Melanikov, B., Krivyakin, B., Morozov, L. and Kiristaev, V., 1984.Geology of the Khur Area (Central Iran), Explanatory text of the Khur Quadrangle map, 1:250,000, V/O Technoexport Report TE/No. 20. Geological Survey of Iran, 131 pp.

Alavi, M., 1979, The Virani ophiolite complex and surrounding rocks: Geologische Rundschau, v. 68, p. 334–341.

Alavi, M., 1991b, Sedimentary and structural characteristics of the Paleo-Tethys remnants in northeastern Iran: Geological Society of America Bulletin, v. 103, p.9183–9192.

Alavi, M., 1991a, Tectonic map of the Middle East, scale: 1:5,000,000: Tehran, Iran, Geological Survey of Iran, one sheet.

Alavi, M., 1994, Tectonics of the Zagros orogenic belt of Iran: New data and interpretations: Tectonophysics, v. 229, p. 211–238.

Alavi, M., 2004. Regional stratigraphy of the Zagros fold-thrust belt of Iran, and its proforeland evolution. American Journal of Science 304, 1–20.

Alavi-Naini, M., 1994. Geological map of Khodabandeh-Soltanieh (scale 1:100,000). Geological Survey of Iran, Tehran, Iran.

Alizadeh, A., 2008. Structural evolution of the Tutak gneiss dome, southwestern Iran. Ph.D. Dissertation. Shiraz University, Iran.

Almasian, M., 1997. Tectonics of Anarak Area (Central Iran). Ph.D. thesis,

University of Azad, North Tehran Unit, Tehran, Iran, 164 pp.

Amini Chehragh,1999. Geological map of Meyamey (scale 1:100,000). Geological Survey of Iran Tehran Iran.

Babakhani, A.R., Sadeghi, A., 2005. Geological map of Zanjan (scale 1:100,000). Geological Survey of Iran, Tehran, Iran.

Babakhani, A.R., Susov, M., Dvoryankin, A., Selivanov, E. and Desyaterik, N., 1987. Geological Quadrangle map of Jandaq, 1:250,000. Geological Survey of Iran, Tehran, Iran.

Bagheri, H., Moore, F., Alderton D.H.M 2007. Cu–Ni–Co–As (U) mineralization in the Anarak area of central Iran. Journal of Asian Earth Sciences 29, 651–665.

Bagheri, S., Stampfli, G.M., 2008. The Anarak, Jandaq and Posht-e-Badam metamorphic complexes in central Iran: New geological data, relationships and tectonic implications. Tectonophysics 451:123–155.

Baharifar,A. Moinevaziri, H., Bellon, H., Piqué, A,. 2004. The crystalline complexes of Hamadan (Sanandaj–Sirjan zone, western Iran): metasedimentary Mesozoic sequences affected by Late Cretaceous tectono-metamorphic and plutonic events. C. R. Geoscience 336, 1443–1452.

Berberian, M., 1995. Master blind thrust faults hidden under the Zagros folds: active basement tectonics and surface morphotectonics. Tectonophysics 241, 193–224.

Berberian, M., 1976. An explanatory note on the first seismotectonics map of Iran; a seismotectonics review of the country. In: Berberian, M. (Ed.),Contribution to the seismotectonics of Iran (Part II). Geological Survey of Iran, vol. 39, pp. 7–141.

Berberian, M., 1997. Seismic sources of the Transcaucasian historical earthquakes. In: Giardini, D., Balassanian, S. (Eds.), Historical and Prehistorical Earthquakes in the Caucasus. Kluwer Academic Publishing, Dordrecht, pp. 233–311.

Berberian, F., Berberian, M., 1981. Tectono-plutonic episodes in Iran. In: Gupta HK and Delany FM (eds) Zagros-Hindu Kush-Himalaya Geodynamic Evolution. American Geophysical Union, Geodynamics Series 3, pp 5-32.

Berberian, M., and Hamdi, B.1997. Frist discovery of Ordovician beds and conodonts in slightly metamorphosed rocks of Kuh-e- Agh Baba, Maku Quadrangle map, Azarbaijan. Geological survey of Iran, internal report, 7p.

Berberian, M., King, G.C.P., 1981. Towards a Paleogeography and Tectonic Evolution of Iran. Can J Earth Sci 8:210–265.

Clark, G.C., Davies, R.G., Hamzepour, G., Jones, C.R., 1975. Explanatory text of the Bandar-e-Pahlavi quadrangle map, 1:250,000. Geological Survey of Iran, Tehran, Iran. pp.198.

Colman-Sadd, S., 1978. Fold development in Zagros simply folded belt, southwest Iran. Am. Assoc. Pet. Geol. Bull., 62: 984-1003.

Crawford, A.R., 1972. Iran, Continental drift and plate tectonics. 24th Int. Geol. Congr., Montreal, Sect. 3, pp.106-112.

Crawford, A.R., 1977. A summary of isotopic age data for Iran, Pakistan and India: Memoire Societe Geologique de France 8:251–260.

Davies, R. G., Jones, C. R., Hamzepour, B. & Clark, G. C. 1972. Geology of the Masuleh Sheet, NW Iran, scale, 1:100 000. Geological Survey of Iran, Report, 24.

Davoudzadeh, M., Aghanabati, A., and Shahrabi, M., 1975. An orogenic phase of Mid-Jurassic age in northeast Iran (Binalud mountain range). Proceedings of Tehran Symposium, Geodynamics of SW Asia. Geological Survey of Iran, Special Publication, pp. 425-427.

Delaloye, M.., Jenny, J. and Stampfli, G., 1981. K-Ar dating in the eastern Elburz (Iran): Tectoniphysics, v.79, p. T27-T36.

Dewey, J. F., Pitman, W. C., Ryan, W. B. F., and Bonnin, J., 1973. Plate tectonics and the evolution of the Alpine system: Geological Society of America Bulletin, v. 84, p. 3137-3180.

Eftekhar-Nezhad, J. 1973. The Mahabad Quadrangle map (scale 1:250,000). Geological Survey of Iran. Tehran, Iran.

Eshraghi, S.A., Roshan Ravan, J., Sabzehei, M., 1999. Geological map of the Quatruyeh area, scale 1:100,000. Geological Survey of Iran.

Falcon, N.L., 1969. The geology of the north-east margin of the Arabian basement shield. British. Association for the Advancement of Science Geology Sections.; 1969, p. 13A 15.

Falcon, N.L., 1974. Southern Iran; Zagros Mountains; in Mesozoic-Cenozoic orogenic belt; Data for Orogenic Studes; Alpine-Himalayan orogens. Geol.Soc.Lond., Spec.Publ. No. 4, p. 199-211, illus.

Fazlnia, A.N., Moradian, A., Rezaei, K., Moazzen, M., Alipour, S., 2007. Synchronous activity of anorthositic and S-type granitic magmas in the Chah-Dozdan batholith, Neyriz, Iran: evidence of zircon SHRIMP and monazite CHIME dating. Journal of Sciences, Islamic Republic of Iran 18, 221-237.

Fotoohi Rad, G.R., Droop, G.T.R., Amini, S., Moazzen, M., 2005. Eclogites and blueschists of the Sistan Suture Zone, eastern Iran: A comparison of P–T histories from a subduction mélange. Lithos 84:1-24.

Furon, R., 1941. Géologie du plateau iranien (Perse, Afghanistan, Béloutchistan), Mém. Mus. Hist. Nat. Paris vii 2 177–414.

Gansser, A., 1951. Geological reconnaissance in the Gorgan and surrounding areas. Unpublished Geological Report no. 18 of National Iranian Oil Company.

Gansser, A., Gupta, H.K., Delany, F.M., 1981. The geodynamic history of the Himalaya, Zagros, Hindu Kush, Himalaya; geodynamic evolution. Geodynamics Series 3, 111–121.

Gansser, A., Huber, H., 1962. Geological observations in the central Elburz, Iran. Schweizerische Mineralogische und Petrographische Mitteilungen 42, 583-630.

Ghasemi, H., Juteau, T., Bellon, H., Sabzehei, M., Whitechurch, H., Ricou, L. E, 2002. The mafic–ultramafic complex of Sikhoran (central Iran): a polygenetic phiolite complex. C. R. Geoscience 334 431–438.

Gealey, W.R.1977. Ophiolite obdution and geologic evolution of the Oman mountains and adjacent areas. Geological Society of America Bulletin, 88, pp.1183-1191.

Geological Survey of Iran. 1984a. Anarak, scale1:100 000. Geological Survey of Iran,
Geological Survey of Iran. 1:100 000 geological map of the Hamadan.

Ghavidel-syooki, M., 2007. Palynostratigraphy and Palaeogeography of Gorgan schist, in the southeastern Caspian Sea, northern Iran. Book of Abstracts of CIMP.

Ghazi, M., Pessagno, E., Hassanipak, A., Kariminia, M., Campbell K., Tectonogenesis of the Khoy ophiolite, NW Iran: results from biostratigraphic/ chronostratigraphic and [40]Ar/[39]Ar studies. 2001, in: Int. Conf. Geology of Oman, Abstract Volume, Sultan Qaboos University, Oman.., pp. 34–35.

Golshani, F., 1990. The upper Proterozoic-lower Paleozoic stratigraphy of Iran with remarks on tectonics, magmatism, and metamorphism (Ph.D. thesis): Hokkaido University, Hokkaido, Japan, pp. 272.

Haghipour, A., 1974. Etude geologique de la region de Biabanak-Bafq (Iran Central); petrologie et tectonique du socle Precambrien et de sa couverture. These, Universite Scientifique et Medicale de Grenoble, France, 403p.

Haghipour, A., 1977. Geological Map of the Biabanak-Bafq Area. Geological Survey of Iran.

Haghipour, A., Pelissier, G., 1977. Geology of the Saghand Sector. In: Haghipour, A., Valeh, N., Pelissier, G., Davoudzadeh, M. (Eds.), Explanatory Text of the Ardekan Quadrangle Map, vol. H8. Geological Survey of Iran, pp. 10–68.

Hassanzadeh, J., Stockli, D.F., Horton, B.K., Axen, G.J., Stockli, L.D, Grove, M., Schmitt, A.K., Walker. J.D., 2008. U-Pb zircon geochronology of late Neoproterozoic–Early Cambrian granitoids in Iran: Implications for paleogeography, magmatism, and exhumation history of Iranian basement. Tectonophysics 451:71–96.

Hempton, M.R., 1987. Constraints on Arabian plate motion and extensional history of the Red Sea. Tectonics 6, 687–705.

Hubber, H., 1957. Geological report on the south Gorgan Mountain front between Neka and Shahpasand: National Iranian Oil Company, unpublished internal geological Report, no. 164,39p.

Huckriede, R., Kursten, M., Venzlaff, H., 1962. Zur geologie des gebiets zwischen Kerman und Saghand (Iran). Beihefte zum Geologischen Jahrbuch, vol. 51. 197p.

Hushmandzadeh, A., 1969. Metamorphisme et granitisation du massif Chapedony (Iran Central). These, Universite Scientifique et Medicale de Grenoble, France, 242p.

Hushmandzadeh, A., Alavi-Naini, M., Haghipour, A., 1978. Geological evolution of Torud area (Precambrian to Recent). Geological Survey of Iran H5 pp138 (in Farsi).

Hushmandzadeh, A., Berberian, M., 1973 The relation of orogenic movements to metamorphic episodes in Iran; A short review. Geological survey of Iran.

Hushmandzadeh, A., Soheile, M., Hamdi, B., 1990. Explanatory text of the Eqlid Quadrangle map 1:25000, Geological Survey of Iran, Ministry of mines and metals. Geological Quadrangle, No. G 10.

Hynes, S.J., Reynolds, P.H., 1980. Early development of Tethys and Jurassic ophiolite displacement. Nature 283, 561e563.

Jafarian, M.B., 2000. Geological map of Kalateh-Reshm (scale 1:100,000)sheet No 6860. Geological Survey of Iran Tehran Iran.

Jenny, J.G., 1977. Geologie et Stratigraphie de 1'Elbourz oriental entre Aliabad et shahrud, Iran, These Geneve, 238 pp.

Kadinsky-Cade, K. and Barazangi, M., 1982. Seismotectonics of southern Iran: The Oman Line. Tectonics, 1: 389-412.

Kent, P.E., 1958. Recent studies of south Persian salt plugs. Am. Assoc. Pet. Geol. Bull., 42: 2951-2972.

Khalatbari-Jafari, M., Hatami, M., 2009. Suprasubduction Origin for the Nari Ophiolite, Southwestern Belt of Fariman, Northeast Iran. American Geophysical Union, Fall Meeting 2009.

Khalatbari-Jafari, M., Juteau, T., Bellon, H., Emami, H. 2003 Discovery of two ophiolite complexes of different ages in the Khoy area (NW Iran) C. R. Geoscience 335 917–929.

Khalatbari-Jafari, M., Mobasher, K., Davarpanah, A., Babaie, H., La Tour, T. 2008. A backarc basin origin for the Eocene volcanic rocks North Abbas Abad, East of Shahrud, Northeast Iran. American Geophysical Union, Fall Meeting 2008.

Koohpeyma, M., 2007. Structural analysis of ductile deformation of metamorphic rocks in the south of Mashhad. MS Thesis of Research Institute for Earth Seciences, Geological Survey of Iran.

Krumsiek, K. 1976. Zur Bewegung der Iransch-Afghanisten Platte. *Geol. Rundsch,* 65, 909–929.

Lam, P.J., 2002, Geology, geochronology, and thermochronology of the Alam Kuh area, central Alborz Mountains northern Iran [M.S. thesis]: Los Angeles,

McDougall, I., Harrison, T.M., 1999. Geochronology and thermochronology by the 40Ar/39Ar method. Oxford University Press, New York.

Majidi, B., 1978 E tudepetrostructural de la region de Mashhad, N.E Iran. Thesis. Univ. Grenobl. Farance.

McQuarrie, N., Stock, J.M., Verdel, C., and Wernicke, B.P., 2003, Cenozoic evolution of Neotethys and implications for the causes of plate motions: Geophysical Research Letters, v. 30, no. 20, 2036.

Mohajjel, M., Fergusson, C.L., and Sahandi, M.R., 2003, Cretaceous-Tertiary convergence and continental collision, Sanandaj-Sirjan zone, western Iran: Journal of Asian Earth Sciences, v. 21, p. 397–412.

Moritz, R., Ghazban, F., and Singer, B.S., 2006, Eocene gold ore formation at Muteh, Sanandaj-Sirjan tectonic zone, western Iran: a result of late-stage extension and exhumation of metamorphic basement rocks within the Zagros orogen: Economic Geology, v. 101, p. 1497-1524.

Nabavi, M.H., 1976. An introduction to the Iranian geology. Geological Survey of Iran. 110 pp. (in Persian).

Nadimi, A., 2005. The basement complexes in Iran, with special regards to those exposed in the Central Iran. International Conference on Precambrian Continental Growth and Tectonism (abstract), Jhansi, Feb. 22–24, 2005, India, pp. 32–34.

Nadimi A, 2007 Evolution of the Central Iranian basement. Gondwana Research 12: 324–333

Navai, I., 1987. Geological map of Khar Touran (scale 1:250,000), Geological Survey of Iran, Tehran, Iran.

Omrani, J., Khabbaznia, A.R., 2003. Geological map of Alut (scale 1:100,000), Geological Survey of Iran, Tehran, Iran.

Rachidnejad-Omran N., Emami, M.H., Sabzehei, M., Rastad, E., Bellon, H., and Piqué, A., 2002 Lithostratigraphie et histoire paléozoïque à paléocène des complexes métamorphiques de la région de Muteh, zone de Sanandaj- Sirjan (Iran éridional): Comptes rendus Geoscience, v. 334, p. 1185–1191.

Rahmati Ilkhchi M, 2002. Geological map of Razveh (scale 1:100,000).Geological Survey of Iran, Tehran Iran

Ramezani J, Tucker RD, 2003. The Saghand Region, Central Iran: U–Pb geochronology, petrogenesis and implications for Gondwana tectonics. Am J Sci 303: 622–665

Reyre, D., Mohafez, S., 1970. Une premiere contribution des accordc NIOC-ERAP a la connaissanca geologique de l' Iran. Deuxieme partie. Rev. Inst.F.Petrole; France.

Ricou, L.E., 1974. L' e´volution ge´ologique de la re´gion de Neyriz (Zagros Iranien) et l' e´volution structurale des Zagrides. Thesis, Universite Paris-Sud, Orsay (unpublished).

Ricou, L.E., 1976. Evolution structurale des Zagrides. La region Clef de Neyriz (Zagros iranien). Mem. Sot. Geol. Fr., Nouv. Ser., 55 (125): 140 pp.

Ricou, L.E., Braud, J., Brunn, J.A., 1977. Le Zagros. Me´moire Societe Ge´ologique de France, Hors-Se´rie 8, 33–52.

Romanko, E.F., Morozov, L.N., 1983. The Anarek-Khvor Massif in Central Iran: structure and history of development. Geotectonics 17 (1), 70–75.

Roshan Ravan, J., Amini, B., 1995. Geological map of the Kor-e-Sefid area, scale 1:100,000 Geological Survey of Iran.

Sabouri, J., 2002. Recognition of index Fossil, Cochleatina from top of the Kahar Formation in Firooz-Abad of Chalus, and interpretation of age of this Formation in Iran.The 18th Symposium of Geosciences Conference, Tehran

Sabzehi, M., 1974. Les Melanges ophiolitiques de la Region d'Esfandagheh (Iran m&idional). Etude petrologique et strueturale. Interpretation dans le Cadre iranien. These, Grenoble, 306 pp.

Sabzehi, M., 1977. Petrology of Iranian ophiolites, internal report, GSI Teheran, 700 p. (in Persian)..

Salehi-Rad, M. R., 1979. Etude Geologique de la région de Gorgan (Alborz Oriental, Iran): Ph.D. thesis, Universities de Paris Sud, 162p.

Samani, B.A., Zhuyi, C., Xuetao, G., Chuan, T., 1994. Geology of Precambrian in central Iran: on the context of stratigraphy, magmatism and metamorphism. Geosciences Quarterly 3 (10), 40–63 (Geological Survey of Iran, in Farsi with English abstract).

Sarkarinejad, K. Alizadeh A. 2009. Dynamic model for the exhumation of the Tutak gneiss dome within a bivergent wedge in the Zagros Thrust System of Iran. Journal of Geodynamics 47, 201–209

Schröder, J.W., 1944, Essai sur la structure de l'Iran: Eclogae Geologicae Helvetiae, v. 37, p. 37–81.

Sengör, A.M.C., Altiner, D., Cin, A., Ustaomer, T., and Hsu, K.J., 1988, Origin and assembly of the Tethyside orogenic collage at the expense of Gondwana Land, in Audley-Charles, M.G., and Hallman, A., eds., Gondwana and Tethys: Geological Society [London] Special Publication 37, p. 119–181.

Sharkovski, M., Susov, M. & Krivyakin, B. 1984.Geology of the Anarak area (Central Iran). Explanatory Text of the Anarak Quadrangle Map 1:250 000. Geological Survey of Iran, V/O 'Tecnoexport' USSR Ministry of Geology, Reports, 19.

Sheikholeslami, R., Bellon, H., Emami, H., Sabzehei, M., Piqué, A., 2003. Nouvelles données structurales et datations 40K-40Ar surles roches métamorphiques de la region de Neyriz (zone de Sanandaj-Sirjan, Iran méridional). Leur intérêt dans le cadre du domaine néo-tethysien du Moyen-Orient. Compates Rendus Geoscience 335, 981-991.

Sheikholeslami, M.R., Pique, A., Mobayen, P., Sabzehei, M., Bellon, H., Emami, M. H., 2008 Tectono-metamorphic evolution of the Neyriz metamorphic complex,

Quri- Kor-e-Sefid area (Sanandaj-Sirjan Zone, SW Iran). Journal of Asian Earth Sciences 31 504–521

Stahl, A. F., 1911. Handbuck der regionalen geologie – Persian: V Band 8, Hildelberg.

Stampfli, G.M., 1978.Etude géologique générale de l'Elburz oriental au S de Gonbad-e-Qabus, Iran N-E. Fac Sci Univ Genève Thesis No 1868 pp 329

Stampfli, G.M., 2000. Tethyan oceans. In: Bozkurt, E., Winchester, J.A., Piper, J.D.A. (Eds.), Tectonics and Magmatism in Turkey and Surrounding Area. Geological Society of London, Special Publication, pp. 1–23.

Stampfli, G.M., Borel, G.D., 2002. A plate tectonic model for the Paleozoic and Mesozoic constrained by dynamic plate boundaries and restored synthetic oceanic isochrons. Earth and Planetary Science Letters 196, 17–33.

Stampfli, G.M., Kozur, H., 2007. Europe from the Variscan to the Alpine cycles. In: Gee, D.G., Stephenson, R. (Eds.), European Lithosphere Dynamics. Memoir of the Geological Society (London), pp. 57–82.

Stampfli, G., Marcoux, J., and Baud,A., 1991, Tethyan margins in space and time: Palaeogeography, Palaeoclimatology, Palaeoecology, v. 87, p. 374–409.

Stöcklin J, 1968. Structural history and tectonics of Iran: a review. Amer Assoc Petroleum Geol Bull 52 (7): 1229–1258

Stocklin, J., 1971. Statigraphic Lexicon of Iran (Part I). Rep.Geol.Surv.Iran, 18:1-337.

Stocklin, J., 1974. Possible Ancient Continental Margins in Iran. In: Burke, C.A., Drake, C.L. (Eds.), The Geology of Continental Margins. Springer Verlag, New-York, pp. 873–887.

Stöcklin, J., 1977. Structural correlation of the Alpine ranges between Iran and Central Asia. Mémoires hors Série de la Société Géologique de France 8:333–353

Stöcklin, J., Eftekharnezhad, J., 1969. Explanatory text of the Zanjan quadrangle map. Geological Survey of Iran, Tehran, Iran.

Stocklin, J., Eftekharnejad, J., and Hushmandzadeh, A., 1965, Geology of the Shotori Range (Tabas area, East Iran): Geological Survey of Iran Report 3, 69 p.

Stocklin, J., Eftektar-Nezhad, J. and Hushmand-Zadeh, A., 1972. Central Lut reconnaissance, East Iran. Geol. Surv. Iran Rep., 22: 62 pp.

Takin M, 1972. Iranian geology and continental drift in the Middle East: Nature 235: 147–150.

Talbot, C. J., and Alavi, M., 1996, The past of a future syntaxis across the Zagros, *in* Alsop, G. I., Blundell, D. J., and Davidson, I., editors, Salt tectonics: London, Geological Society Special Publication 100, p. 89–109.

Talbot, C.J. and Jarvis, R.J., 1984. Age, budget, and dynamics of an active salt extusion in Iran. J. Struct. Geol., 6: 521-533.

Thiele, O., 1966, Zum Alter der Metamorphose in Zentraliran: Mitteilungen der geologischen Gesellschaft [Wien], v. 58, p. 87–101.

Thiele, O., Alavi, M., Assefi, R., Hushmand-zadeh, A., Seyed-Emami, K., and Zahedi, M., 1968, Explanatory text of the Golpaygan quadrangle map 1:250,000: Geological Survey of Iran, Geological Quadrangle E7, 24 p.

Tietze, E., 1877. Ein Ausflug nach dem Siahkuh (Schwarzer Berg) in Persien. Mitt.geogr. Ges.Wien. (N.F.) 18/8, pp.257-267.

Tirrul, R., Bell, I.R., Griffis, R.J., Camp, V.E., 1983. The Sistan Suture Zone of eastern Iran. Geol. Soc. Amer. Bull. 94, 134– 150.

Zanchetta, S., Zanchi, A., Villa, I., Poli, S. & Muttoni, G. 2009. The Shanderman eclogites: a Late Carboniferous high-pressive event in the NW Talesh Mountains (NW Iran). In: Brunet, M.-F., Wilmsen, M. & Granath, J.W.(eds) South Caspian to Central Iran Basins. Geological Society, London, Special Publications, 312, 57–78.

CHAPTER 2

Magmatic and metamorphic evolution of the Shotur Kuh Metamorphic Complex (Central Iran)

Mahmoud Rahmati-Ilkhchi[1,2], Shah Wali Faryad[1], František V. Holub[1], Jan Košler[3], and Wolfgang Frank[4]

[1] Institute of Petrology and Structural Geology, Charles University in Prague, Albertov 2, 128 43 Prague, Czech Republic

[2] Geological Survey of Iran

[3] Department of Earth Science and Centre for Geobiology, University of Bergen, Allegaten 41, N-5007 Bergen, Norway

[4] Central European Argon Laboratory, Slovak Academy of Sciences, Valasška, Bratislava

Abstract

Metamorphic basement rocks, that are exposed beneath the very-low-grade to unmetamorphosed Upper Jurassic-Eocene formations north of the Torud fault zone within the Great Kavir Block, were investigated in order to elucidate origin of their protoliths and the pressure and temperature conditions of metamorphism. The basement, previously assumed as a pre-Cambrian metamorphic complex, is mostly formed by amphibolite facies orthogneisses (tonalite, granodiorite, and granite) with amphibolites and small amounts of metasediments-micaschists. Major- and trace-element geochemistry in combination with U-Pb age dating of zircon showed that the protoliths formed during Late Neoproterozoic continental arc magmatism that has also been identified in other tectonic blocks of Central Iran. In addition to quartz, feldspar(s), micas in orthogneisses, and amphibole + plagioclase in amphibolite, all rocks may contain garnet that shows prograde zoning. Kyanite was found only in some Al-rich amphibolite together with gedrite. The PT conditions of the rocks, based conventional geothermobarometry and the pseudosection method, show a medium-pressure amphibolite facies metamorphism. Ar-Ar age dating of muscovite reveals that this metamorphism occurred 166 Ma ago (Middle Jurassic) and related to the closure of the Neotethyan basin.

2.1. Introduction

The Central Iranian Terrane is a composite of fold-and-thrust belts with basement blocks covered by thick sedimentary sequences. Comparative stratigraphy and tectonics, combined with geochemistry of igneous rocks in Central Iran, led to the identification of several crustal blocks (e.g., Stöcklin, 1968, 1977; Takin, 1972; Crawford, 1977; Berberian et al., 1981). Ramezani and Tucker (2003) summarized tectonic and geochronological data from Central Iran and focused on igneous rocks in the Saghand area that previously had been thought to represent the Precambrian basement. The igneous/metaigneous rocks occur along a north-south-trending belt, the Kashmar-Kerman Tectonic Zone (KKTZ), which separates the Yazd block to the west and the Tabas block to the east in Central Iran (Fig. 1a). Based on U-Pb ages and geochemical data, Ramezani and Tucker (2003) postulated that these rocks are remnants of a Late Neoproterozoic arc that developed along the Proto-Tethyan margin of the Gondwanaland supercontinent. Metamorphism of these rocks that reached amphibolite facies conditions occurred in Eocene times. However, several basement rocks exposed beneath the Paleozoic-to-Mesozoic sedimentary sequences west of the KKTZ are still assumed to be Pre-Cambrian metamorphic basement, even though detailed information about their composition and metamorphic evolution is lacking. Bagheri and Stampfli (2008) investigated amphibolite facies metaigneous and metasedimentary rocks exposed along the boundary between the Yazd and Great Kavir blocks and postulated a Paleozoic accretionary complex with a 320 Ma age of greenschist-to-amphibolite facies metamorphism and a Permian-Triassic (280–230 Ma) high-pressure metamorphism. It seems that boundaries between different crustal blocks were significant in the formation of igneous and metamorphic rocks during the geological evolution of Central Iran.

In this work, we focus on the Shotur Kuh metamorphic complex in the Great Kavir Block (GKB) (Fig. 1a). It forms a tectonic window beneath the Mesozoic and Cenozoic sediments near the Torud fault zone. Similar to other crystalline windows exposed in Central Iran, it has been assumed to represent a Pre-Cambrian metamorphic basement. In addition to geochemistry and metamorphic evolution, we present new U-Pb zircon and Ar/Ar mica ages. The implications of our results for the metamorphic and tectonic evolution of the GKB along the Torud tectonic zone, as

well as relationships to other igneous and metamorphic complexes in Central Iran, are discussed.

2.2. Geological setting

From east to west, the Central Iranian Terrane consists of four major crustal domains (Fig. 1a): the Lut Block, the Tabas Block, the Yazd Block and the Great Kavir Block (see for example, Berberian et al., 1981; Bagheri and Stampfli, 2008). These blocks are separated by a series of intersecting regional-scale faults. Although the stratified cover rocks are largely comparable among different blocks, locally significant facies and/or thickness variations occur across the domain boundaries. Each block features a particular overall deformation style and pattern of recent seismicity, distinguishable from those in the adjacent domains (Berberian, 1981). The Tabas and Yazd blocks are separated by a nearly 600-kilometer-long, arcuate, and structurally complex belt, the KKTZ, composed of variably deformed and fault-bound supracrustal rocks.

The Rezveh area with the Shotur Kuh metamorphic complex (SKMC) is a part of the Great Kavir Block (GKB) and occurs north of the Torud fault zone (Fig. 1b). This tectonic zone is followed by a series of Eocene volcanic rocks of dacitic and andesitic composition. The SKMC represents an E-W-trending elliptical tectonic window (c. 20 km long and 11 km wide) that, together with its Pre-middle-Triassic tectonic cover, is exposed beneath the Jurassic-Miocene sedimentary sequences (Fig. 1c). Most of the basement rocks have igneous precursors, and only small amounts of micaschists and phyllites, which represent the lower part of the Pre-middle Triassic (Permian-Lower Triassic?) sequence with metamorphosed limestone and dolomite are present. These rocks occur along the southern and northern boundaries of the SKMC. The main rocks are orthogneisses of tonalitic, granodioritic, and granitic compositions with various amounts of amphibolites (probably former dykes) that have lengths up to several tens of meters and widths from centimeters to 20 m. The amount and thickness of the amphibolite bodies decreases from meta-granodiorite to granite, and they are most common in the central and western part of the complex. In some cases, amphibolite and orthogneiss may form parallel stripes and bands that are locally deformed into isoclinal folds. The metagranite occurs along the northern border and in the central part of this complex.
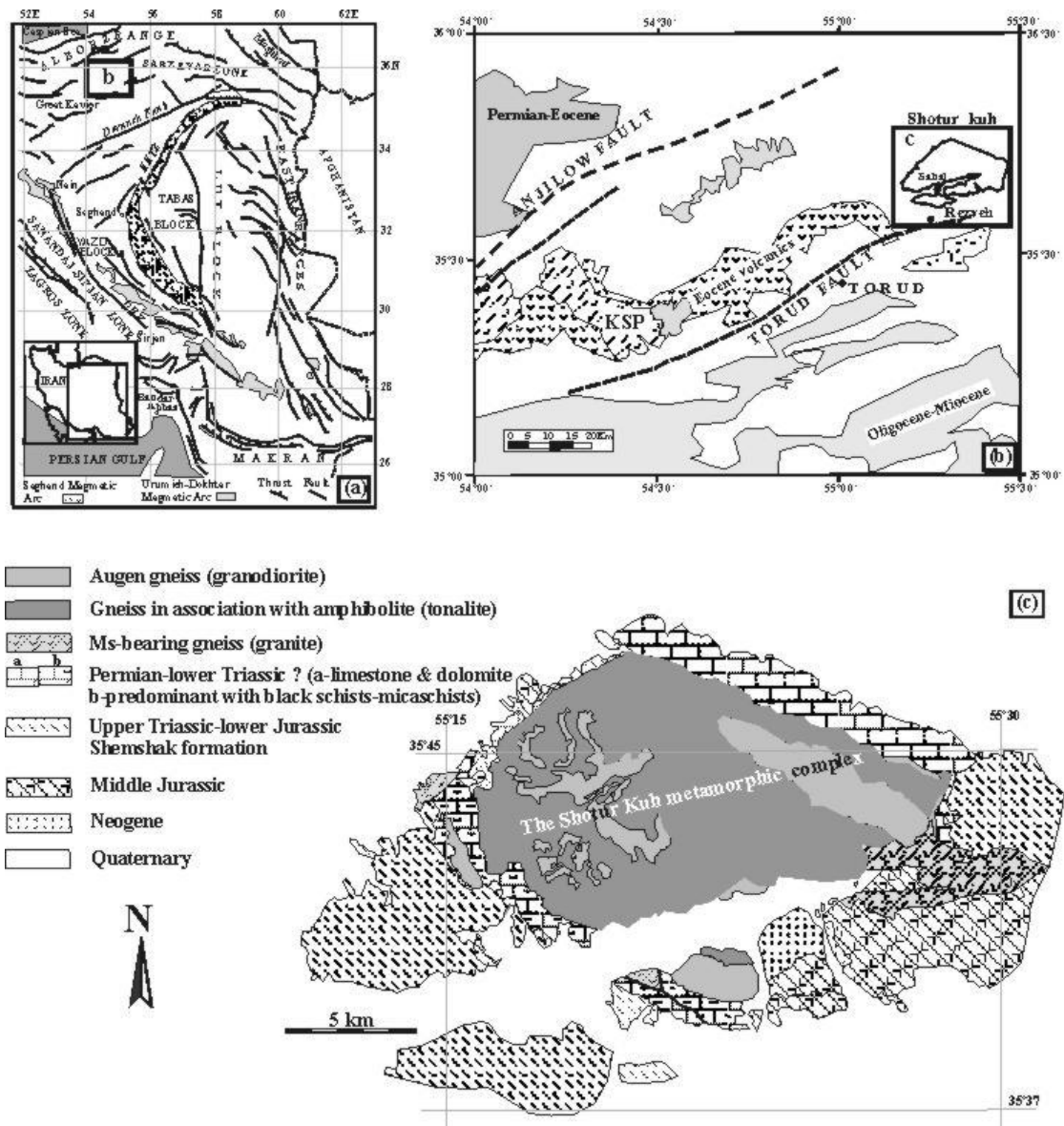
Fig. 1. Simplified tectonic map of eastern Iran showing constituent crustal blocks (compiled from Ramezani and Tucker, 2003; Alireza Nadimi, 2006). KKTZ- Kashmar-Kerman Tectonic Zone, DBF-Dehshir Fault, TFZ. (b) Schematic map of the Torud area with important faults (after Hushmandzadeh et al., 1978). (c) Simplified geological map of the Rezveh area (Rahmati-Ilkhchi, 2002).

Metapelitic rocks (black shale-phyllite-garnet micaschist) rimming the southern border of the complex form the lower part of the Pre-middle Triassic (Permian-Lower Triassic?) formation. They intercalate with calcitic and dolomitic marbles that upward become a massif carbonatic sequence with few or no pelitic rocks. Marbles and garnet micaschists are isoclinally folded together with metaigneous rocks and are tectonically juxtaposed with phyllites, which show a lower degree of metamorphism. The Pre-middle Triassic pelitic-carbonatic rocks are covered by the Upper Triassic-

Lower Jurassic Shemshak formation, which is represented by the intercalation of psammopelitic rocks with conglomerates. They show metamorphic fabrics similar to those in the Pre-middle Triassic rocks, but in lower greenschist facies conditions that are characterized by the presence of chlorite, fine-grained white mica and quartz. The uppermost (Middle Jurassic) part of the Mesozoic sequence, beneath the Neogene sediments, is characterized by very-low-grade sandstones, shales and conglomerates, which contain pebbles of the basement rocks (Rahmati-Ilkhchi, 2002).

2.3. Analytical methods

We studied the rocks using bulk-rock geochemistry, mineral composition, and age dating of zircon and micas. Powdered whole-rock samples were analyzed in the Activation Laboratories (Actlabs), Ltd. (Ancaster, Ontario) using the lithium metaborate/tetraborate fusion technique followed by a combination of (1) inductively coupled plasma emission spectroscopy (ICP-OES) for major elements plus Sc, Be, and V; and (2) inductively coupled plasma mass spectrometry (ICP-MS) for all other trace elements. The analytical results (see Table 1) are illustrated in geochemical diagrams using the GCDkit software (Janoušek et al., 2006).

Mineral chemical analyses were carried out with a CAMECA SX 50 electron microprobe at the Institute of Mineralogy, Technische Universität Stuttgart, which is equipped with four wavelength-dispersive spectrometers. The following synthetic standards were used: pyrope (Si, Al, Mg), andradite (Ca, Fe), jadeite (Na), spessartine (Mn), K-silicate glass (K), Ba-silicate glass (Ba), and NaCl (Cl), as well as natural rutile (Ti) and topaz (F). The operating voltage was 15 kV using beam currents between 10 and 15 nA. The beam was focused to 1–2 μm diameter, except for micas, for which an 8–10 μm beam was used. The peak counting times were 20 seconds. Some compositional profiles of garnet were obtained using the scanning electron microscope JEOL 6310 at the Institute for Petrology and Structural Geology, Charles University, Prague. Representative mineral analyses are given in Table 2.

U/Pb dating of zircons was performed by laser ablation inductively coupled plasma mass spectrometry (LA-ICPMS) using a New Wave UP-213 (213 nm, Nd:YAG) laser system coupled to a Thermo Finnigan Element 2 ICP-MS instrument at the Department of Earth Science, University of Bergen. The analytical technique and data reduction were modified from Košler et al. (2002). Ar-Ar age dating was

obtained by measuring the $^{40}Ar*/^{39}Ar$ isotopic ratio using the mass spectrometry VG 5400 at the Central European Ar-Laboratory in Bratislava.

Petrography

The main rock groups of the SKMC are orthogneisses that are derived from rocks of granitic, granodioritic and tonalitic compositions. The metatonalite are characterized by the presence of amphibolite bodies, and they are exposed in the central and eastern parts of the complex. Phyllites to micaschists studied here come from the southern border of the SKMC.

Orthogneisses

The rocks are medium- to coarse-grained (partly) display augen textures with various degrees of foliation. At least three varieties of orthogneisses can be distinguished based on the present mineral assemblages: amphibole + plagioclase + biotite + quartz ± garnet (metatonalite); plagioclase + biotite + quartz ± garnet; and plagioclase + biotite + muscovite ± garnet (metagranodiorite to metagranite). Grain size and augen structure in the orthogneisses increase from tonalites to granites. In addition to feldspars, quartz and biotite, some tonalitic and granitic varieties may additionally contain amphibole and muscovite, respectively. Zircon, apatite, rutile, titanite, allanite, and monazite are accessory phases. Metagranites are strongly foliated and they are rich in muscovite (up to 10 vol %); together with biotite and thin quartz bands, they define the foliation (Fig. 2a). Such rocks occur along the northeastern border and also in the central part of this complex. Garnet is not found often but occurs in all compositional varieties of the orthogneisses. The relict K-feldspar is slightly perthitic, but microcline and myrmekite can be also observed. An interesting feature in metatonalites and metagranodiorites is the presence of dark-brown allanite, which may form up to 1 mm long crystals oriented parallel to the foliation. It is usually rimmed by epidote.

The rocks show various degrees of retrogression and recrystallization, which is characterized by the presence of several mineral phases. Large plagioclase crystals contain small grains of zoisite-clinozoisite, and also, though rarely, of calcite in the cores. Both feldspars can be partly replaced by fine-grained white mica. Garnet is usually cracked, and along cracks and rims it is partially replaced by fine-grained

biotite and chlorite. The fine-grained variety of biotite is also present in some mylonitized orthogneisses. Compared with the coarse–grained, red-brown biotite, which shows textural equilibrium with garnet, the fine-grained variety has light-brown
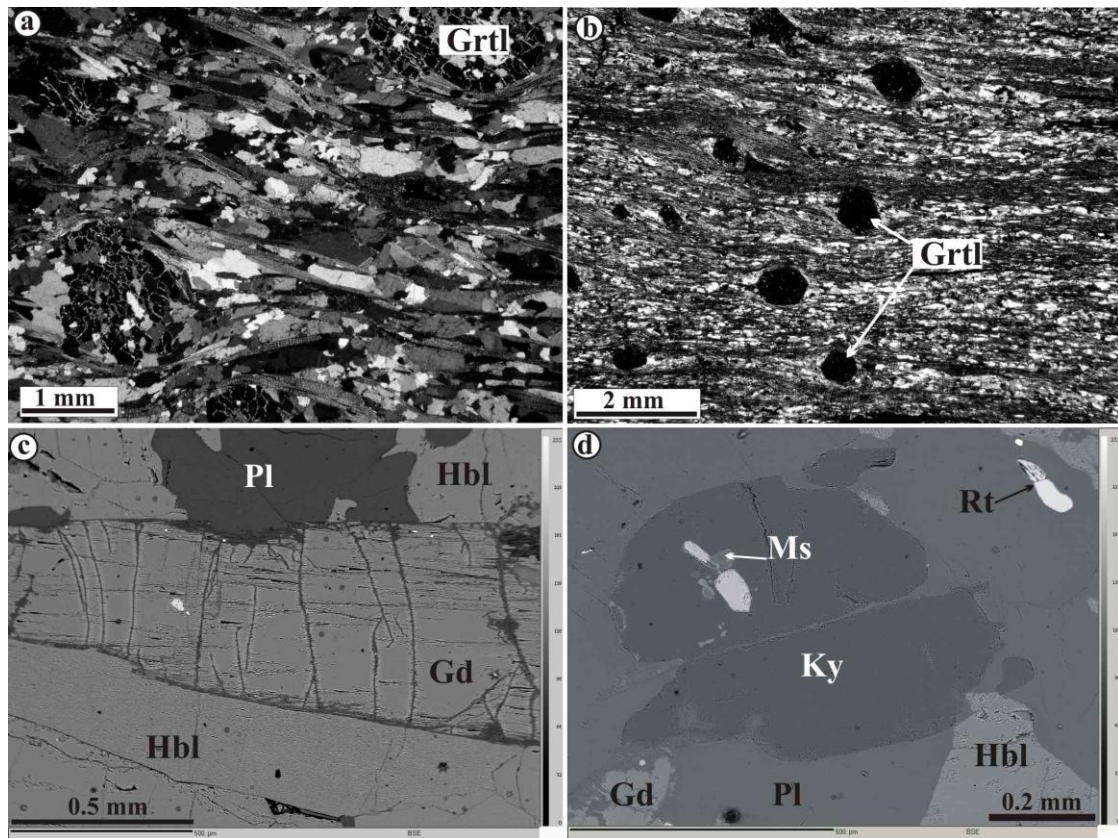
and green colours.

Fig. 2. Microphotos of an muscovite-bearing orthogneiss metagranite (a) and micaschist-phyllite (d) from the Shotur Kuh metamorphic complex. (b) and (c) are backscatter images of gedrite and kyanite-bearing amphibolite.

Amphibolites

Amphibolites are mostly garnet-free, and the major phases are plagioclase and amphibole, which define the foliation of the rock. Porphyroblastic garnet (up to 5 mm in size) and quartz can each be present up to 15 vol %. Accessory phases are zircon, apatite, titanite, and opaque minerals, secondary minerals involve epidote and chlorite which replace amphibole. Relict igneous clinopyroxene was observed in one sample (I-10a) and it forms large crystals (1 to 3 mm in size) that are mostly replaced by actinolite and epidote. Plagioclase crystals (1–2 mm in size) are partly replaced by sericite.

In one case (sample P182), kyanite and gedrite were found (Figs. 2b and c). This rock is coarse-grained and well foliated, and consists of calcic amphibole, plagioclase, gedrite, and accessory rutile, kyanite, biotite, and phengite. Gedrite, which is characterized by crystals up to 7 mm long that show a weak pleochroism from pale to yellow-grey, forms intergrowths with calcic amphibole and contains inclusions of plagioclase. Phengite was found in kyanite, which together with partial replacement of amphibole by chlorite along the cleavage indicates very weak retrogression.

Micaschists

The fine-grained rocks grading from phyllites to micaschists come from the southern border of the SKMC. The micaschists are strongly foliated and consists of quartz, white mica, garnet, biotite, and small amounts of plagioclase. In contrast to muscovite-bearing orthogneisses they contain a very fine graphitic substance that is indicative of a sedimentary protolith. Garnet crystals (up to 0.5 mm in size) form idioblasts, with pressure shadows consisting of quartz and large flakes of biotite and muscovite (Fig. 2d). The rocks are retrogressed to various degrees, with garnet grains being replaced by calcite and chlorite, biotite being replaced by chlorite, and plagioclase containing numerous flakes of fine-grained white mica.

2.5. Geochemistry

In order to characterize the tectono-magmatic evolution of the rocks, 16 samples (10 orthogneisses and 6 amphibolites) were selected for whole-rock analyses. Representative data are listed in Table 1. Since we did not recognize any particular evidence for major-element transport during post-magmatic evolution and regional metamorphism, we assumed that the present compositional variations of the orthogneisses and amphibolites may largely reflect the original characteristics of the igneous rocks. No chemical element, however, may be considered as fully "immobile", and therefore all of the geochemical conclusions should be regarded with caution.

Orthogneisses

Orthogneisses represent a heterogeneous group of subalkaline rocks with SiO_2 ranging from 63.7 to 76.9 wt % and variable amounts of alkalis (Na_2O 2.8 to 3.9 wt %, K2O 0.5 to 4.6 wt %).

Table 1 Representative whole-rock chemical analyses of the Shotur Kuh orthogneisses and amphibolites. Major oxides are in weight percent, trace elements in parts per million.

	I-10	P8	P160	P109	P122	P203	P147	P183	P108	P202	P182	I-5	P179	P29	P68	P74
Rock	Orthogneiss										Amphibolite					
SiO_2	63.72	64.29	71.74	72.21	73.66	73.72	74.54	75.16	75.91	76.89	46.21	49.58	51.12	51.57	49.91	51.6
TiO_2	0.57	0.73	0.12	0.44	0.24	0.38	0.19	0.18	0.12	0.06	0.69	0.72	1.65	2.12	2.26	1.40
Al_2O_3	13.42	16.30	12.11	13.23	13.36	12.71	13.06	13.02	12.27	12.22	18.36	16.35	15.35	14.91	13.73	17.46
Fe_2O_3 tot.	10.42	5.88	1.67	3.77	2.57	2.80	2.02	1.84	1.54	0.90	8.88	8.63	11.98	13.25	13.41	13.45
MnO	0.18	0.05	0.01	0.04	0.04	0.03	0.01	0.02	0.04	0.01	0.12	0.12	0.18	0.20	0.21	0.22
MgO	1.74	3.06	0.40	0.81	0.58	0.56	0.39	0.36	0.27	0.13	12.19	8.80	6.95	5.75	5.32	2.49
CaO	5.68	2.22	2.81	3.13	1.63	1.43	0.91	1.56	1.15	0.44	8.65	11.47	9.59	9.29	9.19	8.29
Na_2O	3.21	3.88	3.19	3.39	3.36	2.89	3.43	3.48	2.78	3.21	2.80	2.68	2.27	1.63	2.65	2.44
K_2O	0.47	2.47	3.35	1.33	3.23	4.61	4.30	3.86	4.08	4.59	0.20	0.53	0.31	0.43	1.69	1.33
P_2O_5	0.06	0.22	0.59	0.12	0.08	0.11	0.23	0.05	0.05	0.06	0.09	0.07	0.23	0.30	0.34	0.45
LOI	0.30	1.09	2.86	0.89	1.09	0.56	1.20	0.28	0.79	0.68	1.62	0.90	1.20	1.47	1.11	0.61
Total	99.20	100.20	98.86	99.36	99.83	99.81	100.30	99.81	98.98	99.19	99.63	99.85	100.80	100.90	99.82	99.74
Mg	24.9	50.8	32.2	29.9	30.9	28.4	27.7	27.9	25.8	22.3	73.1	66.9	53.5	46.2	44.0	26.8
A/CNK	0.83	1.24	0.87	1.04	1.11	1.03	1.09	1.02	1.11	1.11	0.89	0.63	0.71	0.74	0.60	0.85
MALI	-2.0	4.1	3.7	1.6	5.0	6.1	6.8	5.8	5.7	7.4	-5.6	-8.3	-7.0	-7.2	-4.9	-4.5
Rb	5	100	86	49	104	215	107	128	131	267	8	14	6	18	54	50
Sr	287	247	139	240	110	65	82	73	104	26	207	166	142	206	154	283
Ba	130	603	598	792	720	332	706	305	526	77	36	83.2	49	103	126	389
Y	23.1	35.4	33.0	14.2	23.6	59.6	32.8	46.2	21.7	52.0	19.0	17.5	42.3	41.0	46.1	41.3
Zr	609	220	132	215	161	226	127	139	101	64	66	48	127	198	223	209
Nb	11.4	16.4	10.4	7.7	9.3	11.3	6.5	8.8	5.8	6.7	3.0	1.7	7.1	19.5	16.4	14.4
Hf	15.2	5.3	3.7	4.7	4.1	6.4	4.0	4.8	3.1	3.0	1.5	1.5	3.3	4.4	5.9	4.8
Ta	0.6	1.3	0.9	0.4	0.8	1.2	0.9	0.9	1.0	1.8	0.2	0.1	0.4	1.1	1.2	0.8
Th	6.4	12.9	14.8	9.6	14.8	34.9	14.3	17.9	16.1	14.5	0.4	0.7	1.73	2.41	3.4	3.19
La	29.3	30.0	33.6	40.5	30.9	49.1	28.6	22.8	16.2	11.3	4.0	3.6	10.4	17.8	18.2	37.2
Ce	59.2	63.8	68.7	74.5	60.7	105	57.9	49.4	32.8	28.1	10.8	9.6	24.6	40.8	42.7	89.9
Sm	7.00	5.73	5.78	4.07	3.97	8.67	5.54	6.40	2.72	4.23	1.84	2.30	4.43	5.68	7.02	7.75
Eu	1.85	1.19	0.63	1.29	0.61	0.93	0.86	0.44	0.49	0.19	0.80	0.94	1.65	2.00	2.31	2.01
Gd	5.37	5.92	5.79	3.53	3.78	8.14	4.87	6.77	2.89	4.52	2.58	2.73	6.21	7.08	7.28	7.9
Yb	2.39	2.76	2.98	1.13	2.33	5.30	2.95	4.86	2.33	5.66	1.68	1.47	3.59	3.30	4.04	3.46

Atomic ratio mg = 100Mg/(Mg+Fe$_{tot}$.); molar ratio (alumina saturation index) A/CNK = Al_2O_3/(CaO+Na_2O+K_2O); Modified Alkali-Lime Index MALI = Na2O + K2O – CaO (from wt%, Frost et al., 2001)

Based on normative composition (CIPW), they correspond to tonalite, granodiorite, and monzogranite, with small amounts of syenogranite and alkali-feldspar granite.

Except from two samples of metaluminous tonalite (sample I-10) and granite (P160) and one strongly peraluminous granodiorite (P8) with A/CNK = 1.245, all other orthogneisses have weak-to-moderate peraluminous composition with A/CNK 1.01–1.12. Almost all samples correspond to calc-alkaline rocks. The only exception is the tonalite gneiss (I-10) with unusually high Fe_{tot} (10.42 wt % Fe_2O_3) and low K_2O (0.5 wt %).

Some geochemical characteristics of the orthogneisses are shown on a spiderdiagram (Fig. 3) and on two element-element variation diagrams proposed by Pearce et al. (1984) for discrimination of tectonomagmatic position of granitic rocks (Fig. 4). Most orthogneisses have high large-ion lithophile elements (LILE) and Th (Fig. 3) and display high LILE/HFSE elemental ratios. Only the tonalitic gneiss (I-10) has low LILE (K, Rb, and Ba) but significantly higher Zr and Hf contents, which are close to those in "ocean-ridge granites" (ORGs) (Fig. 3). Geochemical features of this sample are generally similar to some dacitic volcanic rock from the Cambrian Volcano-Sedimentary Unit (Lower Cambrian dacite porphyry JR95-G47 from Zarigan Mountain; Ramezani and Tucker, 2003), however, it is more evolved and thus has higher SiO_2 and lower CaO.

Amphibolites

Mafic rocks associated with orthogneisses are generally low in SiO_2 (46.2 to 51.6 wt %), high in total Fe as Fe_2O_3 (8.6 – 13.5 wt %) and have variable contents of MgO (12.2 – 2.5 wt %), Na_2O (1.6 – 2.8 wt %) and K_2O (0.2 – 1.7 wt %). They correspond to subalkaline basalts or gabbros of tholeiitic affinities. The high MgO and mg-value of sample P182 suggests a primitive composition. However, this rock contain gedrite and kyanite and it is rich in Al_2O_3 (18.36 wt %). Samples P182 and I-5 have low TiO_2, P_2O_5 and incompatible elements including rare earth elements (Fig. 5) that could result from accumulation of early magmatic phases (calcic plagioclase, olivine, orthopyroxene). In contrast, sample P74 shows evolved basaltic composition with high total Fe but with a very low mg-number and increased contents of incompatible elements. Geochemical features of amphibolite samples are illustrated in a spiderdiagram (Fig. 5) and selected widely used tectonic discrimination plots (Fig. 6).

They show high Th/Ta ratios and plot both in different fields of within plate, MORB and volcanic arc basalts. Their geotectonic interpretation is discussed later.
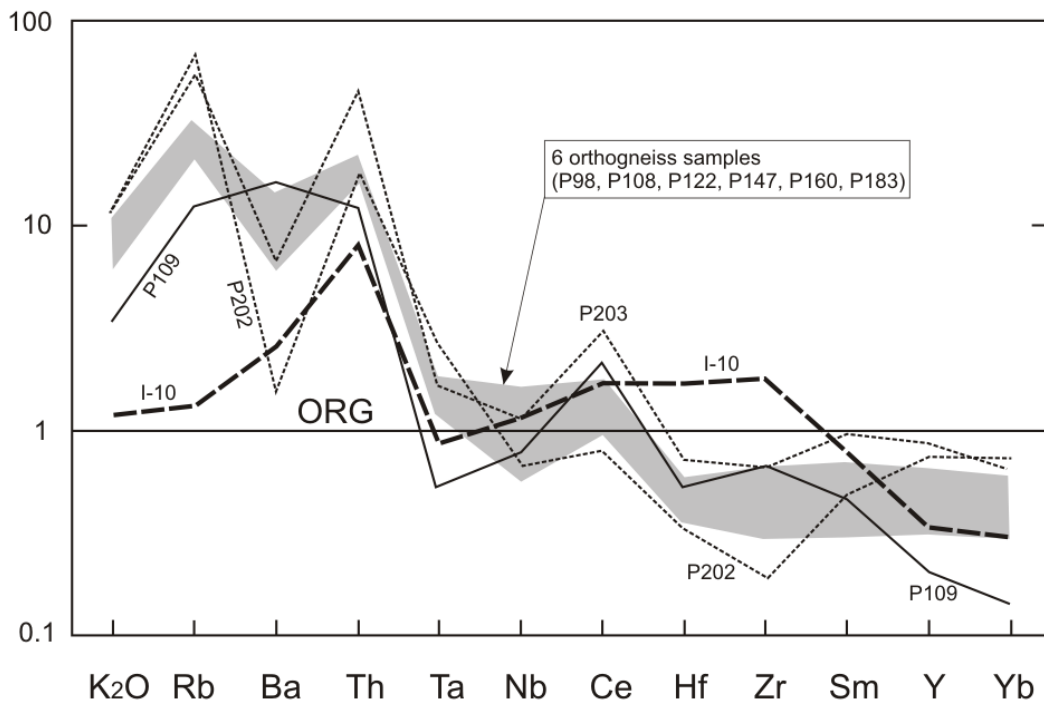
Fig. 3. Spidergram of selected elemental abundances in orthogneisses normalized with the "ocean-ridge granite" (ORG). Normalizing values are from Pearce et al. 1984).
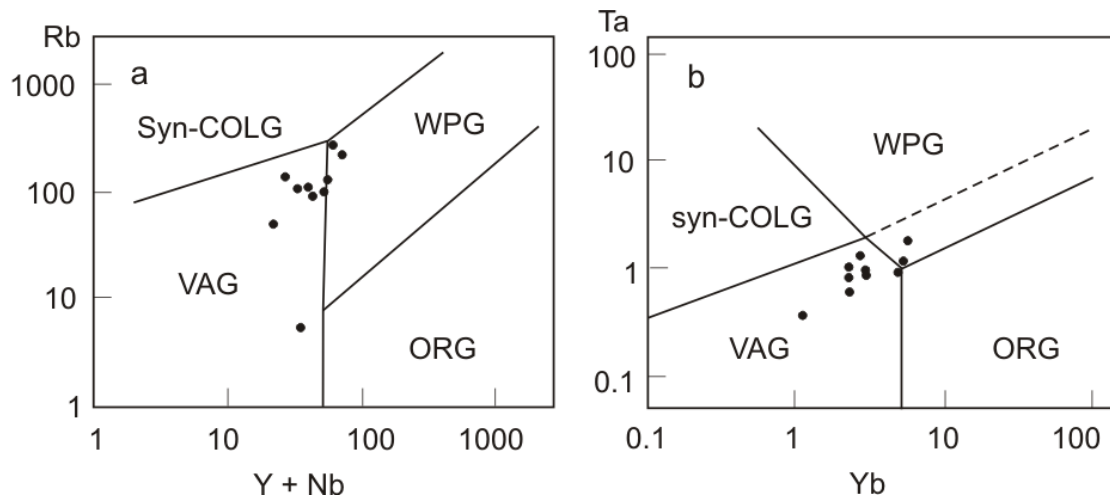
Fig. 4. Position of the studied orthogneisses in selected discrimination diagrams for the tectonic setting of granitoid rocks according to Pearce et al. (1984).
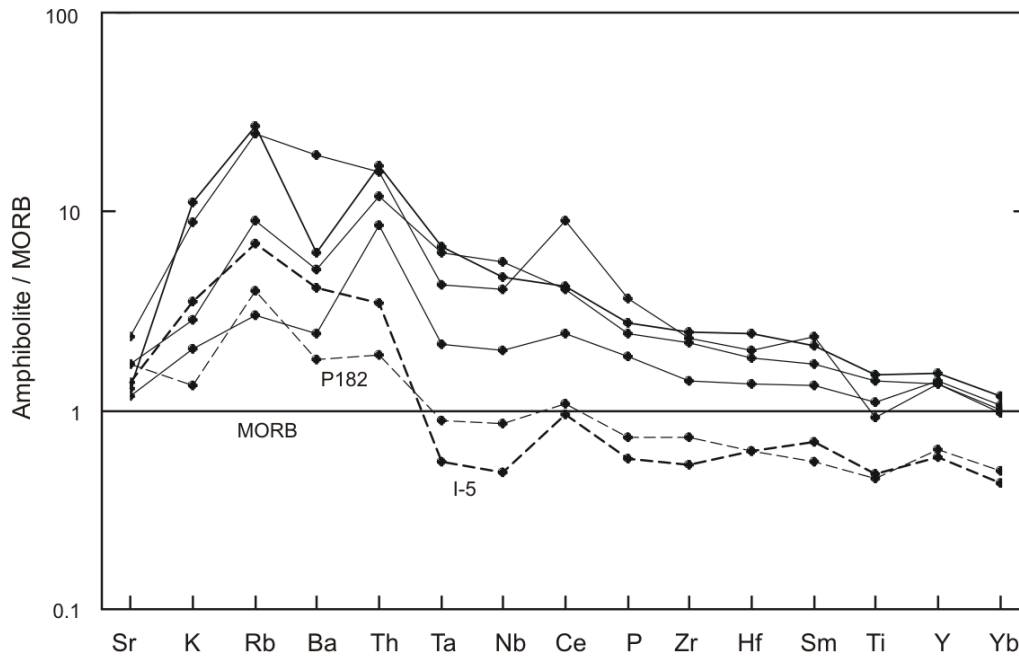
Fig. 5. Spidergram of MORB-normalized abundances of selected trace elements after Pearce (1983) for amphibolites associated with orthogneisses from the Shotur Kuh metamorphic complex.
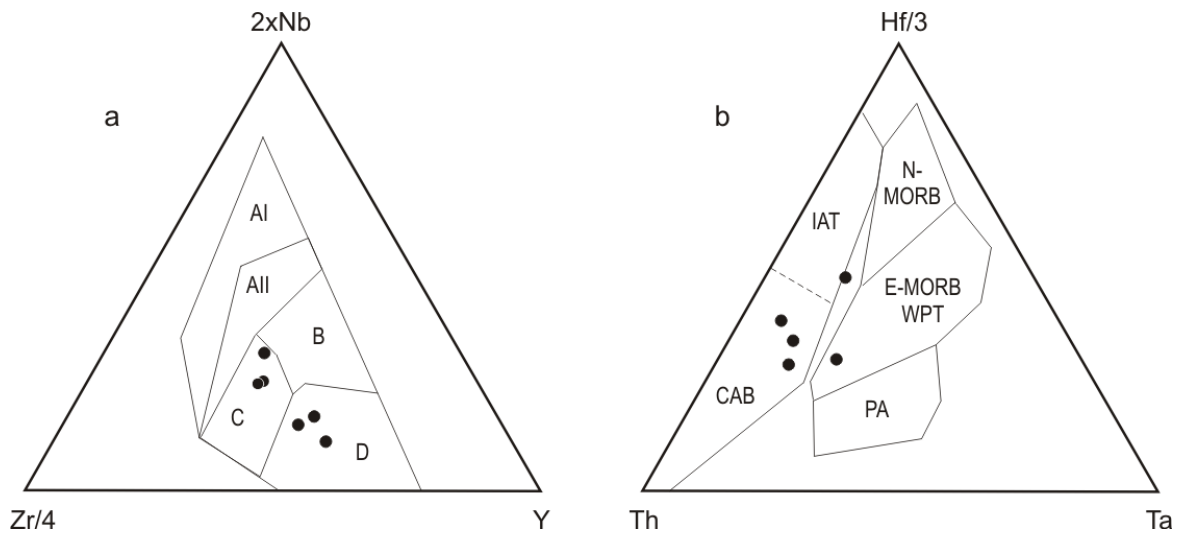
Fig. 6. Selected discrimination plots for the tectonic setting of analyzed amphibolites. a – Zr/4 - 2×Nb - Y (Meschede 1986); b – Th - Hf/3 - Ta (Wood 1980). AI – within-plate alkali basalts; AII – within-plate alkali basalts and within-plate tholeiites; B – E-type MORB; C – within-plate tholeiites and volcanic-arc basalts; D – N-type MORB and volcanic-arc basalts.

48

Table 2. Selected microprobe analyses of minerals used for PT calculations

	Garnet								Biotite			Chlorite	Amphibole			Plagioclase					
Sample	I-12	P95	P99 (c)	P99 (r)	P34	P200	I-10a	I-10b	I-12	P95	P99	P200	I-10a	I-10b	P34	I-12	P95	P99	P34	I-10a	I-10b
Rock		Orthogneiss				Mic	Amphibolite			Orthogneiss		Mic	Amphibole				Orthogneiss			Amphibolite	
SiO_2	37.37	37.97	36.67	37.89	37.54	36.72	38.49	38.19	36.58	37.19	36.70	24.11	41.43	42.39	39.50	63.71	62.87	60.65	62.3	61.81	63.42
TiO_2	0.07	0.04	0.03	0.00	0.11	0.03	0.12	0.00	2.03	2.71	2.43	0.06	0.72	0.73	1.15						
Al_2O_3	21.10	21.38	20.48	20.85	20.97	20.92	20.75	21.38	17.63	19.10	17.79	21.69	14.68	13.50	15.22	22.82	23.05	24.85	23.68	24.59	22.98
Fe_2O_3	0.75	0.00	0.94	0.73	0.00	0.00	2.16	0.03					2.38	0.00		0.01	0.14	0.00	0.04	0.12	0.00
FeO	32.84	32.35	32.82	31.89	28.15	32.15	21.48	26.73	17.87	16.37	18.12	25.79	14.38	21.03	17.62	0.00	0.00	0.00	0.00	0.00	0.00
MnO	2.69	2.25	1.69	1.54	1.54	0.76	3.84	0.47	0.00	0.04	0.00	0.16	0.16	0.00	0.00	0.00	0.00	0.00	0.00	0.00	0.00
MgO	3.84	3.89	3.81	3.86	2.63	2.48	2.10	1.31	11.61	12.03	11.16	15.11	8.65	5.51	8.24	0.00	0.00	0.00	0.00	0.00	0.00
CaO	2.21	2.61	2.58	3.27	8.61	6.36	11.41	12.22	0.02	0.34	0.00	0.06	11.34	11.09	11.30	3.94	4.93	6.44	5.04	6.37	4.22
Na_2O	0.07	0.00	0.01	0.07	0.11	0.01	0.43	0.00	0.11	0.00	0.12	0.03	1.79	1.78	2.26	9.35	8.74	7.86	8.82	7.66	9.31
K_2O	0.00	0.00	0.00	0.00	0.00	0.00	0.00	0.00	9.75	9.10	9.73	0.03	1.32	1.13	0.70	0.11	0.16	0.18	0.00	0.14	0.00
Total	100.90	100.5	99.03	100.1	99.75	99.43	100.8	100.3	95.59	96.88	96.05	87.05	96.85	97.17	96.00	99.93	99.89	99.99	99.86	100.7	99.93
Si	2.942	3.022	2.948	3.032	2.993	2.967	3.023	3.029	2.755	2.726	2.754	2.209	6.254	6.480	6.081	2.811	2.785	2.700	2.763	2.723	2.805
Ti	0.004	0.003	0.002	0.000	0.007	0.002	0.007	0.000	0.115	0.149	0.137	0.004	0.082	0.084	0.133	0.00	0.00	0.000	0.000	0.00	0.000
Al	1.958	2.006	1.940	1.966	1.959	1.993	1.921	1.998	1.565	1.650	1.573	2.342	2.612	2.433	2.762	1.186	1.204	1.304	1.238	1.277	1.195
Fe^{3+}	0.044	0.000	0.057	0.044	0.074		0.128	0.002					0.270	0.059	0.000	0.000	0.005	0.000	0.000	0.004	0.000
Fe^{2+}	2.162	2.009	2.206	2.134	1.792	2.172	1.411	1.774	1.126	1.004	1.137	1.976	1.815	2.688	2.269	0.00	0.00	0.000	0.001	0.00	0.000
Mn	0.179	2.154	0.115	0.105	0.103	0.052	0.255	0.032	0.000	0.002	0.000	0.012	0.020	0.000	0.000	0.00	0.00	0.000	0.000	0.00	0.000
Mg	0.451	0.222	0.457	0.460	0.311	0.551	0.246	0.156	1.303	1.315	1.248	2.064	1.947	1.256	1.892	0.00	0.00	0.000	0.000	0.00	0.000
Ca	0.186	0.461	0.222	0.280	0.731	0.299	0.960	1.039	0.002	0.027	0.000	0.006	1.834	1.816	1.864	0.186	0.234	0.307	0.239	0.301	0.200
Na	0.011	0.152	0.001	0.010	0.017		0.065	0.000	0.016	0.000	0.019	0.000	0.524	0.527	0.674	0.800	0.751	0.679	0.758	0.654	0.798
K	0.000	0.000	0.000	0.000	0.000	0.000	0.000	0.000	0.937	0.851	0.932	0.003	0.254	0.220	0.137	0.006	0.009	0.010	0.000	0.008	0.000
alm	0.726	0.414	0.735	0.714	0.610	0.707	0.491	0.591								An 0.188	0.236	0.308	0.240	0.312	0.200
py	0.151	0.046	0.152	0.154	0.105	0.179	0.086	0.052								Ab 0.806	0.755	0.681	0.760	0.679	0.800
grs	0.063	0.095	0.074	0.094	0.248	0.097	0.334	0.346								Or 0.006	0.009	0.011	0.000	0.008	0.000
sps	0.060	0.444	0.038	0.035	0.035	0.017	0.089	0.011													
X_{Mg}	0.17	0.10	0.172	0.177	0.15	0.20	0.15	0.08	0.54	0.57	0.52	0.51	0.52	0.32							

*-micaschist

2.6. Mineral chemistry

Orthogneisses

Garnet

   Garnet from muscovite-free varieties is mostly rich in Fe and Ca (Alm59-66, Grs16-18, Py15-18, Sps1-7). The amphibole- or epidote-bearing varieties have garnets with relatively low Mg and higher Ca contents (Fig. 7). The most Ca-rich garnet comes from the orthogneiss containing allanite rimmed by epidote (sample I8b). Most garnets show weak but clear prograde zoning characterized by the decrease of Mn and $X_{Fe} = Fe^{2+}/(Mg+Fe^{2+})$ from the core toward the rim. In some cases, garnet may show a retrograde zoning (an increase of Mn and X_{Fe}) at the outermost rim part of the grains (Fig. 8). The variation of Ca differs from sample to sample but mostly shows an increase from core to rim. Garnet in the muscovite-bearing variety, including that with microcrystalline texture, has relatively high Fe (Alm69-73) and Mg (Py14-20) and low Ca (Grs5-9) abundances. Similar to garnet from Ms-free rocks, slight zoning from core to rim can be observed in some grains. The spessartine content ranges between 3and 8 mol %.
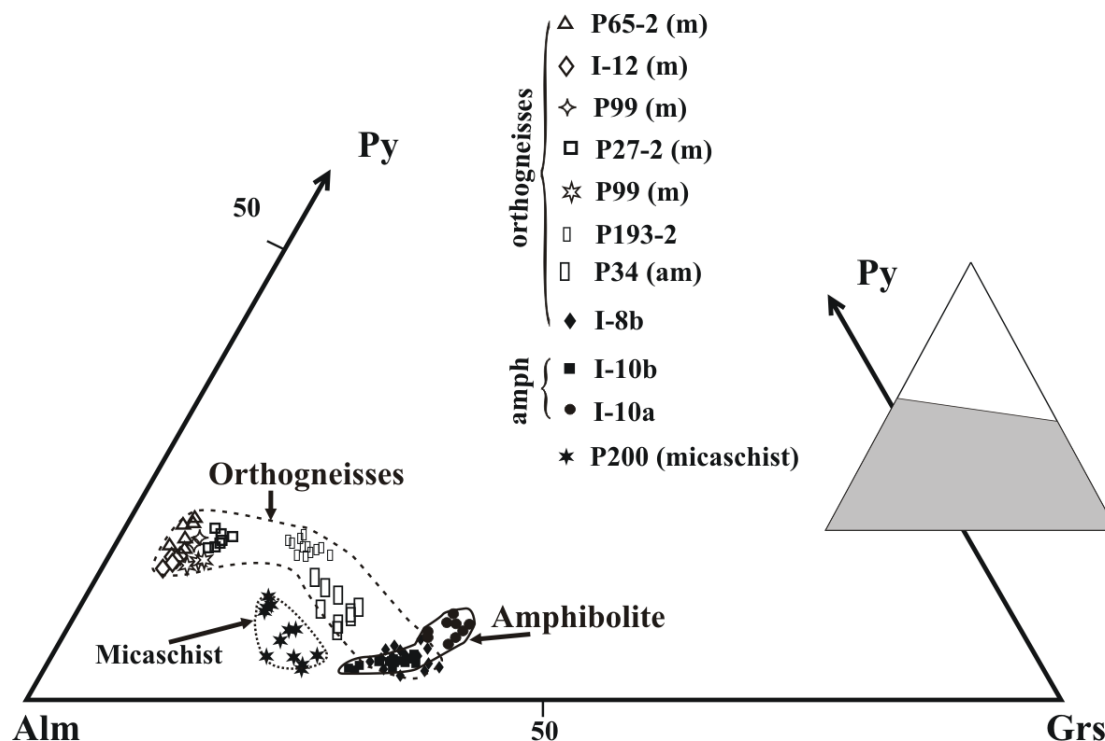
Fig. 7. Composition of garnet from orthogneisses, amphibolites, and micaschists in the Shotur Kuh complex. ´m´ and ´am´ are muscovite- and amphibole-bearing varieties, respectively.

Micas

Biotite from muscovite-free samples has lower $X_{Mg} = 0.26–0.36$ compared with that in the muscovite-bearing variety ($X_{Mg} = 0.51–0.55$), but the two varieties have similar Al (1.6–1.7 atoms per formula unit (a.p.f.u)) and Ti (0.1–0.2 a.p.f.u.) contents. Biotite associated with chlorite, muscovite, and albite in mylonitized orthogneiss has $X_{Mg} = 0.32–0.34$, which is similar to that in the muscovite-free orthogneisses, but with lower Al (1.4 a.p.f.u.) content. Muscovite has low Si (3.0–3.1 a.p.f.u.) with relatively high paragonite content (10–20 mol %), and only the microcrystalline variety of orthogneiss has low (3 mol %) paragonite content.

Plagioclase

Plagioclase in the muscovite-free varieties has a high anorthite content (An_{22-31} mol %), and some higher An contents come from the cores of large plagioclase grains. The coarse-grained, muscovite-free variety has An_{18-24}, while that from the microcrystalline variety has relatively high Ca content (An_{23-30}).

Other minerals

Epidote was analysed in muscovite-free orthogneisses, and it has X_{Al} (Al/(Al + Fe^{3+})) = 0.75–0.86.
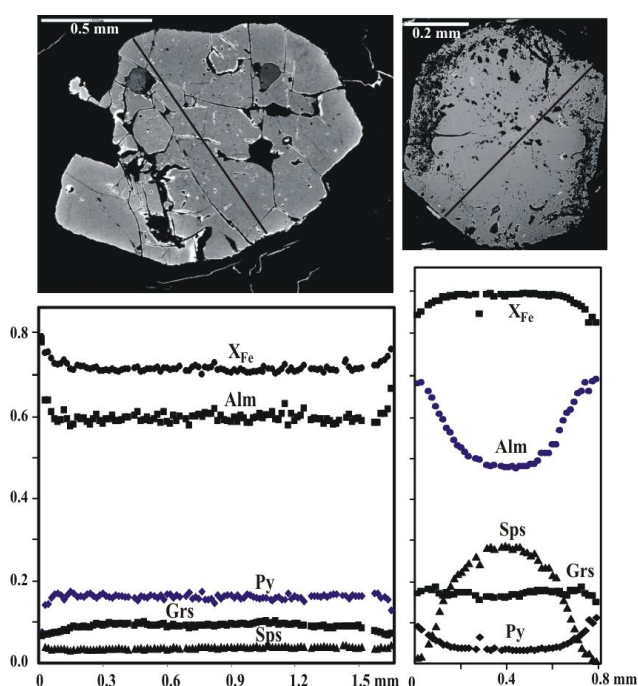
Fig. 8. Compositional profiles of garnet from muscovite-bearing orthogneiss (a, sample P99) and from micaschist (b, sample P200).

Amphibolite

Garnet

Garnet from amphibolite is mostly almandine-grossular solid solution. Its composition varies from sample to sample between Alm_{49-64}, Grs_{31-34}, Py_{3-9} and Sp_{1-9}. Garnet from biotite-amphibole gneiss (sample P34) has higher Mg and lower Ca (Alm_{56-63}, Grs_{21-25}, Py_{10-13}, Sps_{2-9}) and it is mostly homogeneous, although slight zoning characterized by an increase in Mg and Fe and a decrease in Mn and Ca toward the rim can be seen.

Amphiboles

Amphibole in kyanite-free amphibolites is mostly pargasite and ferropargsite, with Si = 6.2– 6.4 and X_{Mg} = 0.53–0.30. Ferropargasite is present in sample I-10a, along with relatively high-Fe garnet (Fig. 7). The A-site of amphibole is occupied by 0.50–0.65 atoms, and Na^{M4} position is in the range of 0.25–0.45 a.p.f.u. Amphibole from biotite-bearing amphibolite has X_{Mg} = 0.38–0.45 with Na^{M4} about 0.2, and Mg-rich tschermakite with X_{Mg} = 0.9 (Na^{M4}= 0.40–0.44 a.p.f.u., Si = 6.3 a.p.f.u.) is associated with gedrite in kyanite-bearing amphibolite (sample P182). The coexisting gedrite, which has X_{Mg} = 0.7, is rich in Al (Al_2O_3 = 17.3 wt.%) and Na (Na_2O = 2.3 wt %), and the A-site occupancy is about 0.4 a.p.f.u. Considering the coupled substitution of tschermakite (Ts): $Al^{VI} + Al^{IV} = Mg^{VI} + Si^{IV}$ and edenite (Ed): $Na_A + Al^{IV} = \square A + Si^{IV}$ (Robinson et al., 1971), the analysed orthoamphibole shows Ed/Ts = 0.33 and has a composition close to ideal gedrite.

The analysed gedrite in the kyanite-bearing amphibolite has Al = 2.9 a.p.f.u. and Na = 0.55 a.p.f.u., which are slightly lower compared with typical literature data (Spear, 1980). Robinson et al. (1971) emphasized the importance of Na in the A site of gedrite and postulated an ideal end-member gedrite composition of $Na_{0.5}(Mg,Fe^{2+})_2$ $(Mg,Fe^{2+})_{3.5}Al_{1.5}Si_6Al_2O_{22}(OH)_2$. This formula represents a combination of the edenite and tschermak's substitutions in a ratio of one to three. The analysed gedrite has lower A-site occupancies and Al^{VI} compared with ideal gedrite, with A = 0.5 and Al^{VI} = 2.0 (Spear, 1980).

Plagioclase

Plagioclase composition in amphibolite is An_{30-31} in sample I-10a and An_{18-20} in sample I-10b. Oligoclase-andesine with 28–30 mole % of An occurs in the biotite-bearing amphibolite, and more Ca-rich andesine with An_{33-35} is present in the kyanite-bearing amphibolite (sample P182).

Micas

Biotite from the kyanite-bearing amphibolite (P182) has $X_{Mg} = 0.7$. The phengite analysed in this sample has a high Si content (Si= 3.36–3.40 a.p.f.u).

Micaschist

Garnet (sample P200) is rich in almandine and shows strong zoning (Fig. 8) with a Mn-rich core ($Alm_{49},Grs_{16},Py_3,Sps_{31}$), a progressive increase in Mg and a decrease in Mn and X_{Fe} ($Alm_{70},Grs_{18},Py_{10},Sps_1$) towards the rim. *Biotite* has X_{Mg} =0.52–0.55, the silica and paragonite contents in muscovite correspond to 3.0 a.p.u. and 11–16 mol %, respectively. *Plagioclase* is pure albite.

2.7. PT conditions of metamorphism

Most of the studied rocks have simple mineral assemblages containing feldspars, biotite ± garnet in orthogneisses and amphibole ± garnet in amphibolite. Plagioclase is not always totally equilibrated and may preserved its igneous composition in the cores of large porphyroclasts. In one case, relics of clinopyroxene were also observed in amphibolite. To constrain the PT conditions of metamorphism, well-foliated and recrystallized samples of orthogneisses and amphibolites were selected. Temperature was calculated using the exchange thermometers of garnet-biotite (Ganguly et al., 1996; Holdaway, 2000), garnet-muscovite (Hynes and Forest, 1988), and amphibole-garnet (Graham and Powell, 1984; Perchuk and Lavrentjeva, 1983; Dale et al., 2000). Because of the lack of Al-silicate in garnet-bearing gneisses, pressure was estimated using the garnet-biotite-plagioclase-quartz barometer of Wu et al. (2006) and the plagioclase-garnet-amphibole-quartz of Kohn and Spear (1990) in combination with the occurrence of kyanite in amphibolite. Possible plausibility of the calculated PT conditions was tested by the pseudosection method, using the Perplex 07 software (Connolly, 2005: version 07) with the internally consistent thermodynamic data set of

Holland & Powell (1998: 2003 upgrade) for muscovite-bearing orthogneiss (P99). The solution models of minerals that were used are plagioclase (Newton et al., 1980) biotite, chlorite, and garnet (Holland and Powell, 2003).

Three orthogneiss samples (I-12, P95 and P99) and one micashist sample (P200) were selected for garnet-biotite thermometry, and the temperatures obtained using three calibrations for the orthogneisses are in the range of 577–645 °C (Table 3) but show a slight increase from the calibration of Ganguly (1996) through Holdaway (2000) to Wu and Cheng (2006). Relatively higher temperatures (615–695 °C) were obtained for the garnet-bearing the amphibolite and amphibole-garnet-bearing orthogneiss using garnet-amphibole thermometry with the calibration of Graham and Powell (1984) and Dale et al. (2000). The calibration of Perchuk and Lavrentjeva (1983) gave about 70 °C lower temperatures for these samples.
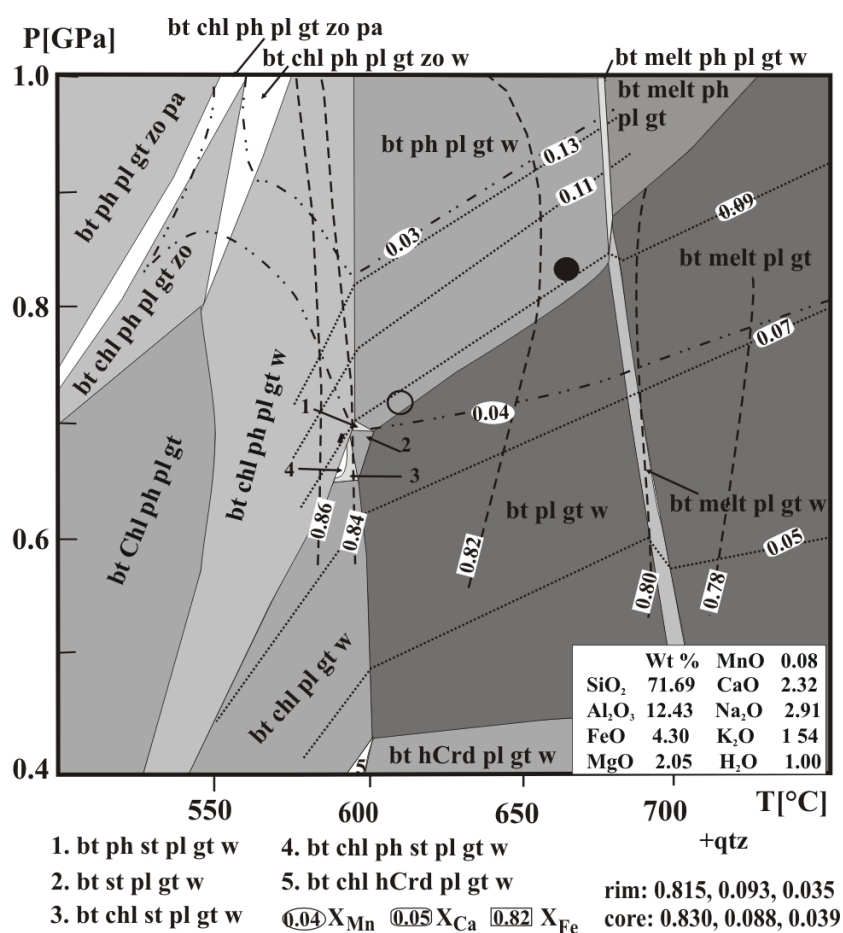
Fig. 9. Pseudosection (MnNCKFMASH system) constrained for garnet-muscovite-bearing gneiss (sample P99) from the Shotur Kuh complex. All fields contain excess quartz. The open and filled circles indicate intersections of isopleths (X_{Fe}, X_{Ca} in squares and X_{Mn} in ellipses) for core and rim compositions of garnet.

54

Pressures obtained by the exchange barometry of Wu and Cheng (2006) for the orthogneisses were in the range of 6.8–7.6 kbar, but the garnet-plagioclase-amphibole-quartz barometry in amphibolite gave higher pressures of 10–12 kbar using the calibration of Kohn and Spear (1990) and Dale et al. (2000). The higher pressure for sample I-12b is due to its more sodic plagioclase composition (An_{18}) compared with the other samples that have plagioclase with An_{29-31}. Similar pressures (10±0.3 kbar at 570 ±46 °C) for garnet-amphbole-plagioclase-equilibria were obtained using average PT (Thermocalc, version 2.7) and the thermodynamic data set of Holland and Powell (1998).

Table 3. Results of exchange thermobaromery for gneisses and amphibolite

----

Gneisses sample	Grt-Bt: T (°C)			Grt-Bt-Pl-Qtz: P (Kbar)
	Ganguly	Holdaway	Wu	Wu
I-12	577 ± 6	608 ± 7	631 ± 5	7.45±0.14
p95	596 ± 42	610 ± 58	629 ± 20	6.82±1.53
p99	602 ± 46	645 ± 75	633 ± 16	7.62±0.71
p200	541 ± 42	544 ± 46	578 ± 37	

Amphibolite sample	Grt-Hbl: T (°C)			Grt-Hbl-Pl-Qtz: P (Kbar)	
	GP	PL	DHP	KS	DHP
I-10a	660±35	530±54	615±21	10.1±0.5	9.8±0.1
I-10b	684±26	558±16	680±14	11.±0.4	11.8±0.5
p34	668±48	601±49	695±24	9.9±0.3	10.2±0.4

Ganguly-Ganguly et al. (1996), Holdaway-Holdaway (2000), Wu-Wu et al. (2006), GP-Graham and Powell (1984), PL-Perchuk and Lavrantjeva (1983), DHP-Dale et al. (2000). KS -Kohn and Spear (1990). Grt-garnet, Bt-biotite, Pl-plagioclase, Hb-Hornblende, Qtz-quartz,

The results of pseudosection with isopleths of X_{Ca}, X_{Fe} and X_{Mn} in garnet for sample P99 indicate 7.2 kbar/610 °C for core compositions and 8.4 kbar/660 °C for rim compositions of garnet (Fig. 9). These PT conditions are confirmed by all three isopleths of X_{Ca}, X_{Fe}, and X_{Mn} that intersect one another in the four variant fields with garnet, muscovite, biotite, and plagioclase. This temperature is about 20 °C higher than the average temperatures obtained by all exchange thermometers, but it is within the error range resulting from analytical measurements and calculations. Pressure conditions obtained from the pseudosection fit well with those derived from the exchange barometry in orthogneisses. Such pressures are confirmed also by the presence of kyanite in the Al-rich metabasite (sample P182), which, according to data from the literaure (e.g., Cooper, 1980; Ward, 1984; Spear, 1982), indicates a pressure greater than 6 kbar. For amphibolite-facies temperatures, Selverstone et al. (1984)

suggested that kyanite reflects pressures higher than those appropriate for the stability of the common amphibolite assemblage. Experimental studies corroborate this idea, and it was predicted (Schreyer and Seifert, 1969) that Ged + Ky should be stabilized at pressures of about 10 kbar and that they are a precursor of Tlc + Ky "whiteschists" (Schreyer, 1973).

The phyllitic-micaschist (sample P200) gave temperatures of 541–578 °C (Table 3), which are 50–60 °C lower than those in the orthogneisses. Pressure conditions were not estimated, but they seem to be close to that in the orthogneisses.

2.8. Geochronology

The age of igneous crystallization of the Shotur Kuh orthogneiss-amphibolite complex was obtained by laser ablation ICPMS U-Pb dating of zircon extracted from an orthogneiss sample of granodiorite composition (P160). The data constrain the crystallization age of the granodiorite to be 547 ± 7 Ma (2 sigma Concordia age; Fig. 10, Table 4). A similar age of 566 ± 31 Ma (n = 8, MSWD=1.3) has been recently obtained for the Shotur Kuh Complex orthogneisses using ion microprobe and thermal-ionization zircon dating (Hassanzadeh et al., 2008).
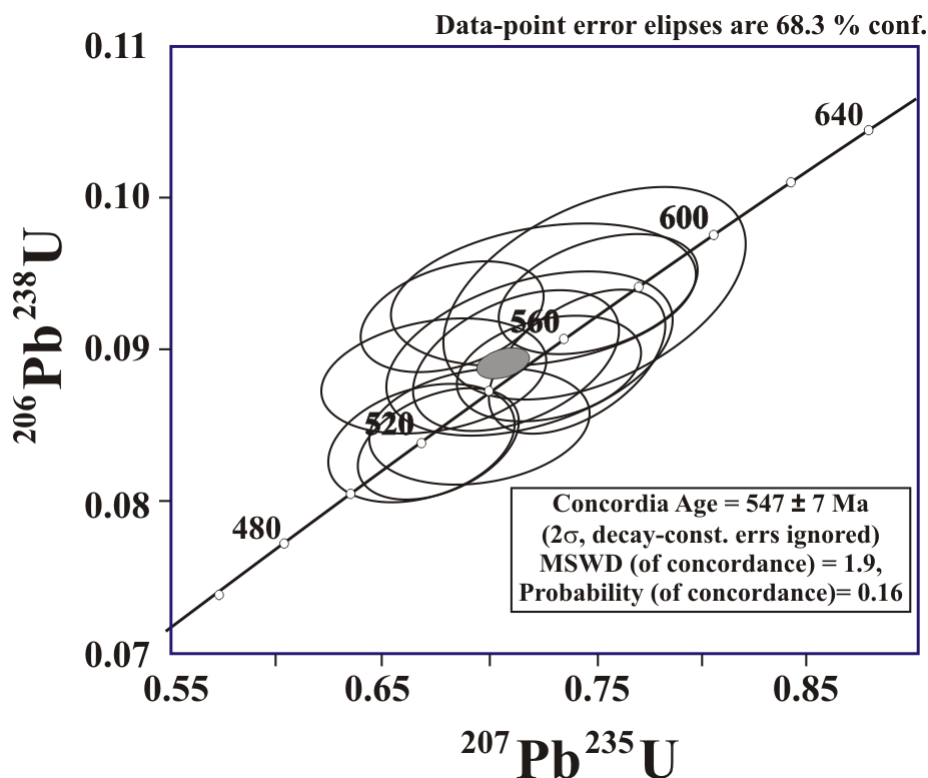
Fig. 10. Pb concordia diagram for zircon from orthogneiss (sample 160) in Shotur Kuh complex.

Both ages are consistent with the U-Pb zircon ages of granitic and volcanic rocks reported from several localities in Central Iran, including Saghand area (Ramezani and Tucker, 2003) and Sanandaj– Sirjan region (Hassanzadeh et al., 2008).

Ar-Ar age dating was performed on metamorphic muscovite from a metagranite sample showing well–preserved, equilibrated fabric in amphibolite facies conditions. However, a distinct low-temperature alteration is clearly visible and caused severe alteration of biotite and also minor alteration of feldspars. The age pattern of the muscovite from this sample corresponds well with the crystallization sequence observed in thin section. It shows a distinct saddle-shaped pattern that points to a moderate age rejuvenation due to diffusional loss of radiogenic Ar during low-temperature reheating (Fig. 11). A single sample may not be sufficient to make far-reaching conclusions, but from our experience we conclude that the mica flakes contain age domains that are older than 166 Ma (probably about 170–180 Ma), which reflects the original cooling after metamorphism. A Lower Jurassic age of 171.8 ± 2.7 was also obtained by K-Ar dating of muscovite (sample I-13), although biotite from the same sample gave 208 Ma (Table 5). A younger age of 141 Ma was obtained for biotite in sample I-12.
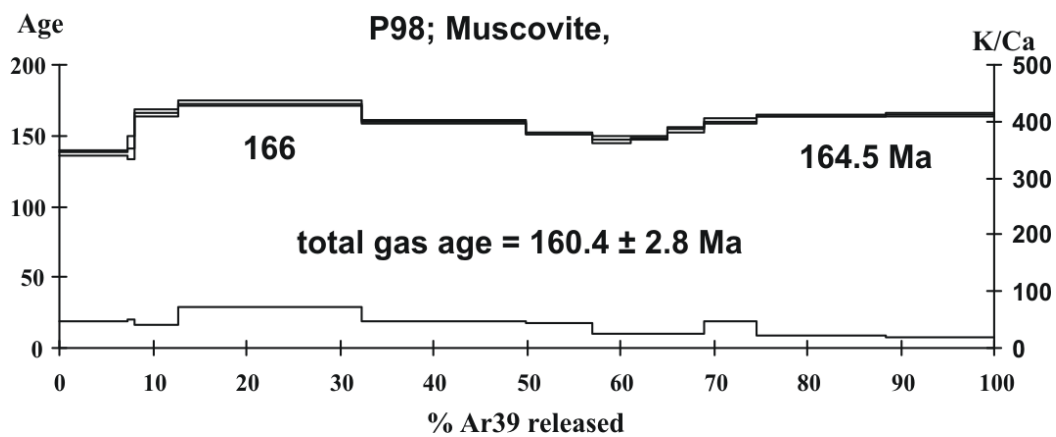
Fig. 11. Ar/Ar ages of 166 Ma for muscovite in micaschist (sample P98) from the Shotur Kuh complex (Central Iran).

Table 4. U-Pb and Pb-Pb Laser Ablation ICPMS data for zircons from sample P160

Analysis no.	Isotopic ratios						Ages Ma					
	$^{207}Pb/^{235}U$	± 1 sigma	$^{206}Pb/^{238}U$	± 1 sigma	$^{207}Pb/^{206}Pb$	± 1 sigma	$^{207}Pb/^{235}U$	± 1 sigma	$^{206}Pb/^{238}U$	± 1 sigma	$^{207}Pb/^{206}Pb$	± 1 sigma
1	0.6685	0.0294	0.0839	0.0026	0.0578	0.0007	519.8	22.8	519.1	16.0	522.6	25.8
2	0.7143	0.0315	0.0889	0.0032	0.0583	0.0007	547.3	24.1	549.0	19.5	540.2	27.8
3	0.6824	0.0284	0.0920	0.0024	0.0538	0.0012	528.2	22.0	567.6	14.8	361.6	49.4
4	0.6750	0.0243	0.0838	0.0025	0.0584	0.0006	523.8	18.8	518.7	15.4	545.9	21.7
5	0.7023	0.0181	0.0904	0.0015	0.0564	0.0005	540.1	13.9	557.6	9.5	467.1	20.4
6	0.6947	0.0343	0.0848	0.0027	0.0594	0.0010	535.6	26.5	524.9	16.5	581.5	36.3
7	0.7496	0.0460	0.0936	0.0046	0.0581	0.0009	568.0	34.9	576.9	28.2	532.5	32.4
8	0.6739	0.0348	0.0883	0.0025	0.0554	0.0015	523.1	27.0	545.3	15.3	427.4	61.9
9	0.7252	0.0474	0.0935	0.0030	0.0562	0.0009	553.7	36.2	576.4	18.7	461.5	37.3
10	0.7203	0.0445	0.0897	0.0035	0.0582	0.0012	550.9	34.0	553.9	21.7	538.2	43.3
11	0.7500	0.0297	0.0936	0.0026	0.0581	0.0009	568.2	22.5	576.5	16.2	535.3	34.8
12	0.7280	0.0285	0.0887	0.0022	0.0596	0.0009	555.4	21.8	547.6	13.7	587.5	33.4
13	0.7397	0.0283	0.0892	0.0031	0.0601	0.0006	562.2	21.5	550.9	18.9	608.2	22.3

Table 5. Results of K-Ar dating from muscovite and biotite in the Shotur Kuh metamorphic complex

Samples	Rock type	Mineral	K_2O (wt.%)	% $\underline{rad.\ ^{40}Ar}$ tot. ^{40}Ar	$rad.^{40}Ar$ (10^{-11} mol/g)	Age (± 2σ) in Ma
I- 12	orthogneiss	biotite	8.446	93.3	178.6	141.2 ± 2.2
I- 13	orthogneiss	biotite	8.383	90.3	266.9	208.7 ± 3.2
I- 13	orthogneiss	muscovite	8.454	96.4	219.4	171.8 ± 2.7

2.9. Discussion

Evidence for a Pre-Cambrian to Cambrian magmatic arc

The new geochronological data for crystallization ages of granitoid protoliths of orthogneisses from the SKMC are quite comparable with the granitoid ages reported by Ramezani and Tucker (2003) from the Saghand area in East-Central Iran who interpreted the igneous rocks as a magmatic arc of Late Neoproterozoic to Early Cambrian age (Fig. 12). This interpretation was recently confirmed by geochronological data from granites and orthogneisses from central Iran (Hassanzadeh et al., 2008). These ages, which range from Late Neoproterozoic to Early Cambrian, match the mostly juvenile Arabian–Nubian shield and Peri-Gondwanan terranes that have formed after the main phase of Pan-African Orogeny.
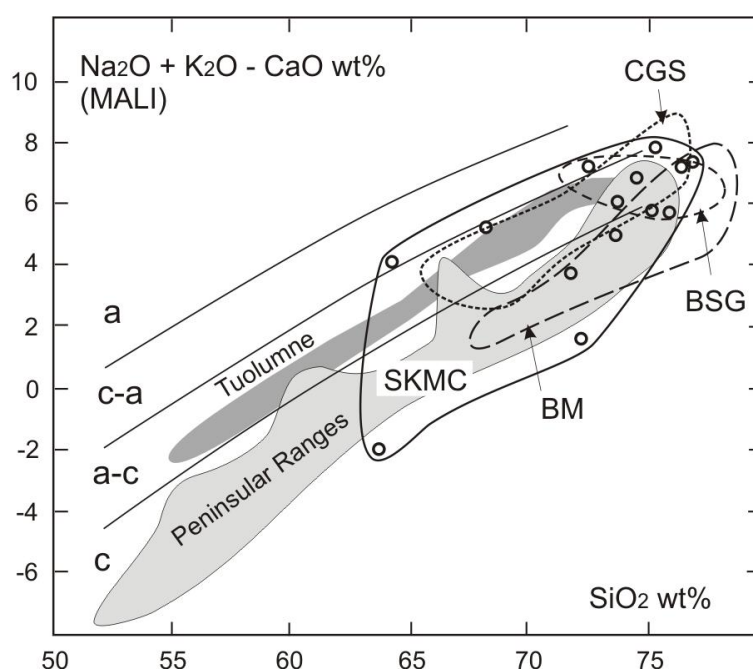
Fig.12. The "Modified Alkali-Lime Index" (MALI) vs SiO2 diagram after Frost et al. (2008) for Shotur Kuh Metamorphic Complex orthogneisses (field labelled SKMC, circles represent individual analyses). Other fields represent: BSG - Boneh Shurow granitic gneisses from Central Iran (Ramezani and Tucker, 2003), CGS - Cambrian Granitic Complex from Central Iran (Ramezani and Tucker, 2003), BM- granitoids of the Bitlis Massif in SE Turkey (Ustaömer et al., 2008). For comparison, variation fields for typical magmatic arc intrusive complexes of the Peninsular Ranges and Tuolomne Batholith are displayed (from Foster et al., 2008). Terminology for individual igneous suites: a – alkalic, a-c – alkali-calcic, c-a – calc-alkalic, c – calcic.

Consistent with paleogeographic reconstructions for the Late Neoproterozoic (Powell, 1980; Laver and Scotes, 1987; De Wit et al., 1988; Unrug, 1997) the arc was formed by the closure of the Chapedony Ocean (Proto- Tethys, Fig. 13) (Ramezani and

Tucker, 2003). Following the Pan-African Orogeny and the consolidation of the basement, the Precambrian craton of Iran, Pakistan, central Afghanistan, southeastern Turkey and Arabia became a relatively stable continental platform with epicontinental shelf deposits (mainly clastics) and was characterized by a lack of major magmatism or folding (Nadimi, 2007).
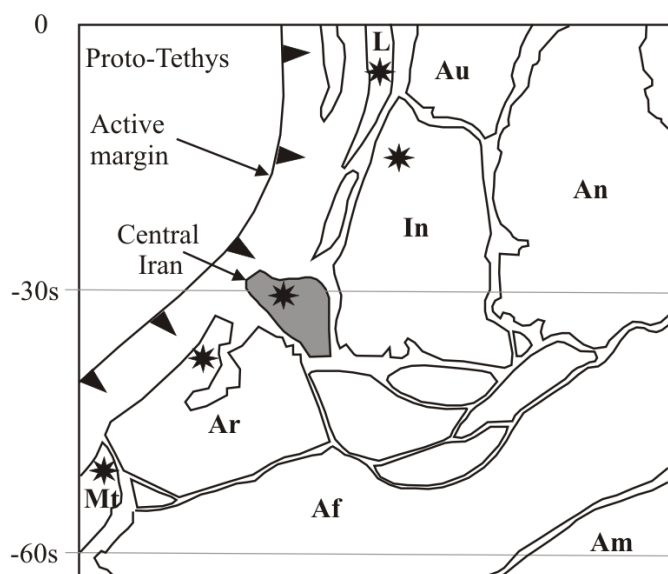
Fig.13. Schematic Gondwanaland reconstruction in Early Cambrian based on Molleweide projection of tectonic plates at 540 Ma by the PLATES Project (1999), with modifications by Remezani and Tucker (2003). Precambrian cratons are: Af- African, Am- South American, An- Antarctic, Au-Australian and In- Indian plates, Ch-South China, L-Lhasa and MT- Menderes-Tauruns Blocks. Stars refer to Peri-Gonwana arc plutons.

Despite large compositional variability, the overall geochemistry of the orthogneiss varieties from the Shotur Kuh complex is compatible with an origin of their granitoid protoliths within a magmatic arc. Based on the trace-element discrimination diagrams (Pearce et al. 1984), the majority of orthogneisses plot within the "volcanic arc granite" field (Fig. 4). We suggest that the arc was situated at a continental margin where melting and recycling of abundant older continental material could play a significant role. Some orthogneiss analyses are very comparable with rocks described by Ramezani and Tucker (2003) as being members of the Late Neoproterozoic to Early Cambrian arc igneous assemblage from the Saghand area (see Fig. 1 and Table 6)—namely, with the "Cambrian Granitoid Suite" (CGS) and with the acidic orthogneiss "Boneh-Shurow Granitic Gneiss" (BSG) dated as Late Neoproterozoic. When comparing these orthogneisses with Late Neoproterozoic to Early Cambrian igneous and metaigneous rocks in the nearby regions they show close

similarity to continental arc-related granitoids and metagranitoids in SE Turkey (Ustaömer et al., 2009). Fig. 12 displays geochemical signatures of the Shotur Kuh orthogneisses in the Frost et al. (2001) diagram and compare them with some plutonic rocks from other parts of the peri-Gondwanan and also much younger arc related plutonic complexes from North America. Despite of their rather broad scatter, the Shotur-Kuh orthogneisses fit well with arc-related calcic and calc-alkalic suites and together with other granitoid or metagranitoid complexes from the peri-Gondwanan arc they correspond to silica-rich, evolved rocks. Although some geochemical features, namely the high total Fe and Zr contents, of the tonalitic orthogneiss (sample I-10) appear to be far from typical arc assemblages they are broadly similar to some subvolcanic members of the Cambrian Volcano- Sedimentary Unit of Saghand, which has been interpreted as arc-related (Ramezani and Tucker, 2003).

Table 6 Comparison of selected geochemical parameters for the studied orthogneisses with other Late Neoproterozoic to Cambrian granitoids in Central Iran and SE Turkey

	Orthogneisses, Shotur Kuh Metam. Complex (this study)	Cambrian Granitoid Suite (Ramezani & Tucker 2003)	Boneh-Shurow Granitic Gneisses (Ramezani & Tucker 2003)	Bitlis Massif, SE Turkey (Ustaömer et al. 2008)
SiO_2	(63.72) 64.3 - 75.9	65.9 - 76.3	71.7 – 77.7	68.0-78.3
K_2O	(0.47) 1.33 - 4.61	2.86 - 4.92	2.7 – 4.8	0.2 – 4.6
K_2O/Na_2O	(0.146) 0.39 - 1.6	0,8 - 1,39	0.6 – 1.3	0.02 – 1.2
MALI	(-2.0) 1.6 – 6.8	2.9 – 8.7	5.8 – 7.2	1.6 – 7.8
A/CNK	(0.833) 0.866 -1.24	0.923 - 1.004	0.94 – 0.99	0.82 – 1.09
Th/Ta	9.9 - 29.3	17.5 - 44.4	11 - 22	-
Eu/Eu*	0.20 - 1.02	0.38 - 0.59	0.30 – 0.68	-

Values in parentheses represent the orthogneiss I-10 that is significantly different from other rock analyses representing the Shotur Kuh metamorphic complex. MALI is "Modified Alkali-Lime Index" $Na_2O + K_2O – CaO$ (Frost and Frost, 2001); A/CNK is molar ratio $Al_2O_3/(CaO + Na_2O + K_2O)$.

The tectonic positions of mafic rocks (amphibolites) spatially associated with orthogneisses, are difficult to interpret, mainly because of metamorphism and deformation, which could have modified their original geological relationships. Some small amphibolite bodies could represent original mafic enclaves. However, the majority of mafic bodies may represent metamorphosed primary dykes.

The geochemical indications for the original tectonic setting of mafic rocks are rather ambiguous. In various discrimination diagrams, amphibolites plot in the fields of "within-plate basalts"and MORBs, and also of volcanic arc basalts. Because of the relatively high Th contents, most samples are shifted toward the "Calc-alkaline basalt" field or plot within this field (Fig. 6). The increased Th/Ta ratios (Fig. 5) may

indicate that the original basaltic magmas were derived from a mantle source affected by subduction-related processes.

Some geochemical features of amphibolites are consistent with the origin of their protolith magmas at a destructive plate margin – i.e., in a magmatic arc (increased LILE/HFSE and Th/Ta element ratios, Fig. 5). However, the "subduction fingerprint" is rather weak and could also be explained in terms of partial melting of the sub-continental lithospheric mantle (with the long term "subduction memory") and/or contamination of mafic magmas by continental crust (including protoliths of orthogneisses). Except for the two most mafic samples that are probably affected by the accumulation of early mineral phases, the rocks display relatively high TiO_2 content, which is in contrast to the composition of typical volcanic arc magmas. Mafic to intermediate rocks with strong, typical fingerprints of subduction-related magmas are absent, and therefore the arc igneous assemblage is incomplete and the outcropping rock complexes involving metamorphosed mafic dykes may represent an extensional setting of the continental back-arc rather than a true arc near the volcanic front. However, even such a setting can be supposed to be a part of a much greater Late Neoproterozoic-Early Paleozoic orogenic system that was active along the Proto-Tethyan margin of the Gondwanaland supercontinent, extending at least from its Arabian margin to the Himalayan margin of the Indian subcontinent (Ramezani and Tucker, 2003).

Metamorphic evolution

Mineral assemblages observed in the studied rocks indicate a medium-pressure, barrovian-type metamorphism for which a maximum pressure of c. 8 kbar and a temperature of about 650°C were obtained. This metamorphism produced garnet, biotite, plagioclase, quartz, and muscovite in orthogneisses, and garnet, amphibole, plagioclase, and quartz in amphibolite. The overlaying Pre-middle Triassic sedimentary sequences were also affected by this metamorphism, but they show a lower temperature (550 °C). Garnet, both in metaigneous and metapelitic rocks, indicates prograde zoning from cores to rims of grains. This zoning is strong in metapelites and weak in metaigneous rocks, where it shows additional modification at rims (retrograde zoning) that probably occurred during cooling. The weak prograde zoning in metaigneous rocks could be the result of either higher temperatures or longer relaxation times at high temperature. Lithological similarity but different PT

conditions between Pre-middle Triassic pelitic rocks and garnet micaschists suggest either tectonic juxtaposition of single unit with differing metamorphic grade or the micaschists belong to an older basement unit, which reached PT conditions close or similar to the orthogneisses.

The limitation of the Middle- to Lower-Jurassic ages of 165 Ma for the amphibolite facies metamorphism, obtained by Ar-Ar data on muscovite, is supported by the presence of the Upper Triassic-Lower Jurassic Shemshak formation and by the Middle-Jurassic pasammopelitic rocks with conglomerates containing pebbles of the basement orthogneisses and amphibolite. The stratigraphically well-defined Shemshak formation in Central Iran (e.g., Assereto, 1966; Stampfli, 1978) shows lower greenschist facies metamorphism with fabrics comparable to those in the underlying limestone-dolomite formation (Rahmati-Ilkhchi, 2008). Because the Middle- Jurassic sediments with conglomerates show only very-low-grade metamorphic conditions, the greenschist facies overprint (fine-grained white mica, chlorite with albite, epidote, and, locally, also brown-green biotite replacing garnet or plagioclase) in the basement rocks could be related to retrogression during exhumation.

The results of our petrological and geochronological study agree well with the geodynamic scenario for closure of the Neotethyan basin in the southwestern part of Iran (e.g., Stöcklin, 1968; Barberian and King, 1981; Sengor, 1991; Glennie, 2000; Sheikholeslami et al., 2008; Ghasemi and Talbot, 2006). This basin was formed by continental rifting, separating the Iranian and the Arabian plates (Fig. 14). Formation of a magmatic arc with an accretionary prism during the Early Cimmerian Orogeny (Sheikholeslami et al., 2008; Paul et al., 2003) is coeval with the Middle Jurassic cooling age of white mica from the Shotur Kuh Complex, which defines the collisional processes and metamorphism of the basement rocks of the Central Iran Block.

The significance of the Shotur Kuh metamorphic complex for the geological history of the Great Kavir Block

The investigated metaigneous rocks from the Shotur Kuh complex show arc-related signatures similar to those described by Ramezani and Trucker (2003) and confirm a uniform geotectonic position for the Central Iran micro-continent during the Late Neoproterozoic, including the GKB. This interpretation is also supported by

comparative stratigraphy of Paleozoic to Mesozoic sedimentary sequences among different crustal blocks (Stöcklin, 1968; Takin, 1972; Crawford, 1977; Berberian et al., 1981).
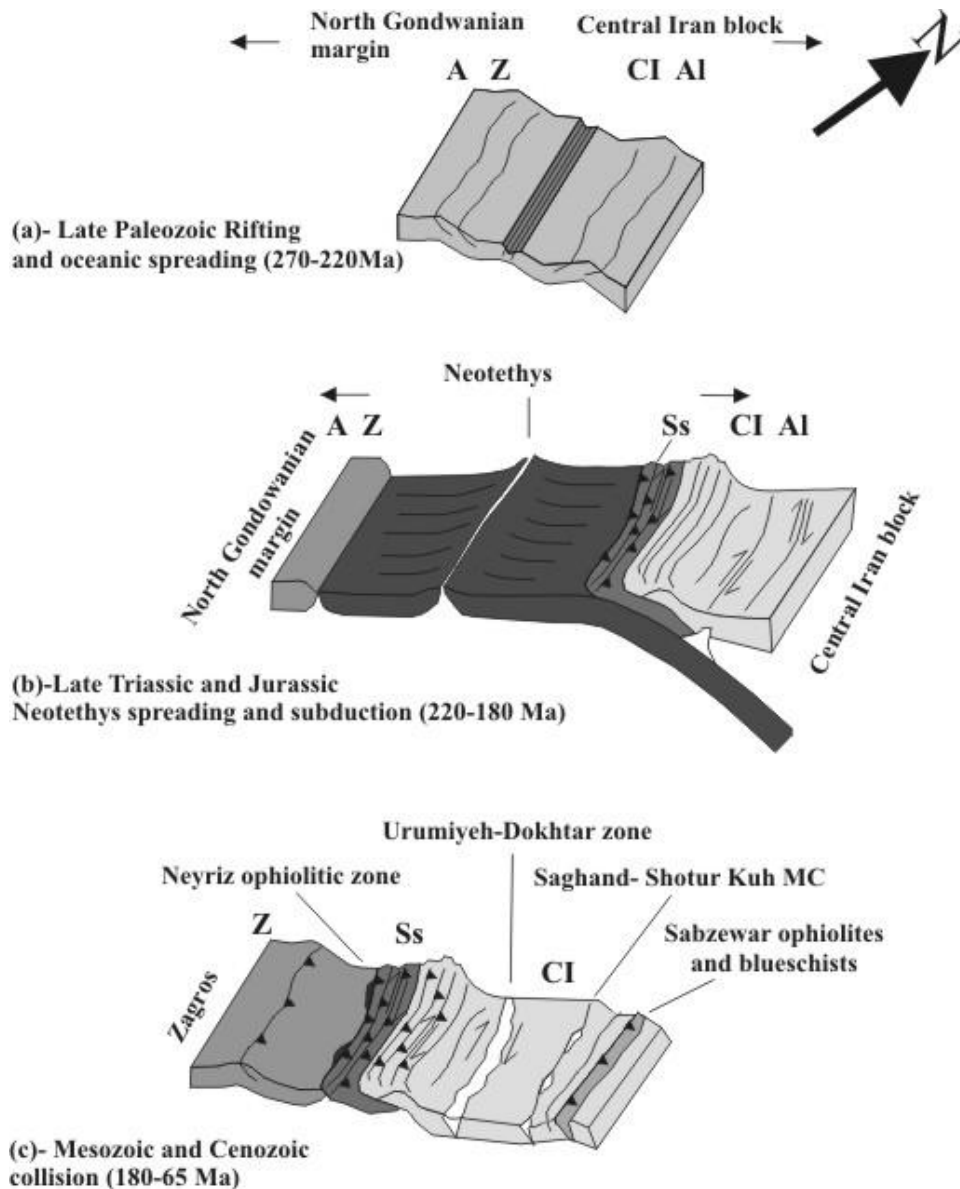
Fig.14. Geodynamic reconstruction of southwest margin of the central Iran and north Gondwanian margin from Late Paleozoic to Cenozoic (modified from Berberian and King, 1981, and Sheikholeslami et al., 2008). a) Development of rift-type basin from Permian. (b) Subduction of the Neotethys oceanic basin in Late Triassic (Early Cimmerian phase) and formation of an accretionary prism and magmatic arc (granite/granodiorite of Chah Dozdan). (d) Collision and generation of an orogenic prism with metamorphism and exhumation of the basement units (Saghand-Shotur Kuh metamorphic complexes) and development of volcanic arc of Urumieh-Dokhtar zone. A-Arabian plate, Z-Zagros, Ss-Sanandaj-Sirjan, CI-Central Iran and Al-Albroz

Most basement rocks in Central Iran are exposed along tectonic zones separating individual blocks. In some cases, these zones are followed by Paleozoic to Cenozoic ophiolites with or without blueschists (Fotoohi Rad et al., 2005; Bagheri and Stampfli, 2008), which suggests large-scale tectonic activity with rifting and subduction. The Sabzevar zone with ophiolites and blueschists is the best example of a back-arc basin that was opened during Cretaceous north from the Neothethys ocean (Bagheri and Stampfli, 2008). The SKMC is exceptional, since it occurs in the central part of the GKB. However, the positions of the SKMC and some mafic and ultramafic rocks near Kuh Siah Poshteh (100 km from the Shotur Kuh complex) along the E-W- trending Torud fault zone may suggest that the Torud fault zone was also active prior to Tertiary volcanism. Considering the N-S compression of the Shotur Kuh complex with south-vergent isoclinal fold axes (Rahmati- Ilkhchi et al., 2008), the Torud tectonic zone may represent a large-scale thrust zone that was responsible for formation (?) and exhumation of the amphibolite facies metamorphic rocks during the Jurassic. The rapid increase in the degree of metamorphism from top to bottom in the Pre-middle Triassic rocks in contact with orthogneiss is either due to tectonic reduction of relatively thick sequences or the result of heating of partially exhumed orthogneiss-amphibolite rocks to the upper-crustal level. To confirm or reject the hypothesis of large thrust and underplate tectonics along this zone, more detailed structural analyses and dating of mafic and ultramafic rocks is needed.

2.10. Conclusions

Geochemical analyses and U-Pb zircon age data from orthogneisses in the Shotur Kuh metamorphic complex indicate that these rocks are derived from granitoid protoliths (granite, granodiorite, and tonalite) formed during Late Neoproterozoic arc-related magmatism. This magmatism, which is known also from other zones and blocks in Central Iran, confirms that the GKB, along with the rest of the blocks of the Central Iran micro-continent, were part of the Neoproterozoic- Early Paleozoic orogenic system that was active along the Proto-Tethyan margin of the Gondwanaland supercontinent. In the Shotur Kuh complex, these rocks were affected by barrovian-type metamorphism that reached amphibolite facies conditions in the deeper part of the exposed basement with orthogneisses and amphibolites, and lower amphibolite facies in the sedimentary cover. Both igneous and sedimentary rocks show evidence

of prograde metamorphism with subsequent cooling. The results of petrological studies with structural data about N-S compression and north-dipping structures suggest that the Lower- to Middle-Jurassic metamorphism and exhumation of the Shotur Kuh complex occurred under conditions of south vergent thrust tectonics along the E-W zone. The latter was probably related to the closure of the Neotethyan basin and subsequent collision during the Early Cimmerian Orogeny.

2.11. References

Assereto R (1966) The Jurassic Shemshak Formation in central Elburz (Iran). Riv Ital Paleont Stratigr 72:1133–1182

Bagheri S, Stampfli GM (2008) The Anarak, Jandaq and Posht-e-Badam metamorphic complexes in central Iran: New geological data, relationships and tectonic implications.Tectonophysics 451:123–155

Berberian F, Berberian M (1981) Tectono-plutonic episodes in Iran. In: Gupta HK and DelanyFM (eds) Zagros-Hindu Kush-Himalaya Geodynamic Evolution. American Geophysical Union Geodynamics Series 3 pp 5-32

Berberian M, King GCP (1981) Towards a Paleogeography and Tectonic Evolution of Iran. CanJ Earth Sci 8:210–265

Connolly JAD (2005) Computation of phase equilibria by linear programming: a tool for geodynamic modeling and its application to subduction zone decarbonation. Earth Planet Sci Lett 236:524–541

Cooper AF (1980) Retrograde alteration of chromian kyanite in metachert and amphibolite whiteschists from the southern Alps, New Zealand, with implications for uplifit on the Alpine fault. Contrib Mineral Petrol 75:153-164

Crawford AR (1977) A summary of isotopic age data for Iran, Pakistan and India: Mémoire Societé Géologique de France 8:251–260

Dale J, Holland T, Powell R (2000) Hornblende-garnet-plagioclase thermobarometry; a natural assemblage calibration of the thermodynamics of hornblende. Contrib Mineral Petrol 140:353-362

De Wit M, Jeffery M, Bergh H, Nicolaysen L (1988) Geological map of sectors of Gondwana reconstructed to their disposition 150 Ma, scale1:10,000,000: Tulsa, Oklahoma, American Association of Petroleum Geologists

Fotoohi Rad GR, Droop GTR, Amini S, Moazzen M (2005) Eclogites and blueschists of the Sistan Suture Zone, eastern Iran: A comparison of P–T histories from a subduction mélange. Lithos 84:1-24

Frost BR, Arculus RJ, Barnes CG, Collins WJ, Ellis DJ, Frost CD (2001) A geochemical classification of granitic rocks. J Petrol 42:2033-2048

Frost BR, Frost CD (2008) A geochemical classification for feldspathic igneous rocks. J Petrol 49:1955-1969

Ganguly J, Cheng W, Tirone M (1996) Thermodynamics of alumosilicate garnet solid solution: new experimental data, an optimized model, and thermodynamic application. Contrib Mineral Petrol 126:137–151

Ghasemi M, Talbot CJ (2006) A new tectonic scenario for the Sanandaj–Sirjan zone (Iran), Journal of Asian Earth Sciences, 26: 683–693.

Glennie KW (2000) Cretaceous tectonic evolution of Arabia eastern plate margin: a tale of two oceans, in Middle East models of Jurassic/Cretaceous carbonate systems. SEPM Spec Publ 69: pp 9–20

Graham CM, Powell R (1984) A garnet-hornblende geothermometer: calibration, testing and application to the Pelona Schist, Southern California. J Metam Geol 2:13-31

Hassanzadeh J, Stockli DF, Horton BK, Axen GJ, Stockli LD, Grove M, Schmitt AK, Walker JD (2008) U-Pb zircon geochronology of late Neoproterozoic–Early Cambrian granitoids in Iran: Implications for paleogeography, magmatism, and exhumation history of Iranian 594 basement. Tectonophysics 451:71–96

Holland TJB, Powell R (1998) An internally consistent thermodynamic data set for phases of petrological interest. J Metam Geol 16:309–343

Holland TJB, Powell R (2003) Activity-composition relations for phases in petrological calculations: an asymmetric multicomponent formulation. Contrib Mineral Petrol 145:492– 501

Holdaway MJ (2000) Application of new experimental and garnet Margules data to the garnet biotite geothermometer. Am Mineral 85:881-892

Hushmandzadeh A, Alavi-Naini M, Haghipour A (1978) Geological evolution of Torud area (Precambrian to Recent). Geological Survey of Iran H5, pp 138 (in Farsi)

Hynes A, Forest RC (1988) Empirical garnet-muscovite geothermometry in low-grade metapelites, Selwyn Range (Canadian Rockies). J Metam Geol 6 (3):297–309

Jafarian MB (2000) Geological map of Kalateh-Reshm (scale 1:100,000) sheet No 6860. Geological Survey of Iran Tehran Iran

Janoušek V, Erban V, Farrow C (2006) Interpretation of whole-rock geochemical data in igneous geochemistry: introducing Geochemical Data Toolkit (GCDkit). J Petrol 47:1255–1259

Kohn M J, Spear F S (1990) Two new geobarometers for garnet amphibolites, with applications to southeastern Vermont. Am Mineral 75: 89-96

Košler J, Fonneland H, Sylvester P, Tubrett M, Pedersen RB (2002) U-Pb dating of detrital zircons for sediment provenance studies - a comparison of laser ablation ICPMS and SIMS techniques. Chem Geol 182:605-618

Lawver LA, Scotese, CR (1987) A revised reconstruction of Gondwanaland. In McKenzie GD (ed). Gondwana Six; Structure, Tectonics, and Geophysics. American Geophysical Union Washington D C, Geophysical Monograph 40:pp 17–23

Meschede M (1986) A method of discriminating between different types of mid-ocean ridge basalts and continental tholeiites with the Nb-Zr-Y diagram. Chem Geol 56:207-218

Nadimi A (2007) Evolution of the Central Iranian basement. Gondwana Research 12:324–333

Newton RC, Charlu TV and Kleppa OJ (1980) Thermochemistry of the high structural state plagioclases. Geochim Cosmochim Acta 44:933-941

Paul A, Kaviani A, Hatzfeld D, Mokhtari M (2003) Lithospheric structure of central Zagros from seismological tomography. Four International Conferences of Earthquake Engineering and Seismology, 12–14 May, Tehran Iran

Pearce JA (1983) Role of sub-continental lithosphere in magma genesis at active continental margins. In Hawkesworth CJ and Norry MJ (eds.) Continental Basalts and Mantle Xenoliths. Shiva, Nantwich pp 230-249

Pearce JA, Harris NBW, Tindle AG (1984) Trace element discrimination diagrams for the tectonic interpretation of granitic rocks. J Petrol 25:956-983

Perchuk LL, Lavrentjeva IV (1983) Experimental investigation of exchange equilibria in the system cordierite-garnet-biotite. In Saxena SK (ed) Kinetics and equilibrium mineral reactions. Adv Phys Geochem 3:199-239

Powell CMcA, Johnson BD, Veevers JJ (1980) A revised fit of East and West Gondwanaland. Tectonophysics 63:13–29

Rahmati Ilkhchi M (2002) Geological map of Razveh (scale 1:100,000). Geological Survey of Iran, Tehran Iran

Rahmati Ilkhchi M, Jeřábek P, Faryad SW, Košler J (2008) Tectono-metamorphic evolution of the Shotur Kuh Metamorphic Core Complex in the Central Iranian Block. 6th Meeting of the Central European Tectonic Group, Upohlav Slovakia SlovTec 08:48-49

Ramezani J, Tucker RD (2003) The Saghand Region, Central Iran: U–Pb geochronology, petrogenesis and implications for Gondwana tectonics. Am J Sci 303: 622–665

Robinson P, Ross M, Jaffe HW (1971) Composition of the anthophyllite-gedrite series, comparisons of gedrite and hornblende, and the anthophyllite-gedrite solvus. Amer Mineral 56:1005-1041

Schreyer W (1973) Whiteschist: A high-pressure rock and its geologic significance. J Geol 81:735-739

Schreyer W, Seifert F (1969) High-pressure phases in the system $MgO-Al_2O_3-SiO_2-H_2O$. Am J Sci 267-A: 407-413

Selverstone J, Spear FS, Franz G, Morteani G (1984) High pressure metamorphism in the SW Tauern window, Austria: P-T paths from hornblende-kyanite-staurolite schists. J Petrol 25:501-531

Sengör AMC (1991) Late Paleozoic and Mesozoic tectonic evolution of the Middle Eastern Tethysides: Implication for the Paleozoic Geodynamics of the Tethyan realm. IGCP Project 276 Newsletter No 2:111–149

Sheikholeslami MR, Pique A, Mobayen P, Sabzehei M, Bellon H, Hashem Emami M (2008) Tectono-metamorphic evolution of the Neyriz metamorphic complex, Quri-Kor-e-Sefid area (Sanandaj-Sirjan Zone, SW Iran). J Asian Earth Sci 31:504–521

Spear FS (1980) The gedrite-anthophyllite solvus and the composition limits of orthoamphiboles from the Post Pond volcanics, Vermont. Amer Mineral 65:1103-1118

Spear FS (1982) Phase equilibria of amphibolites from the Post Pond Volcanics, Mt Cube Quadrangle, Vermont. J Petrol 23:383-426

Stampfli GM (1978) Etude géologique générale de l'Elburz oriental au S de Gonbad-e-Qabus, Iran N-E. Fac Sci Univ Genève, Thesis No 1868 pp 329

Stöcklin J (1968) Structural history and tectonics of Iran: a review. Amer Assoc Petroleum Geol Bull 52 (7):1229–1258

Stöcklin J (1977) Structural correlation of the Alpine ranges between Iran and Central Asia. Mém Soc Géol France, hors Sér 8:333–353

Takin M (1972) Iranian geology and continental drift in the Middle East. Nature 235:147–150

Unrug R (1997) Rodinia to Gondwana: The geodynamic map of Gondwana supercontinent assembly. GSA Today 7(1):1–6

Ustaömer PA, Ustaömer T, Collins AS, Robertson AHF (2009) Cadomian (Ediacaran– Cambrian) arc magmatism in the Bitlis Massif, SE Turkey: Magmatism along the developing northern margin of Gondwana. Tectonophysics *in press*

Ward CM (1984) Magnesium staurolite and green chromian staurolite from Fiordland, New Zealand. Amer Mineral 69:531–540

Wood DA (1980) The application of a Th-Hf-Ta diagram to problems of tectonomagmatic classification and to establishing the nature of crustal contamination of basaltic lavas of the British Tertiary Volcanic Province. Earth Planet Sci Lett 50:11-30

Wu CM, Cheng BH (2006) Valid garnet-biotite (GB) geothermometry and garnet-aluminum silicate-plagioclase-quartz (GASP) geobarometry in metapelitic rocks. Lithos 89:1-23

CHAPTER 3

Mid-Cimmerian, Early and Late Alpine orogenic events in the Shotur Kuh metamorphic complex, Great Kavir block, NE Iran

Mahmoud Rahmati-Ilkhchi[1,2], Petr Jeřábek[1], Shah Wali Faryad and Hemin A. Koyi[3]

[1] Institute of Petrology and Structural Geology, Charles University in Prague, Albertov 2, 128 43 Prague, Czech Republic

[2] Geological Survey of Iran

[3] Hans Ramberg Tectonic Laboratory, Institute of Earth Sciences, Uppsala University, Villava¨gen 16, Uppsala S-752 36, Sweden

Abstract

The Shotur Kuh complex, exposed in the NE part of the Great Kavir block, is composed of amphibolite facies metaigneous rocks and micaschist, and of lower-grade Permian–Miocene cover sequences that experienced four main deformation phases and at least two metamorphic events. The D1 deformation phase is associated with a prograde metamorphism that in the basement reached amphibolite facies conditions. This Barrovian type metamorphism with field gradient of 20–22 °C/km was related to collision-induced crustal thickening. The D2 event corresponds to post-collisional exhumational upflow of middle crust resulting in updoming of the basement core and its top-to-the-Northwest unroofing along a low angle detachment shear zone at the basement/cover boundary. The D1 and D2 events are considered as Mid-Cimmerian in age as they affected also the Lower Jurassic Shemshak Formation and are sealed by the Middle Jurassic conglomerates. The D3 folding event, characterized by NE–SW shortening, affected also the Cretaceous limestones and it is sealed by Paleocene conglomerates. Considering Late Cretaceous age of this deformation, it is related to the Late-Cimmerian–Early Alpine orogeny that resulted from the Cenozoic closure of the Neo-Tethys oceanic tract(s) and convergence between Arabian and Eurasian plates. The D4 folding event, characterized by NW–SE shortening, affected also the Miocene conglomerates implying its Late Miocene to post-Miocene age. This deformation event is associated with Late Alpine Alborz and

Zagros phase of convergence between Arabia and Eurasia during Late Cenozoic and could be combined with a left-lateral activity along the Great Kavir fault bounding system.

3.1. Introduction

The Cimmerian block in Central Iran (Stöcklin, 1968) is part of the Alpine-Himalayan orogenic system in western Asia and consists of individual crustal segments that are represented by Alborz, Sanandaj-Sirjan zone and Central Iranian domain (Fig. 1a). It is formed by crystalline basement consolidated during the Neoproterozoic–Early Cambrian Pan-African orogeny and represents former passive margin of Gondwana that separated in Ordovician to Silurian and collided with Eurasia due to closure of the Paleo-Tethys in Middle to Late Triassic Early-Cimmerian event (Stocklin, 1974; Berberian and King, 1981; Sengör et al., 1988; Sengör, 1990; Stampfli et al., 1991; Sengör and Natal'in, 1996; Bagheri and Stampfli, 2008). In Jurassic–Cretaceous, the ongoing subduction of Neo-Tethys in the south induced back arc spreading and partial fragmentation of Cimmerian block, which again amalgamated with the closure of Neo-Tethys in Upper Cretaceous to Eocene Late-Cimmerian–Early Alpine orogeny (e.g. Ramezani and Tucker, 2003; Bagheri and Stampfli, 2008). Recent increase in number of geochronological age data, obtained from the Cimmerian basement units, have revealed also Jurassic (181–156 Ma) orogenic activity in the Sanandaj-Sirjan zone (Khalatbari-Jafari, 2003; Rachidnejad-Omran et al., 2002; Sheikholeslami et al., 2003, 2008; Falznia et al., 2007) and the Central Iranian domain (Bagheri and Stampfli, 2008; Rahmati-Ilkhchi et al. in press). This activity has been attributed to a series of back-arc extensional events and compressional cycles controlled by the north-dipping Neo-Tethyan subduction zone (Bagheri and Stampfli, 2008) and/or to a collisional interaction with Arabian plate prior to opening of the Neo-Tethys ocean (Falznia et al., 2009). The Late Alpine event is represented by the late Miocene Zagros and Alborz phase of continuous N–S convergence in the region controlled by the movement of Arabian and Eurasian plates following the Neo-Tethys closure (e.g. Alavi, 2004; Guest et al., 2006).

In this work, we further extend the evidence for Lower/Middle Jurassic orogenic activity in the Central Iranian domain and present an overview of deformation structures and related metamorphic record within the basement and para-

autochthonous sedimentary cover of the Shotur Kuh metamorphic complex in the northeastern part of the Great Kavir block. Spatial and temporal variations in the deformation-metamorphic record within the Permian–Miocene cover are used to relate the local deformation pattern to the main orogenic processes that affected the Central Iranian domain.

3.2. Geological setting

The Central Iranian domain consists of several crustal blocks, from east to west the Lut, Tabas, Yazd and Great Kavir (Fig. 1a), distinguished on the basis of lithological correlation and main fault pattern (e.g. Stocklin, 1968; Takin, 1972; Crawford, 1977; Berberian et al., 1981). Although most of the area is covered by thick sedimentary sequences, which despite an occurrence of locally significant sedimentary facies and/or thickness variations are largely comparable, the basement rocks are exposed mostly along the block boundaries.

The Shotur Kuh complex exposed in the northeastern part of the Great Kavir block between two parallel NE–SW trending Anjillo and Torud faults (Fig. 1b), is a metamorphic complex with an E–W trending elliptical basement core domain (ca 20 km long and 11 km wide) and overlying para-autochthonous Permian–Miocene cover sequences (Fig. 1c). The basement as well as the cover is intruded by a series of Eocene volcanic rocks of dacite and andesite composition (Rahmati-Ilkhchi, 2002). Most of the basement rocks are represented by orthogneiss with intercalations of amphibolite and metagranitoids. The orthogneisses are derived from tonalite, granodiorite, monzogranite, syenogranite and alkali-feldspar granite, and the amphibolites represent former basaltic dyke swarms with different orientation intruding the granitoid complex. The relative abundance of amphibolite "dyke" bodies in the western part of the basement vanishes towards the north and east. The granitoids are derived from arc-related magmatism that was active during Neoproterozoic–Early Cambrian (547±7 Ma; Rahmati-Ilkhchi et al, in press).

Small amounts of garnet-bearing micaschists are exposed at the contact between basement orthogneisses and pre-Middle Triassic cover rocks in the south of the Shotur Kuh complex.
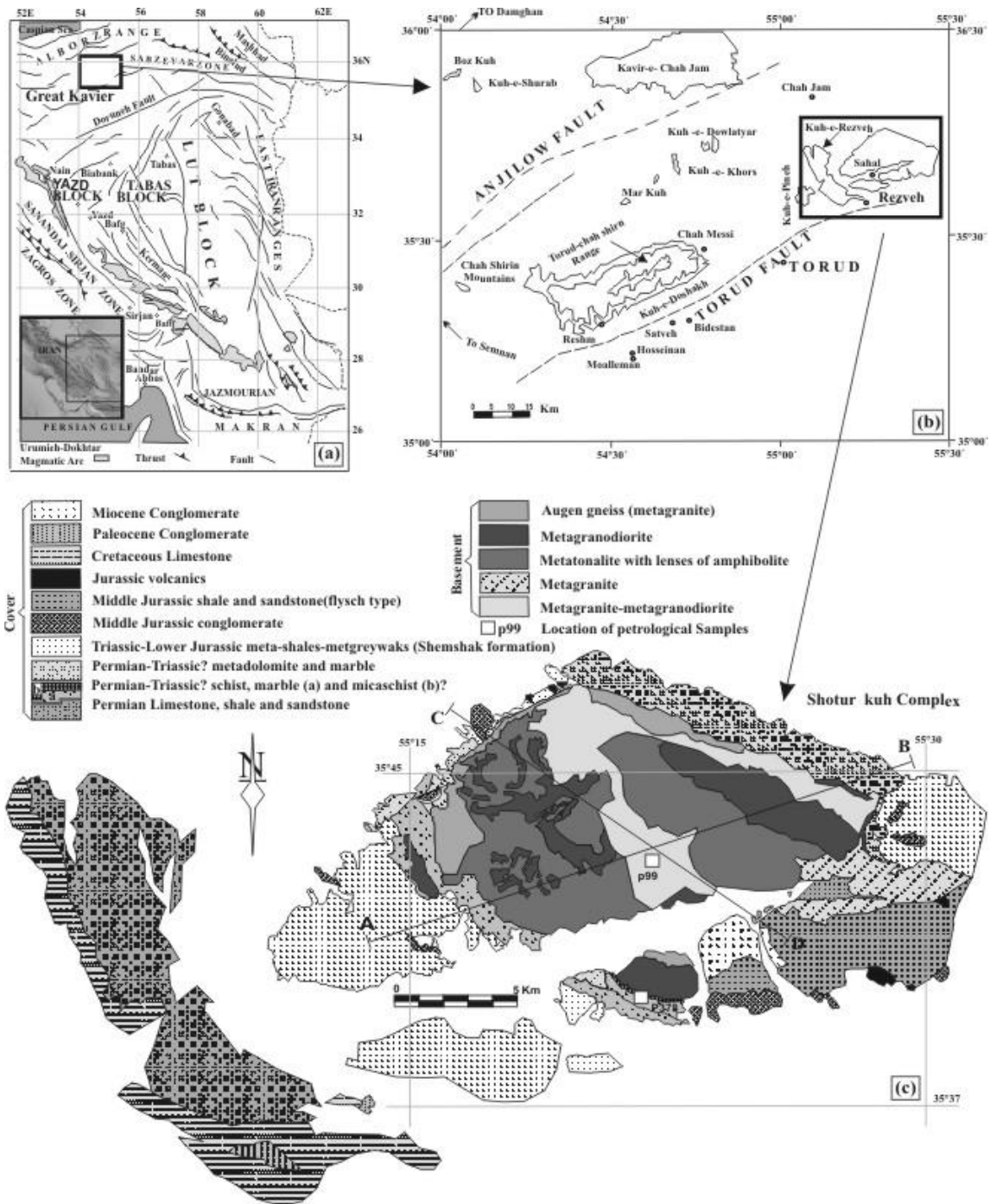
Fig.1. (a) Simplified tectonic map of eastern Iran showing constituent crustal blocks (compiled from Ramezani and Tucker, 2003; Alireza Nadimi, 2006). (b) Schematic map of the Torud area showing location of villages, mountains and important faults after Hushmandzadeh et al. (1978). (c) Simplified geological map of the Rezveh area with location of structural cross-sections A–B and C–D presented in Fig. 4 and of petrological samples p99 (Rahmati Ilkhchi et al. in press) and p378 (this study) used for PT calculations.

75

The micaschists intercalate with marbles and slices of basement orthogneiss, reflecting complex structural relationships. The micaschists are similar in lithology to the greenschist facies pre-Middle Triassic metasediments (see below), but show PT conditions close to the basement rocks.

The pre-Middle Triassic metasedimentary rocks are subdivided into two lithological sequences. The first, exposed along the southern border of the Shotur Kuh basement, is represented by black meta-shales and schists with intercalation of marble (Fig. 2).
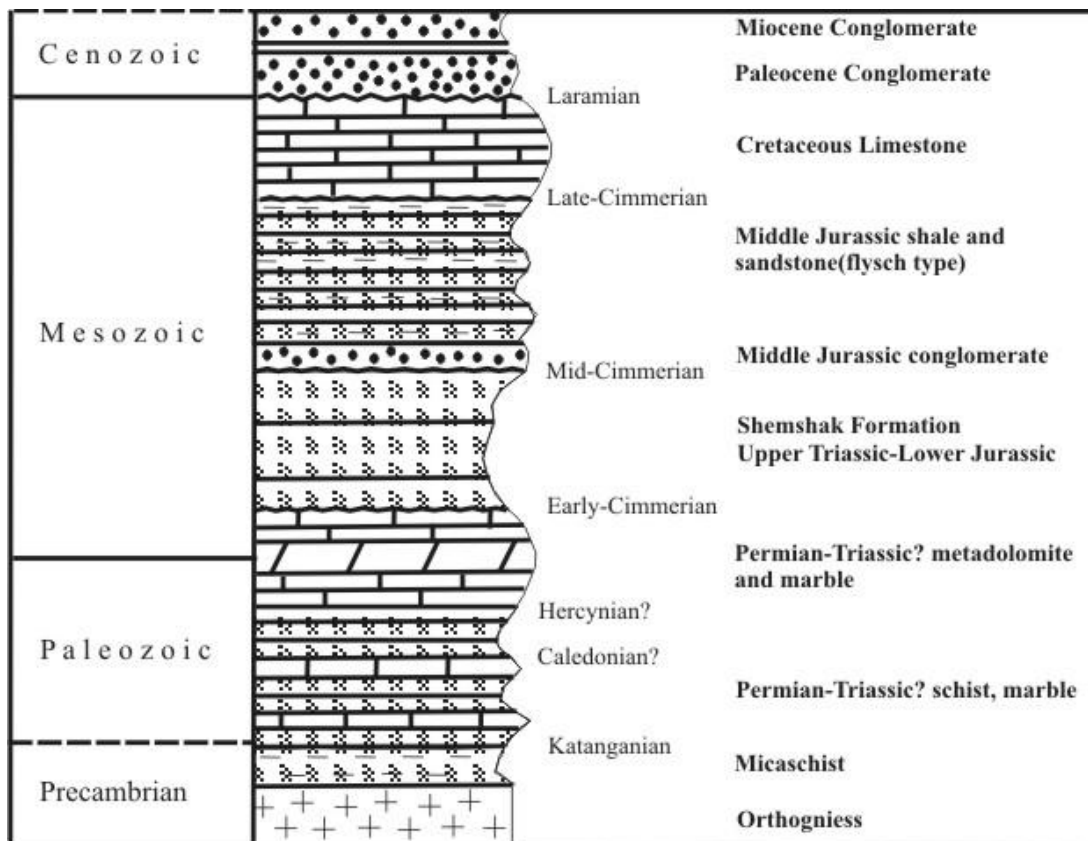
.Fig. 2. Simplified stratigraphic column from the Shotur Kuh complex. Major tectonic events are also indicated in the figure.

The second consists of metadolomite and calcitic marble with intercalation of calc-schist at the bottom of the sequence and occurs in the northern part of the Shotur Kuh (Fig. 1c). As no index fossils were found in these sequences, their precise age cannot be determined. However, based on the presence of some corals, crinoid and *Textularia* (Fig. 3a), the age of these subunits is probably older than middle Triassic (Rahmati-Ilkhchi, 2002). Similar but unmetamorphosed sedimentary sequence in the south-west

of the studied area (Fig. 1c), consists of dolomitic limestone, shale, sandstone and limestone with *Parafusulina* sp., *Schwagerina* sp., *Fusulinides* and *Climacamina* sp (Fig.3b), clearly indicating Permian age.
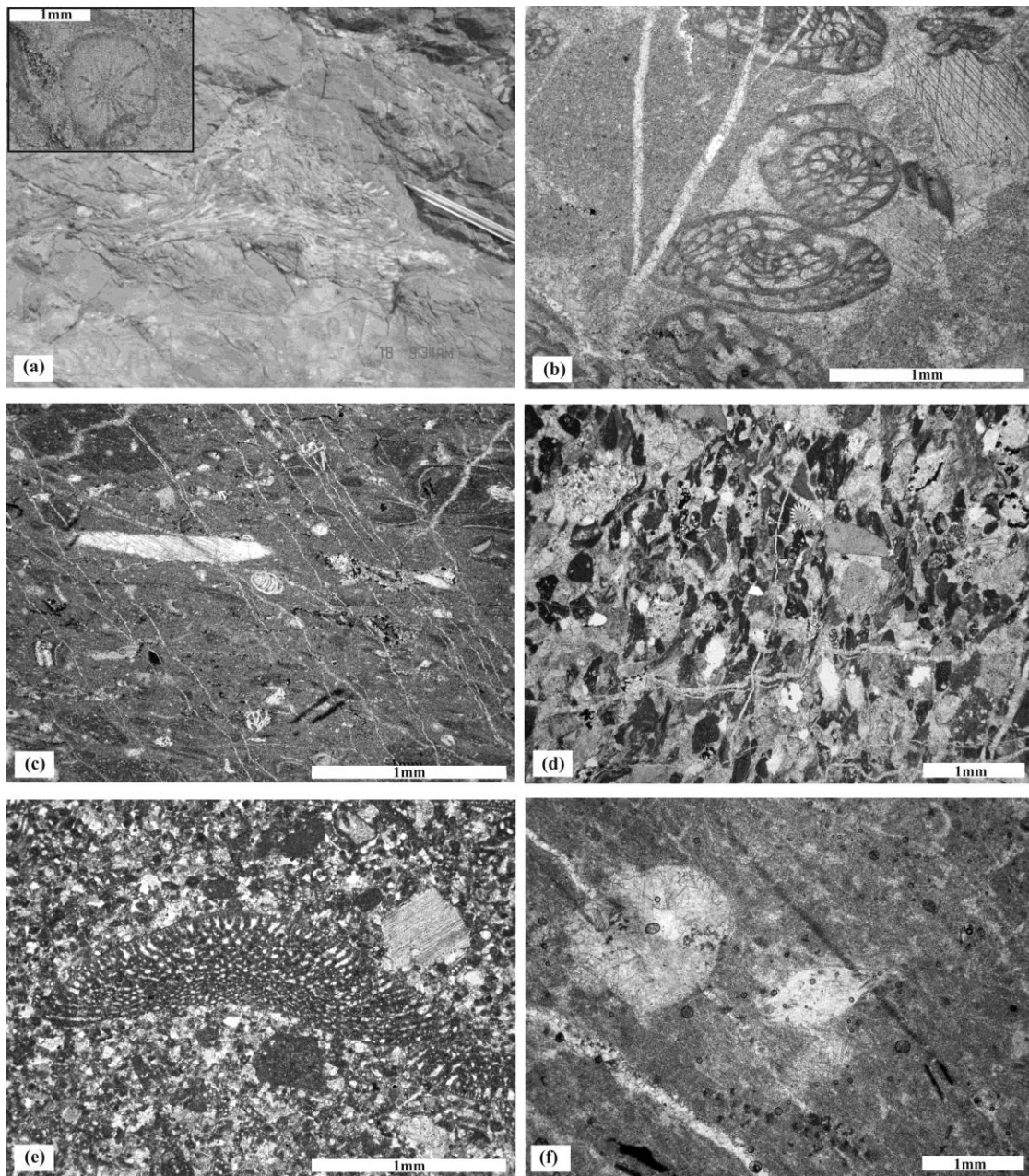
Fig. 3. Fossils from different cover formations of the Rezveh area. (a) Crinoid and Coral bearing marble (Permian–Lower Triassic?), (b) biomicrite with fusulinds (Upper Permian), (c) recrystalized biomicrite with Frondicularia sp., Miliolids, Cristellarias (Upper Triassic), (d) low-metamorphosed clastic sedimentary rock with Crinoids (Jurassic), (e) sandy bio-pel-microsparite with Orbitolina sp. (Lower Cretaceous), (f) biomicrosparite with Operculina (Paleocene?).

Lithological correlation of the above-described formations suggests the presence of one litho-stratigraphic unit of Permian–Middle Triassic age.

The Permian–Triassic metasediments are overlain by the Shemshak Formation (e.g., Assereto, 1966; Stampfli 1978) with a hidden unconformity. This low-grade metamorphosed formation, represented mostly by alternating meta-shales and meta-greywacks, is interbedded with marble and conglomerates with pebbles of slates. The limestones of the Shemshak Formation are fossiliferous and contain *Pseudocyclammina* sp., *Frondicularia* sp., *Cristellaria* sp. and miliolids, (Fig. 3c) suggesting Upper Triassic–Lower Jurassic age.

The Shemshak Formation is unconformably overlain by conglomerate with slaty to very low-grade metamorphosed matrix that contains pebbles of the basement granitoid and orthogneiss, and Permian–Middle Triassic and Shemshak Formation marbles and meta-shales (Rahmati-Ilkhchi, 2002). The conglomerates are succeeded by flysch sediments represented by alternating shales and sandstones interbedded with micro-conglomerate and crinoid-bearing sandy limestone (Fig. 3d). This sedimentary succession is very low-grade metamorphosed and based on fossil record (*Cayexia* Sp., *Lithocudim* Sp., *Eggerlla* Sp., *Cristellaria* Sp., *Pseudocyclammina* sp., *Paleogaudryina* sp.) can be assigned Middle Jurassic in age.

The Jurassic sedimentary rocks are overlain by very low-grade metamorphosed massive limestone with alternating red conglomerates and sandstones at its base, located in the south-west of the studied area (Fig. 1c). The limestone is fossiliferous and contains *Orbitolina* sp., *Pseudochoffatella* sp., *Pseudocyclammina* sp., *Nautiloculina* sp. and *Dictyoconus* sp. (Fig.3e) suggesting Lower Cretaceous (Aptian–Albian) age.

The Cretaceous limestone is unconformably overlain by well consolidated unmetamorphosed conglomerates and red sandstone with *Operculina* (Fig. 3f). Because of superposition, the age of these rocks is assumed to be Paleocene(Rahmati-Ilkhchi, 2002). The Paleocene conglomerates are followed by poorly consolidated unmetamorphosed Miocene conglomerates and sandstones. Their Miocene age is based on lithological correlation of the conglomerate pebbles with Eocene volcanic rocks in the surrounding area (Rahmati-Ilkhchi, 2002).

3.3. Structural record

The Shotur Kuh complex has been affected by four major deformation events D1–D4. The first two events are associated with the development of metamorphic foliation while the later two events are characterized by small to large-scale folding. The differences and similarities in structural record in the basement and overlaying sedimentary rocks are described in the following sections.
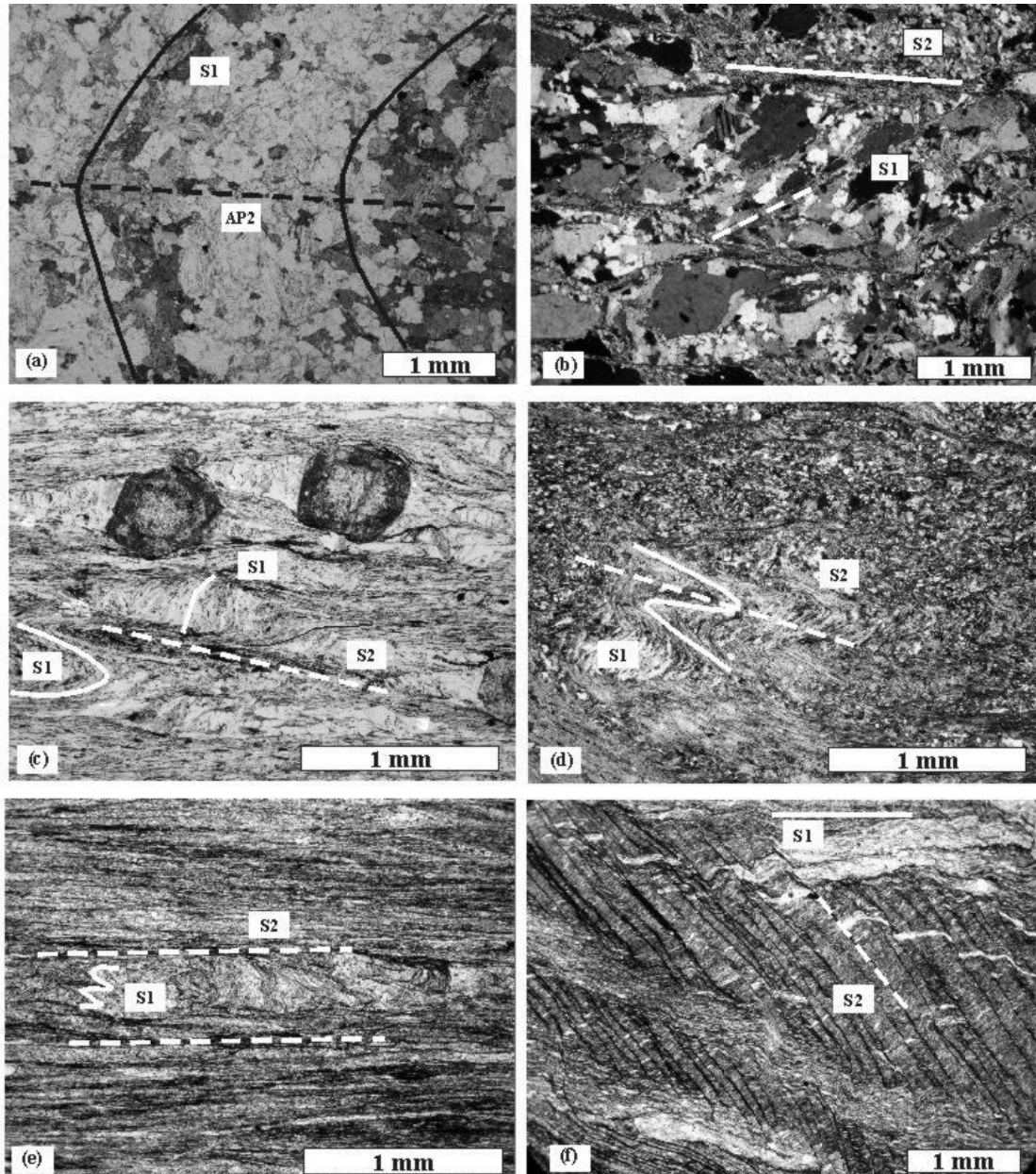
Fig. 4. (a) Metamorphic foliation S1 affected by F2 folding and showing lack of retrogression within amphibolite. Higher grade foliation S1 overprinted by lower grade foliation S2 within orthogneiss (b), micaschist (c), Permian–Triassic cover (d, e) and Lower Jurassic Shemshak Formation (f).

3.3.1. Orthogneisses and amphibolites

The basement rocks are affected by all four deformation events. The first deformation event D1 is associated with the development of amphibolite facies metamorphic foliation S1 defined by shape preferred orientation of muscovite, biotite and recrystallized quartz aggregates in the orthogneiss and of amphibole and biotite or plagioclase/amphibole banding in the amphibolite (Fig. 4a, b).
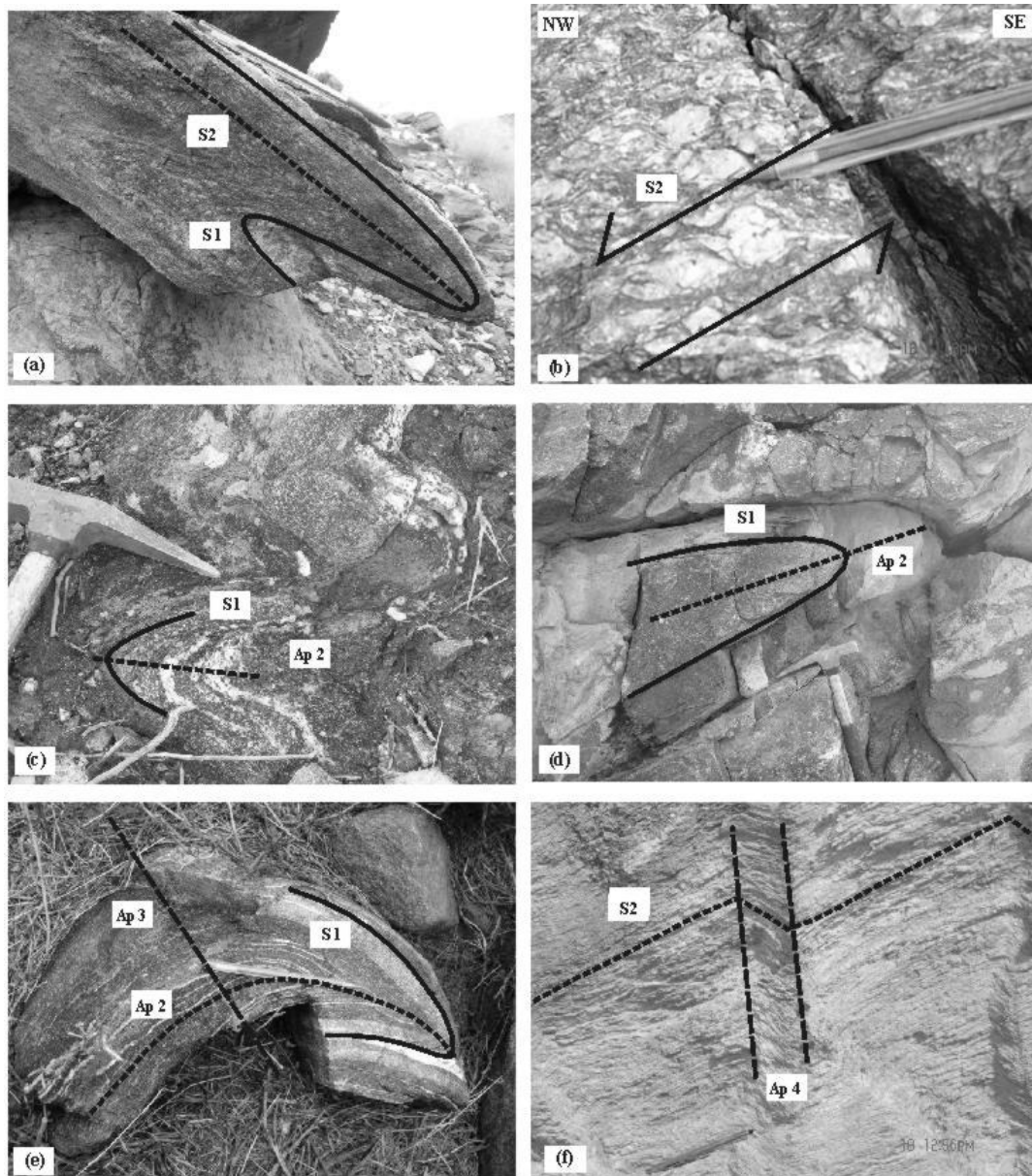
Fig.5. Deformation structures in the basement: (a) relics of S1 fabric within isoclinal folds F2 and transposition of S1 into S2, (b) plagioclase sigma clasts within S2 indicating top-to-the-NW shear sense, (c) isoclinally (F2) folded S1 in amphibolite, (d) isoclinal fold F2 of amphibolite "dyke" body, (e) isoclinal fold F2 affected by F3 folding, (f) F4 kink band affecting the S2.

The S1 foliation has been isoclinally folded, overprinted and/or completely transposed into a new penetrative mylonitic foliation S2 (Fig. 5a–c). The S2 foliation is defined by shape preferred orientation of quartz aggregates, fine-grained muscovite, rarely also biotite and chlorite in orthogneiss (Fig. 4b) and shape preferred orientation of chlorite, biotite and epidote in amphibolite. The S2 fabric is axial planar to the isoclinally folded locally intercalating amphibolite "dyke" bodies (Fig. 5d). D2 structures indicate development and retrogression from amphibolite to greenschist facies conditions manifested by the local occurrence of F2 isoclinally folded amphibolites lacking retrogression (Fig. 5c and 4a) and subsequent formation of retrogressed axial planar S2 cleavages. The S2 fabric shows various orientations reflecting the domal structure of the Shotur Kuh complex (Fig. 6), and it bears subhorizontal NW–SE trending stretching lineation L2 defined by linear arrangement of micas and elongation of quartz aggregates. The L2 is subparallel to axes of isoclinal F2 folds. Macroscopic kinematic indicators within S2 fabric, such as sigma clasts (Fig. 5b), S-C and S-C` shear bands, show top-to-the-Northwest shear sense. Subsequent deformation D3 is responsible for folding of previous fabrics and results in the development of small to large-scale folds (Fig. 5e) with subvertical NW–SE trending axial planes and subhorizontal axes (Fig. 6). The latest ductile deformation D4 in the Shotur Kuh basement results in the development of crenulation cleavage, kink bands (Fig. 5f) and open folds with subvertical NE–SW trending axial planes and subhorizontal axes (Fig. 6).

3.3.1.1. *Quartz deformation microstructures*

Quartz deformation microstructures in the basement orthogneisses were investigated in order to characterize temperature conditions of the observed macroscopic fabrics as well as to evaluate regional microstructural differences. The orthogneisses exhibit two distinct types of quartz microstructure related to recrystallization at different temperature conditions. The first microstructural type, associated with S1 deformation fabric, is characterized by relatively coarse-grained (ca 1 mm) recrystallized quartz and higher temperature features such as lobate grain boundaries and island grains (Fig. 7a). These features are typical for high temperature grain boundary migration recrystallization mechanism (Poirier and Guillope, 1979, Urai et al., 1986), i.e. the GBM recrystallization regime in quartz (Stipp et al., 2002).
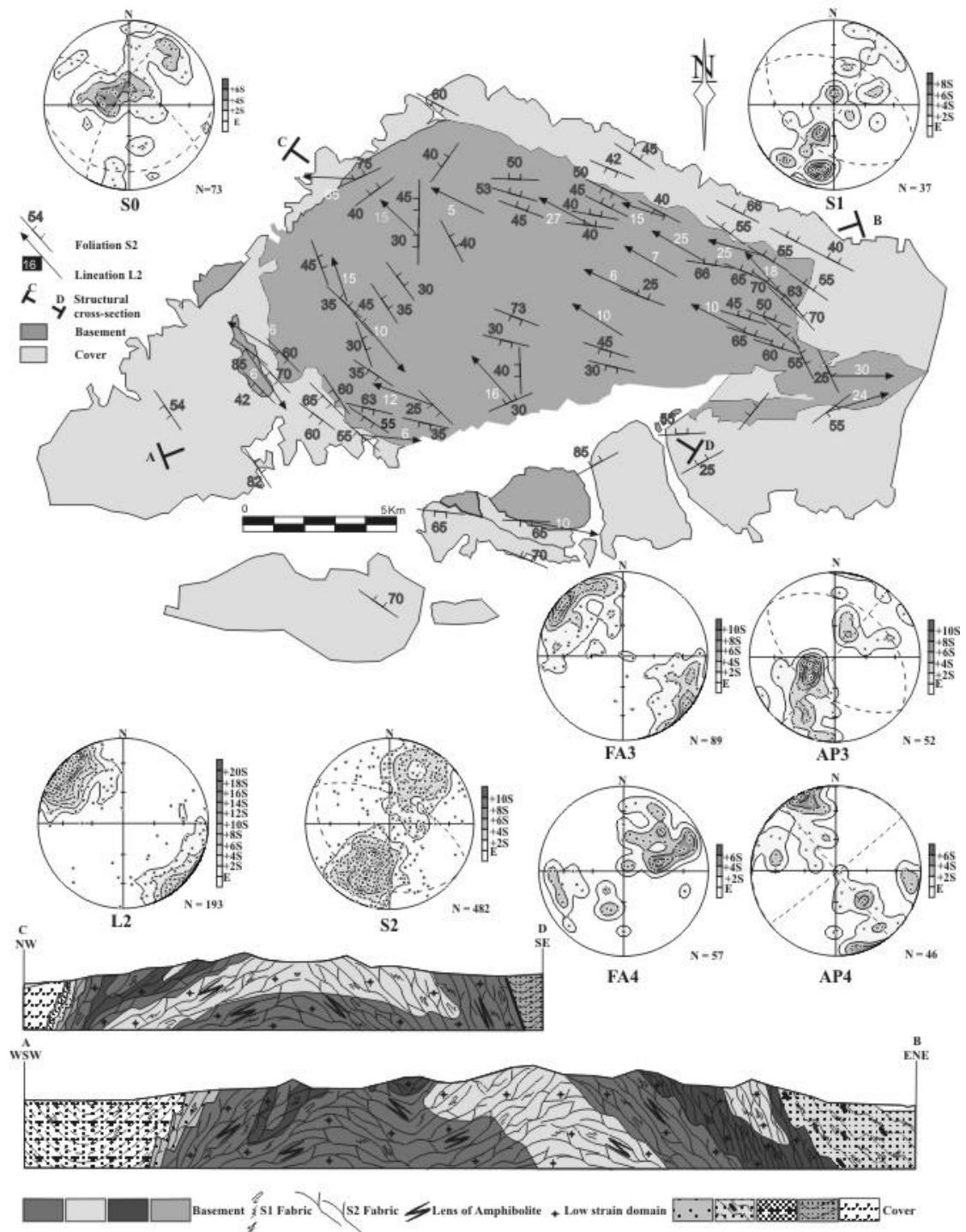
Fig.6. Structural map showing trend and dip of foliation S2 and lineation L2, and two structural profiles; the WSW–ENE trending profile A–B and the NW–SE trending profile C–D. The data in the pole figures cover the whole region and show orientation of following structures: sedimentary bedding S0, D1 and D2 metamorphic foliations S1 and S2 and lineation L2, and D3 and D4 fold axial planes AP3 and AP4 with fold axes FA3 and FA4. The pole figures are in lower hemisphere equal area Schmidt projection. Contours are multiples of angular standard deviation above the uniform distribution.

According to the temperature-microstructure calibration of Stipp et al., (2002), this microstructure is common for amphibolite facies metamorphic conditions. The second microstructural type, associated with S2 fabric, is characterized by relatively fine-grained recrystallized quartz and the development of core and mantle microstructure (Fig. 7b, c). Such microstructure is typical for the subgrain rotation recrystalization mechanism (White, 1979), i.e. the SGR recrystalization regime in quartz (Stipp et al., 2002). According to the temperature-microstructure calibration of Stipp et al., (2002), this microstructure is common for greenschist facies conditions.
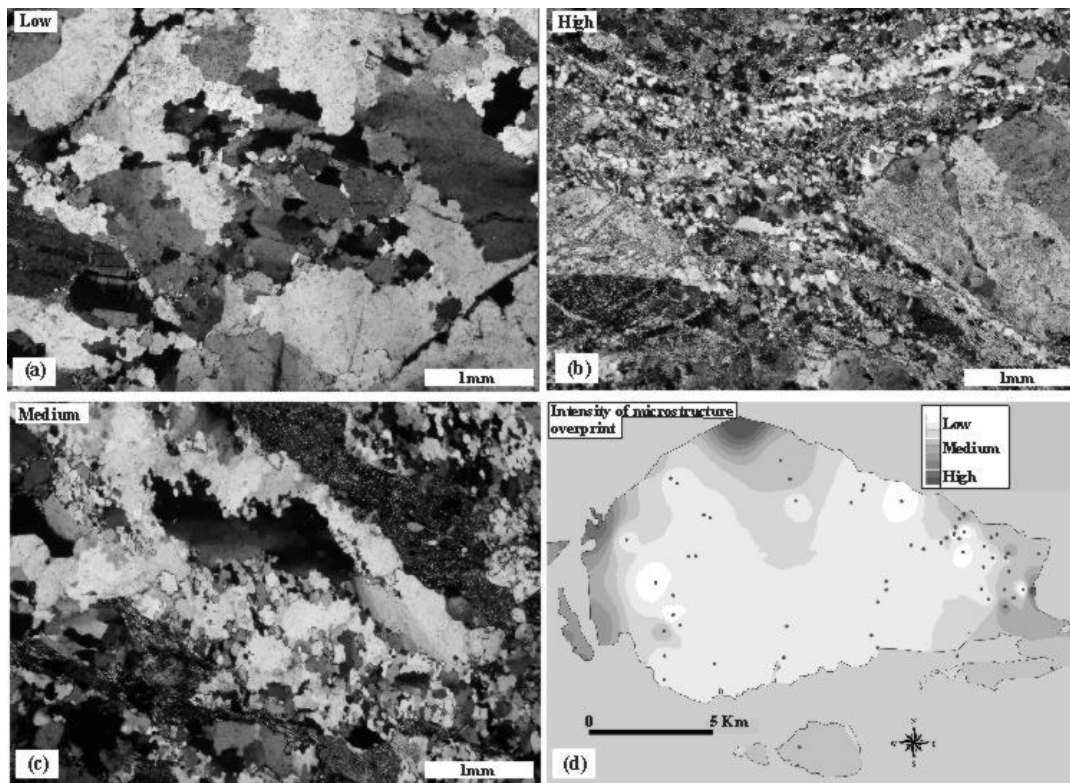
Fig. 7. Quartz deformation microstructure in the basement orthogneiss showing two distinct microstructures: (a) high temperature GBM (D1-related) and (b) lower temperature SGR (D2-related). An example of overprinting relationship of the first D1 microstructure by the second D2 microstructure is shown in (c). The grid in (d) shows spatial variations in an intensity of microstructure overprint across the Shotur Kuh basement; the low and high intensity is exemplified in (a) and (b), respectively.

The micrograph in figure 7c shows clear overprint of the first higher temperature D1 microstructure by the second lower temperature D2 microstructure. The degree of microstructural overprint range from very low (Fig. 7a) to complete obliteration of the first microstructure (Fig. 7b). We attempted to quantify the degree of microstructural overprint on the basis of optical microscopy and determination of extreme cases of

overprinting relationships (Low–High in Fig. 7a-c). The optical analysis of thin sections collected across the Shotur Kuh basement (Fig. 7d) shows that the intensity of microstructural D2 over D1 overprint increases from the central parts of the basement towards the contact with the cover formations.

3.3.2. Micashists

Similarly to the basement rocks, the micaschists exhibit two metamorphic fabrics. The higher grade S1 metamorphic foliation is present within relics of isoclinal F2 folds while the rock is dominated by the lower grade S2 cleavage. The S1 fabric is defined by shape preferred orientation of larger (ca 1 mm) muscovite and biotite grains which are kinked and cleaved during the formation of S2 (Fig. 4c and d). Micaschists in the vicinity of basement orthogneiss contain idioblastic garnets (up to 0.5 mm in size) which together with the relics of micaceous S1 foliation are enclosed within quartz rich microlithons separated by S2 cleavage (Fig. 4c). The S2 cleavage dips to the south or southwest at moderate angles (Fig. 6).

3.3.3. The para-autochthonous cover sequences

The differences in structural record within different litho-stratigraphic sequences of the Shotur Kuh cover have been used to define three distinct tectono-stratigraphic units; Permian–Lower Jurassic, Middle Jurassic–Cretaceous and Paleocene–Miocene.

The Permian–Lower Jurassic rocks record D1–D4 deformation events recognized in the basement. The intensity of deformation increases towards the cover-basement boundary and range from the undeformed meta-shales and marbles to intensely deformed schists and marbles at the contact with the Shotur Kuh basement. Deformation of the Permian–Triassic rocks at the contact with the basement is characterized by boudinage of metadolomites enclosed by thin-bedded limestones and schists. Similarly to the basement orthogneiss and micaschist, the Permian–Lower Jurassic rocks are characterized by the presence of two metamorphic fabrics (Fig. 4e-f). The greenschist metamorphic foliation S1 is sub-parallel to original sedimentary stratification S0 as well as to lower grade metamorphic fabric S2 (cf. Fig. 8a, b). The S1 foliation is defined by shape preferred orientation of larger (ca 0.5 mm) muscovite and chlorite, and contains greenish biotite near the contact with the basement.
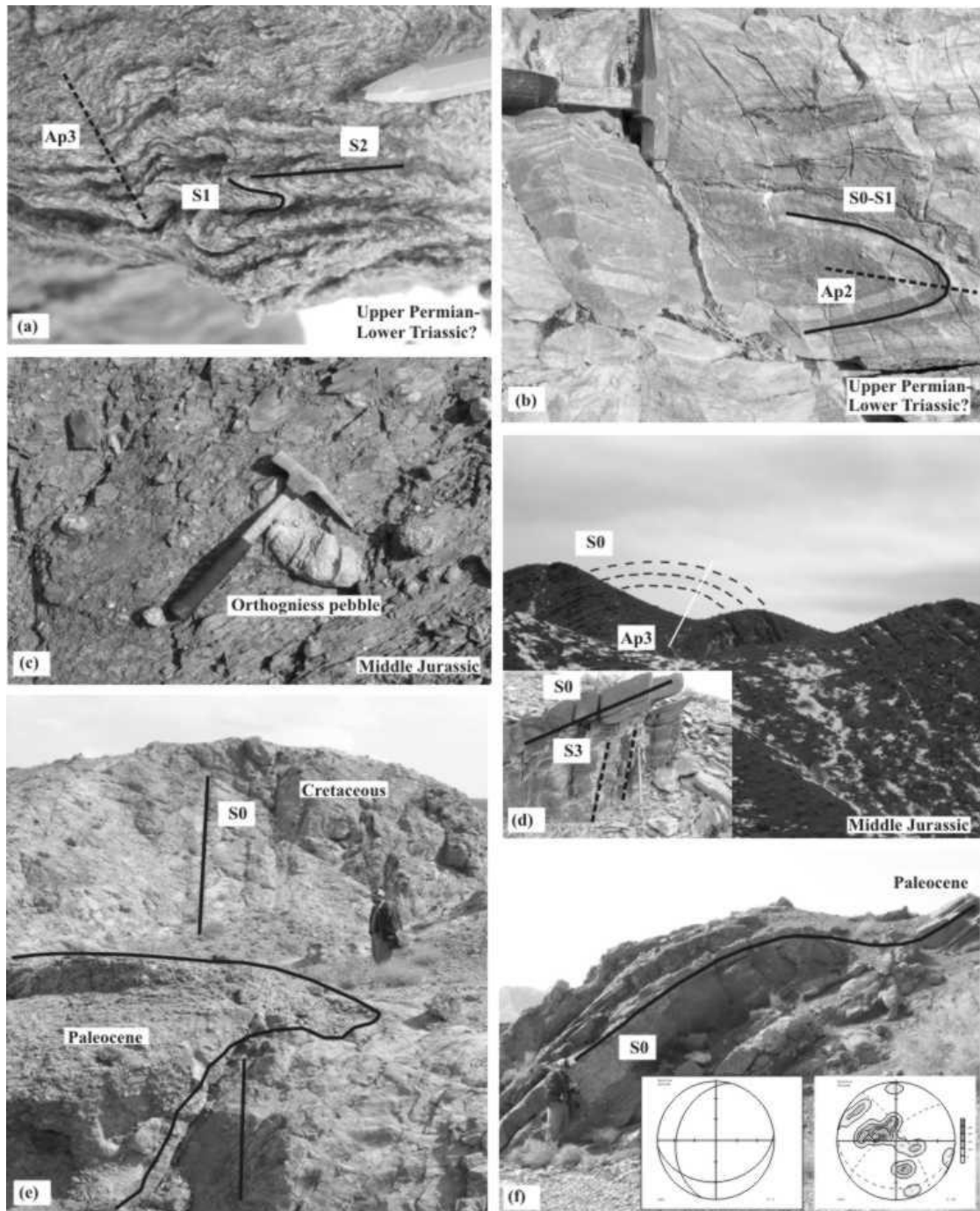
Fig. 8. (a) S1 and S2 fabrics affected by F3 folding in Upper Permian-Lower Triassic? schist, (b) S0-S1 fabrics within isoclinal folds F2 in Upper Permian-Lower Triassic? marble. (c) Middle Jurassic conglomerate with basement orthogneiss pebbles. (d) Large-scale F3 fold affecting S0 in Middle Jurassic flysch sediments: the inset shows S3 cleavage locally developed within folded shale strata. (e) Angular unconformity between folded (D3) Cretaceous limestone strata and Paleocene conglomerate. (f) F4 fold affecting S0 fabric in Paleocene conglomerate; orientation of the two limbs as well as of all measured bedding planes is shown in pole figures.

The S2 fabric, defined by fine-grained white mica, is axial planar to locally observed isoclinal folds F2 affecting the S0-S1 bedding-fabric (Fig. 8b). The F2 fold axes are subparallel to the L2 lineation defined by linear arrangement of micas. The S0-S2 fabric within the Permian–Lower Jurassic rocks exhibits various orientations depending on the location of the cover with respect to the basement so it reflects the D2 related domal structure of the Shotur Kuh complex (Fig. 6).

The S0-S2 fabric orientations are modified by two subsequent folding phases D3 and D4, which result in the development of small to large scale folds and crenulation cleavages with steep NW–SE (D3) and NE–SW (D4) trending axial planes and subhorizontal axes (Fig. 6).

The Lower Jurassic Shemshak Formation is directly overlain by very low-grade metamorphosed Middle Jurassic conglomerates containing pebbles of basement orthogneiss (Fig. 8c). The deformation fabric within orthogneiss pebbles is defined by fine-grained muscovite and show similar microfabric features as the S2 foliation in the basement orthogneiss. Bedding S0 in the Middle Jurassic–Cretaceous rocks is only affected by the D3 and D4 folding events. D3 event is responsible for the development of large scale folds (Fig. 8d) with subvertical NW–SE trending axial planes and subhorizontal axes and locally leads to the development of spaced axial cleavages S3 (inset in Fig. 8d). D4 event is characterized by development of small scale folds and crenulation cleavages with subvertical NE–SW trending axial planes and subhorizontal axes.

Palaeocene conglomerates overlie Cretaceous limestones with clear angular unconformity (Fig. 8e) related to D3 folding of cretaceous limestone. The bedding in the Paleocene–Miocene conglomerates is only affected by D4 folding, which results in the development of tens of metre-scale gentle to open folds (Fig. 8f) with steep NE–SW trending axial planes and subhorizontal axes.

3.4. Petrography and mineral composition

Chemical composition of most minerals was analysed at the Institute for Mineralogy and Petrology in Graz using a JEOL 6310 scanning electron microscope (SEM) equipped with wavelength- and energy-dispersive spectrometers. Standards were pyrope (Mg, Al), adularia (K), rutile (Ti), tephroite (Mn), jadeite (Na, Si), and andradite (Fe, Ca). Na was measured by wavelength-dispersive spectrometers, and

operating conditions were 15 kV and 10 or 15 nA, with 20 s counting time. Representative mineral analyses are given in Table 1. Mineral abbreviations used in the text and figures are after Kretz (1983).

3.4.1. Orthogneisses and amphibolites

Detailed petrology of basement rocks, mainly of orthogneisses and amphibolites, is given in Rahmati-Ilkhchi et al. (in press). The orthogneisses are medium- to coarse-grained and typically consist of feldspars, quartz and biotite ($X_{Mg} = 0.26–0.36$) with small amounts of muscovite, garnet, allanite-epidote and accessories of apatite, zircon and monazite. The garnets are rich in almandine (alm_{59-73}, grs_{6-18}, py_{14-20}, sps_{1-9}) with mostly flat zoning profiles, although in some samples (e.g. p99 for location see Fig. 1) exhibit prograde compositional zoning (for details see Rahmati-Ilkhchi et al. in press). Amphibolite consists of plagioclase (an_{18-30}), pargasite-tschermakite and locally also garnet (alm_{49-64}, grs_{31-34}, py_{3-9} and sps_{1-9}). In one case gedrite with kyanite, phengite and rutile were also found. The basement rocks are retrogressed to various degrees. Feldspars are partly replaced by fine-grained white mica. Biotite is replaced by chlorite with rutile and epidote forms within or adjacent to biotite. Garnet is partially replaced by fine-grained brown to green biotite and chlorite mixture along cracks and garnet rims. Amphibole is partly replaced by chlorite, biotite and epidote.

3.4.2. Micaschist

The micaschists are strongly foliated and contain two metamorphic fabrics (Fig. 4c, d). These rocks consist of quartz, white mica, biotite, sometimes garnet and variable amounts of plagioclase and they mostly contain graphitic substance with fine-grained rutile and other Ti phases. Retrogression in the micaschists is characterized by replacement of garnet into calcite and chlorite, biotite by chlorite, and plagioclase by fine-grained white mica.

Garnet from micaschist (alm_{49-70}, grs_{16-18}, py_{3-10}, sps_{1-31}) shows prograde zoning with rimward increase of X_{Mg} and decrease of spessartine content. Some samples contain two compositional varieties of garnet (Fig. 9a) represented by garnet (I) in the cores (alm_{58-78}, grs_{8-13}, py_{5-11}, sps_{5-24}) and garnet (II) in the rims (alm_{75-78}, grs_{7-12}, py_{11-13}, sps_{0-5}).
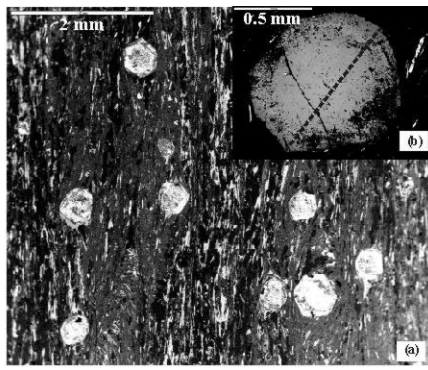
Fig. 9. (a) BSE image of micaschist showing two compositional varieties of garnet core (I) and rim (II). The inset (b) shows detail of zoned garnet with compositional profiles in (c). Sharp change in Grs and Alm contents and a weak decrease of Py and XMg values can be seen at contact between garnet (I) and (II). Sps content generally decrease from core to rim, but small disturbance is visible at the contact of both garnets.
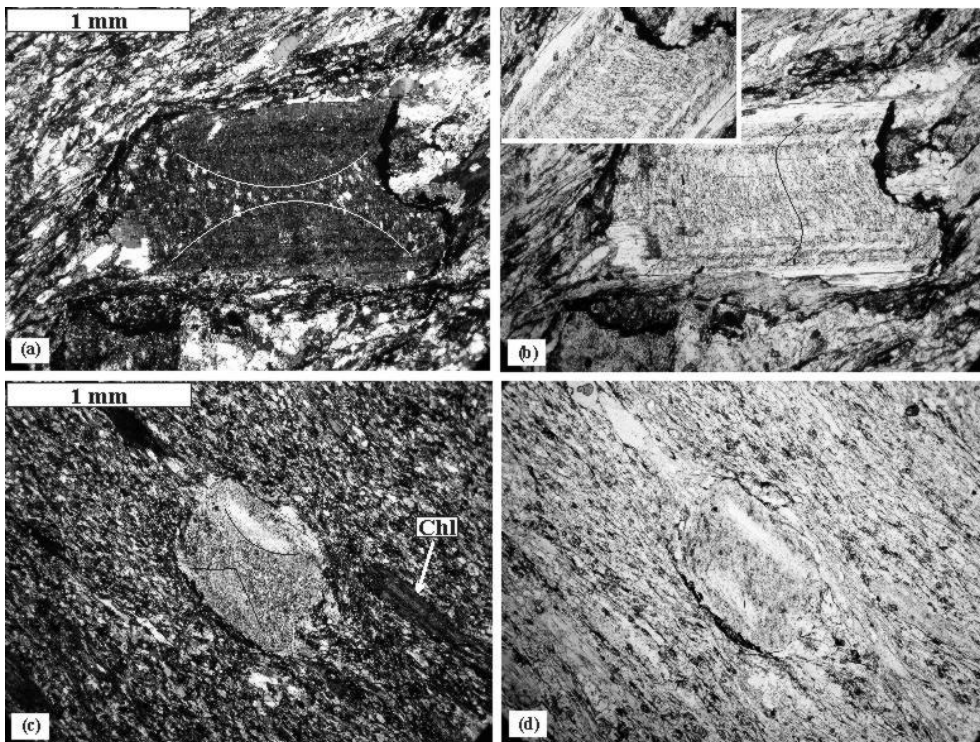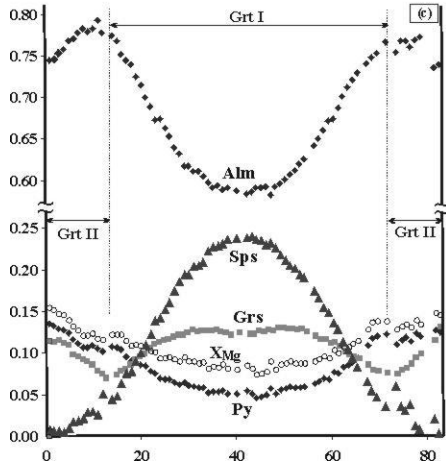

Fig. 10. Photomicrograps of muscovite porphyroblasts with inclusion trails of quartz (a, c) and graphite (b, d). Note concentration of quartz and/or graphite highlight the hourglass structure of chiastolite (andalusite) or sector trilling in cordierite.

Although both garnets show prograde compositional zoning characterized by an increase of X_{Mg} and decrease of sps, garnet (I) exhibits a decrease of calcium and

increase of iron towards the rim, while this zoning pattern is reversal in the garnet (II) (Fig. 9b). Depending on the whole rock composition, plagioclase composition range from pure albite to andesite (an_{40}). Biotite has uniform composition with $X_{Mg} = 0.52$–0.55 and the Si and paragonite contents in muscovite correspond to 3.0 a.p.u. and 11–16 mol %, respectively.

One of the studied garnet-free samples contains large (up to 1 mm) rhomboidal muscovite porphyroblasts within fine-grained matrix. The porphyroblasts show synkinematic growth indicated by the presence of graphite and quartz inclusion trail patterns with s-shaped porphyroblast geometry (Fig. 10). The distribution of quartz and graphite inclusions within these porphyroblasts (Fig. 10a-d) remains an hourglass structure of chiastolite or sector trilling in cordierite and suggests epitaxial replacement of these minerals by muscovite.

3.4.3. The para-autochthonous cover rocks

The above-mentioned tectono-stratigraphic division of the cover into Permian–Lower Jurassic, Middle Jurassic–Cretaceous and Paleocene–Miocene units is consistent with the observed differences in metamorphic grade of the three units. The Permian–Lower Jurassic meta-shales and schists, characterized by the presence of two metamorphic fabrics (Fig. 4e, f), consist of quartz, two varieties of white mica, chlorite and graphitic substance. Near the contact with the basement they also contain greenish biotite. The degree of recrystallization and the grain size of quartz and micas within both fabrics decreases away from the basement/cover boundary towards the younger members of this tectono-stratigraphic unit. The Middle Jurassic–Cretaceous rocks indicate very low-grade metamorphism characterized by the presence of ultra fine-grained mica and chlorite along the bedding planes as well as spaced cleavage S3. The uppermost Paleocene–Miocene conglomerates are characterized by unmetamorphosed matrix.

3.5. PT conditions of metamorphism

PT conditions for the basement orthogneisses and amphibolite were obtained by using various exchange thermobarometres and thermodynamic modelling (Rahmati-Ilkhchi et al., in press). They show a prograde metamorphism that reached 8.5 kbar/650 °C in orthogneisses, while the amphibolite yielded slightly higher pressures of 8–10 kbar.

In contrast to basement orthogneisses and amphibolite with only amphibolite facies mineral assemblages, the micaschists bear evidence for polymetamorphic evolution prior to amphibolite facies metamorphism. In addition to two microstructural and compositional varieties of garnet, the muscovite porphyroblasts showing the hourglass structure with graphite and quartz probably represent former chiastolite that was replaced by a single crystal of muscovite during later metamorphic process. Based on the stability field of minerals in graphite-bearing pelitic rocks (Likhanov et al., 2001), the presumed andalusite without garnet and cordierite suggests low-pressure (below 3 kbar) metamorphism at temperatures ~500–550 °C. To constrain the garnet growth-related metamorphic evolution of micaschist, we used microstructural relationships in combination with phase equillibrium modelling and PT section approach (Connolly 2005), biotite-garnet exchange thermometery (Ganguly et al., 1996; Holdaway, 2000) and garnet-biotite-plagioclase-quartz barometry (Wu et al., 2006).
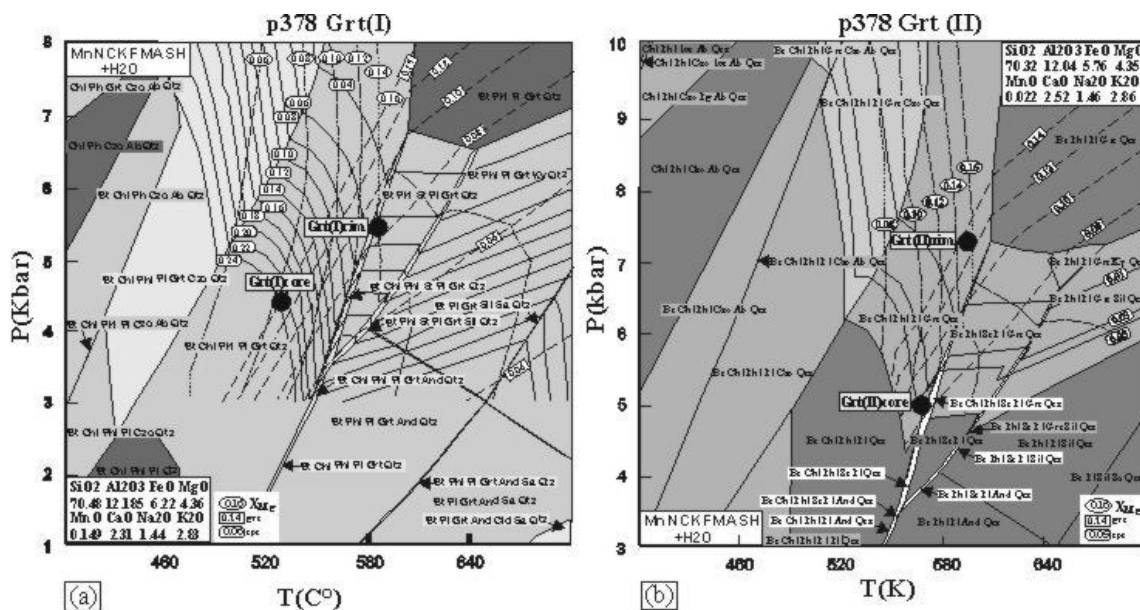
Fig. 11. PT sections (MnNCKFMASH system) constrained for micaschist sample p378 (for location see Fig. 1). (a) shows PT section calculated with the XRF whole rock composition covering the growth of core garnet (I) and (b) shows PT section calculated with the fractionated whole rock composition (see text for details) covering the growth of rim garnet (II). Solid black circles indicate intersection of garnet compositional isopleths (X_{Mg}, grs and sps) for the core and rim compositions of garnet (I) and (II). Bulk rock composition in molar% is indicated in each PT section.

The PT sections were calculated in the thermodynamic software Perple_X (Connolly 2005: version 07), with internally consistent thermodynamic dataset of

Holland & Powell (1998; 2003 upgrade). As for the whole-rock composition, mineral chemistry (particularly high Mn content in garnets) and modal proportion of mineral phases, the P–T sections were calculated in the MnO-Na$_2$O-CaO-K$_2$O-FeO-MgO-Al$_2$O$_3$-SiO$_2$-H$_2$O (MnNCKFMASH) system with excess water. Because the micaschist contains relatively high proportion (5–6 modal%) of garnet with two distinct types of compositional zoning, two PT sections reflecting fractionation of bulk rock composition during garnet (I) and garnet (II) growth have been calculated. To construct the PT section for garnet (I) (Fig. 11a), we used the whole rock composition obtained by X-ray fluorescence (XRF) analysis. The second PT section for the garnet (II) (Fig. 11b) was constructed on the basis of effective bulk rock composition. The effective bulk rock was obtained by extracting the garnet (I) from the whole rock composition. The modal proportion of garnet (I) was determined by image analysis from several BSE images of the studied thin section. In addition to the plagioclase solution model by Newton et al. (1980) and the garnet model by Berman (1990), we used the solution models of White et al. (2001) for NCKFMASH end-member phases expanded by the Mn end-members (Tinkham et al. 2001).

The PT sections calculated for sample p378 (for location see Fig. 1) indicate that garnet (I) and (II) compositions plot into Grt-Bt-Ms-Chl-Pl-Q stability field, which is in a good agreement with observed mineral assemblage (Fig 11). Intersections of isopleths for garnet (I) core and rim (Fig. 9c) suggests an increase in PT conditions from 4.4 kbar/525 °C to 5.4 kbar/585 °C (Fig. 11a, Table 1). An increase in PT conditions from 4.9 kbar/560 °C to 7.3 kbar/600 °C is also recorded by the core and rim composition of garnet (II) (Fig. 11b, Table 1). These values indicate that the garnet (II) core shows lower pressure and temperature than the rim of garnet (I) (Fig. 12). The thermometry of Ganguly (1996) and Wu et al. (2006) indicates slightly higher temperature of 634±25 °C and 651±12, respectively, for the rim composition of garnet (II) and matrix biotite (Table 1). The garnet-biotite-plagioclase-quartz barometry of Wu (2006) gave pressure of 8.1±0.9 kbar (Table 1). All of these PT estimates are similar to those obtained for the basement orthogneisses and amphibolite (Rahmati-Ilkhchi et al., in press).

PT conditions of the Permian–Lower Jurassic have not been treated by mineral composition or other relevant method; however, the newly growing minerals (white

mica, chlorite, calcite and locally albite) suggest that the metamorphism of these rocks correspond to greenschist to lower part of the greenschist facies conditions. Formation of chlorite porphyroblasts with white or brown mica (mixed-layer phyllosilicate), occurring in the Shemshak formation, suggest very low-grade metamorphic conditions below the greenschist facies (Fraceshelli et al., 1986, Arkai et al., 2003).

Table 1. Microprobe analyses of minerals in garnet-bearing micaschist (sample p378)

	Grt(I)-c	Gr (I)-r	Grt(II)-c	Gr(II)-r	Bt	Ms	Pl
SiO_2	37.12	37.45	38.03	37.77	36.27	47.31	59.63
TiO_2	0.05	0.00	0.06	0.00	1.65	0.92	0.01
Al_2O_3	20.34	20.62	20.88	21.24	17.14	33.92	25.15
FeO	28.51	30.07	34.74	34.01	20.43	1.36	0.19
MnO	7.49	5.84	1.36	0.36	0.12	0.00	0.10
MgO	2.04	1.91	2.85	3.34	9.05	1.17	0.02
CaO	3.68	3.80	2.55	3.84	0.07	0.03	7.26
Na_2O	0.08	0.04	0.00	0.00	0.11	0.93	7.59
K_2O	0.04	0.00	0.03	0.00	9.23	10.11	0.04
	99.35	99.74	100.51	100.55	94.05	95.75	99.98
Si	3.019	3.028	3.037	3.004	2.889	3.137	2.660
Ti	0.003	0.000	0.004	0.000	0.099	0.046	0.000
Al	1.952	1.979	1.988	1.991	1.609	2.650	1.322
Cr	0.000	0.000	0.000	0.000	0.000	0.000	0.000
Fe^{3+}	0.094	0.063	0.042	0.044	0.000	0.000	0.007
Fe^{2+}	1.848	1.985	2.305	2.218	1.361	0.075	0.000
Mn	0.516	0.403	0.093	0.024	0.008	0.000	0.004
Mg	0.248	0.232	0.344	0.396	1.075	0.115	0.001
Ca	0.321	0.331	0.221	0.327	0.006	0.002	0.347
Na	0.013	0.007	0.000	0.000	0.016	0.120	0.657
K	0.004	0.000	0.003	0.000	0.938	0.855	0.002
Xmg	0.118	0.105	0.130	0.151	0.441		
Alm	63	67	78	75			
Pyr	8	8	12	13			
Grs	11	11	7	11			
Sps	18	14	3	1			

PT Conditions, calculated garnet-biotite thermometry and garnet-biotite-plagioclase-quartz barometry

	Ganguly	Wu(GB-GBPQ)	Wu(GB-GBPQ)
T	634±25	651±12	8.1±0.5

3.6. Discussion

3.6.1. Polymetamorphic record in the Shotur Kuh complex

As mentioned above, the basement orthogneiss and amphibolites show relatively simple metamorphic history characterized by prograde metamorphism reaching amphibolite facies conditions. The core to rim compositional change in garnets from the orthogneiss documents PT increase from 7 kbar/600 °C to 8.5 kbar/650 °C while amphibolite indicate slightly higher pressures of 8–10 kbar (Rahmati-Ilkhchi et al., in press). Compositional zoning of garnets in orthogneiss (sample p99) and micaschist (sample p378, for location see Fig. 1) indicate similar dP/dT gradients and PT conditions reaching kyanite stability field (Fig. 12). Indeed the presence of kyanite has been documented in amphibolites (Rahmati-Ilkhchi et al., in press) and it is consistent with Barrovian metamorphic field gradient of 20–22 °C km^{-1} obtained from the PT sections (Fig. 12).
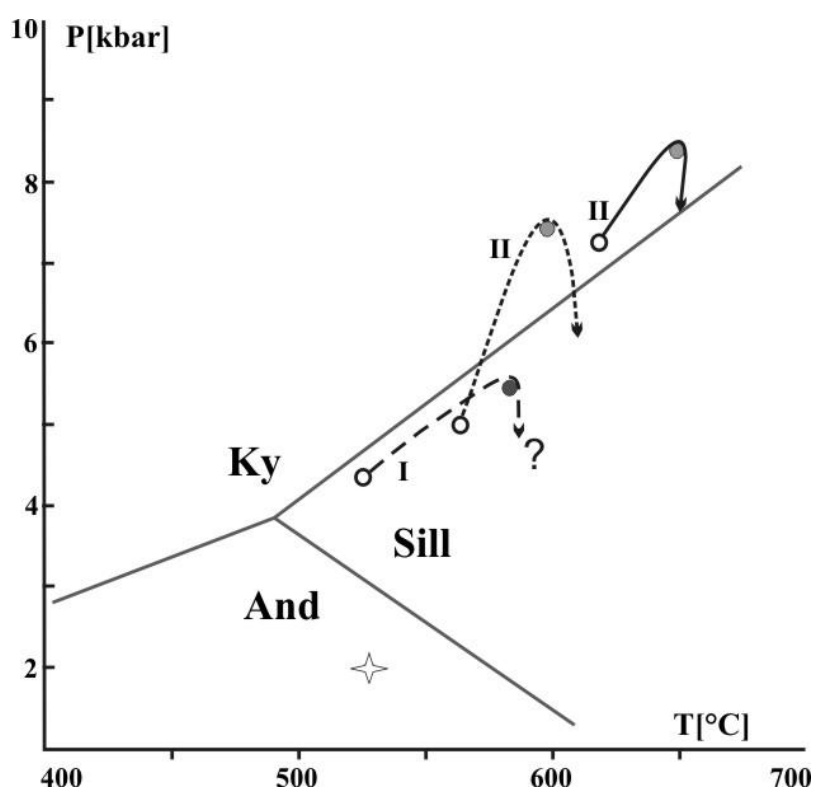
Fig. 12. Summary of PT conditions calculated by using phase equilibrium modelling for basement orthogneisses sample p99 (see Fig. 1 for location) (solid curve, Rhamati-Ilkhchi et al., in press) and for micaschist sample p378 (dashed and dotted curves, this study). PT paths (I and II) in micaschists are based on PT sections (Fig. 10) constructed for the core garnet (I) and rim garnet (II). Star indicates possible thermal event based on the pseudomorphs of muscovite after andalusite or cordierite.

In contrast to the orthogneisses and amphibolite, the micaschists show evidence for polymetamorphic evolution. The earliest metamorphic phase in these rocks is manifested by large rhomboid porphyroblasts of muscovite with hourglass structure or sector trilling inclusion pattern, which probably represents pseudomorphs after chiastolite or cordierite (Fig. 9). As these high-temperature and low-pressure phenomena were observed only in one case, they might be related to a local contact metamorphic event (Fig. 12). Subsequent metamorphism in these rocks is mainly represented by a growth of two compositional varieties of garnet (Fig. 10). By using garnet compositional isopleths in the calculated PT sections (Fig. 11), the compositional zoning of core garnet (I) indicates PT increase from 4.4 kbar/525 °C to 5.4 kbar/585 °C and the rim garnet (II) indicates PT increase from 4.9 kbar/560 °C to 7.3 kbar/600 °C (Fig. 12). As summarized in Fig. 12, both garnets indicate prograde metamorphism although the prograde PT path segments for each garnet differ in dP/dT gradient exhibiting lower gradient for garnet (I) and higher gradient for garnet (II). Furthermore, the reversal in compositional zoning trends of calcium and iron separating the garnet (I) from garnet (II) is marked by a disturbance of manganese and magnesium, which in the calculated PT sections suggests slight (0.5 kbar and 20 °C) drop in pressure and temperature between the garnet (I) rim and the garnet (II) core. It is not clear, whether this compositional change occurs during single metamorphic event as a result of progressive burial, or it relates to two distinct metamorphic events separated by a period of cooling/exhumation. The observed element disturbance, including Mn contents, at the garnet (I)/(II) interface suggests partial resorbtion of the garnet (I) and subsequent formation of garnet (II) supporting a separate metamorphic events. However, such disturbance in compositional zoning could also occur during a single metamorphic event, if the rock had crossed the staurolite stability field. More detailed study on the micashist is needed to confirm one or the other alternative. Another question that remains unclear is the lithological similarity of the micaschist (intercalating marble) with the Permian-Triassic cover rocks. The cover rocks, however, show only greenschist facies conditions where greenish biotite is present at the contact to the micaschist and basement rocks and the degree of metamorphism decrease upwards. There are two alternatives to explain the metamorphic gap between micaschists and the Permian-Triassic metasediments: 1) the micaschists represent an older (pre-Permian) sedimentary formation that was eventually affected by a contact metamorphism prior to its amphibolite facies metamorphism, or 2) they derived from

the Permian-Triassic strata and their present juxtaposition is a result of extensional detachment shearing at the basement/cover contact (see below). The second alternative is supported by the similarities in lithology and deformation character of the micaschist and overlaying Permian-Triassic rocks.

3.6.2. Tectonic evolution of the Shotur Kuh complex

D1 deformation is associated with the development of high grade metamorphic foliation S1 in the basement and Permian–Lower Jurassic cover. In the orthogneiss and micaschist, the S1 fabric contains prograde garnets indicating that it formed during progressive burial of the Shotur Kuh complex. As the S1 fabric exhibits decrease in metamorphic grade from amphibolite facies in the basement to lower greenschist facies towards the Lower Jurassic Shemshak Formation in the cover, the D1 event is probably associated with a period of crustal thickening (Fig. 13). This is supported by the Barrovian type metamorphic field gradient derived for orthogneiss and micaschist imposing collision of continental crustal blocks. The original orientation of S1 fabric is difficult to predict due to an intense overprint by subsequent deformation events. However since S1 is suggested to have formed during a crustal thickening stage, it is likely that it was initially steep. This is supported by the presence of isoclinal F2 folds, which document angular relationship between S1 and subhorizontal, axial planar fabric S2.

D2 deformation is associated with vertical shortening of S1 fabric and formation of axial planar cleavages S2 whose orientation reflects domal structure of the Shotur Kuh complex (Fig. 6). Microstructural analysis of D2 deformation structures (Fig. 4) indicate that they developed at various PT conditions ranging from amphibolite to greenschist facies conditions in the basement and greenschist to very low-grade conditions in the cover. This is manifested by the lack of retrogression within isoclinally folded amphibolite (Fig. 4a) and formation of the greenschist facies S2 cleavage in the orhogneiss (Fig. 7b and 4b), micaschist and Permian–Lower Jurassic metasediments (Fig. 4c-f). In the basement, however, the spatial proximity of D2 structures with contrasting metamorphic grade suggests progressive decrease in PT conditions related to exhumation of the Shotur Kuh complex. In this context, the D2 deformation records buyoancy driven lower crustal upflow, which follows a period of thermal relaxation of previously thickened Shotur Kuh crust. The excess in

gravitational potential energy led to a local extensional collapse and updoming of the Shotur Kuh complex (Fig. 13). At the same time, we cannot rule out the hypothesis that this process is part of a large-scale extension in the Great Kavir Block.

Regional variations in the degree of D2 deformation overprint across the Shotur Kuh basement manifested by quartz deformation microstructures (Fig. 7d) indicate that the intensity of D2 overprint increases towards the basement/cover contact. This observation is in an excellent agreement with rather sharp metamorphic gradient at the basement/cover contact thus proposing the existence of low angle detachment shear zone juxtaposing the higher-grade basement core and lower-grade cover. The updoming/unroofing of the basement core is associated with the development of NW–SE trending lineation and top-to-the-NW kinematic indicators documenting the north-westward transport of the upper crustal portions (Fig. 13). In this concept the alternation of basement and cover rocks in the east of the Shotur Kuh complex (see Fig. 1) represent extensional duplexes

D1 and D2 structural-metamorphic record has been equally recognized in the basement and the Permian–Lower Jurassic cover while the Middle Jurassic conglomerates, directly overlying Lower Jurassic meta-shales of the Shemshak Formation, are virtually unmetamorphosed and contain pebbles of basement orthogneiss. This indicates that D1 burial and D2 exhumation of the Shotur Kuh complex must have occurred close to the Lower/Middle Jurassic boundary and in relatively quick succession. Such time constraint roughly corresponds to the Ar-Ar total gas cooling age of 160.4 ± 2.8 Ma obtained from muscovite in the basement orthogneiss (Rahmati-Ilkhchi et al., in press).

D3 deformation, equally affecting basement and Permian–Lower Cretaceous cover, is associated with folding induced by subhorizontal shortening in the NE–SW direction (Fig. 13). The angular unconformity between upright stratification of Lower Cretaceous limestone and horizontal stratification of Paleocene conglomerate (Fig. 8e) suggests Upper Cretaceous age of the D3 event.

D4 folding affects all the rock units of the Shotur Kuh complex, including Paleocene and Miocene, thus indicating post-Miocene age of this event. Steep NE–SW trending axial planes of the F4 folds indicate subhorizontal shortening in the NW–SE direction (Fig. 13).

Lower / Middle Jurassic

NE   SW

S1   S1

Lower / Middle Jurassic

NW   SE

S2   S2

Late Creataceous

NE   SW

Ap3

Late Miocene to post Miocene

NW   SE

?   ?

Ap4

Basement   Cretaceous Limestone

Permian-Triassic
Dolomaite and Limestone   Paleocene
                                   Conglomerate
Upper Triassic- Lower Jurassic
Shemshak Formation   Miocene
                                   Conglomerate
Middle Jurassic
Conglomerate
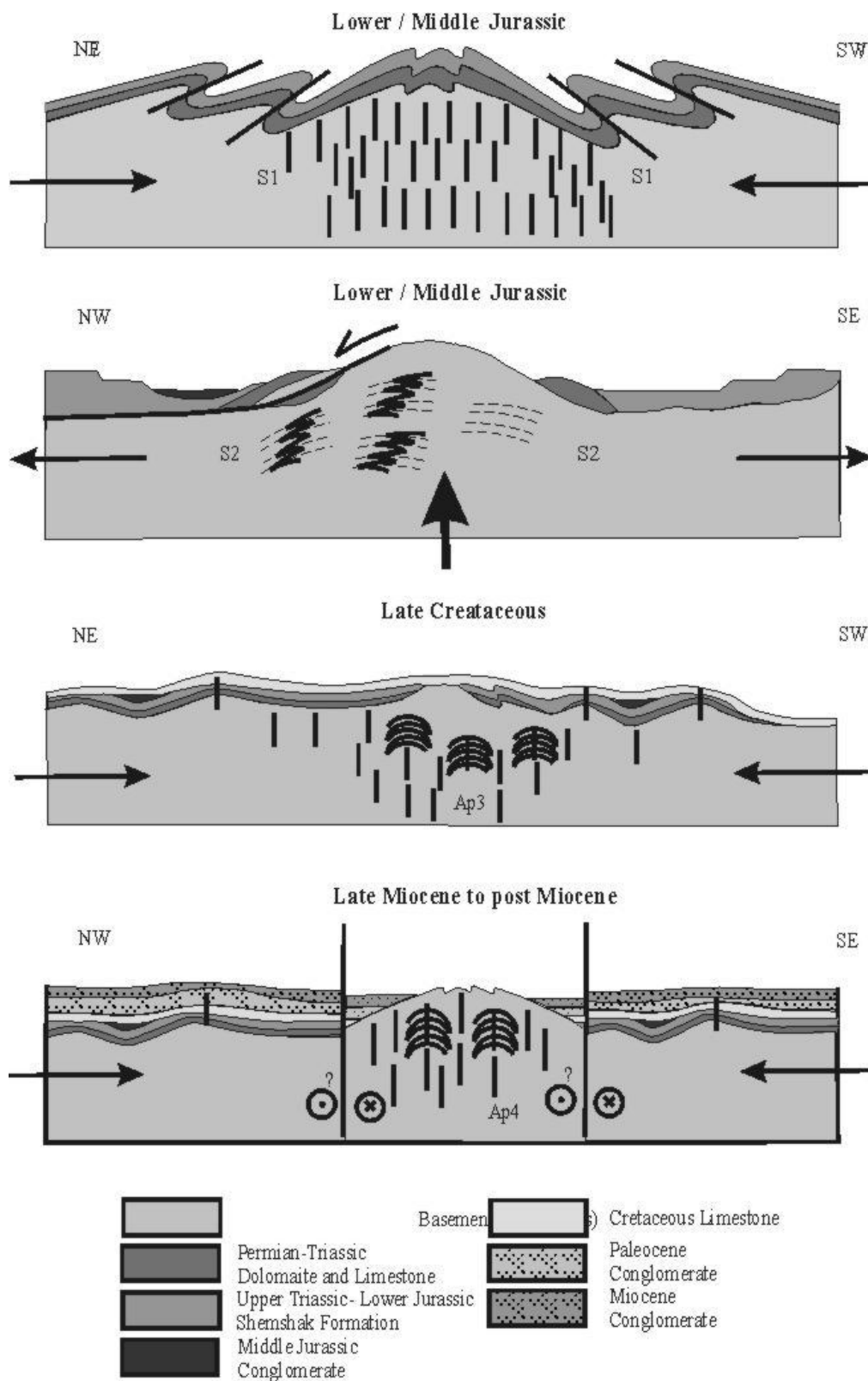
Fig. 13 Sketch showing Summary of tectonic evolution of the Shotur Kuh complex

3.6.3. Regional implications

The Cimmerian tectono-metamorphic processes that occurred in the Central Iranian domain and Sanandaj-Sirjan zone are mostly related to the closure 1) of Paleo-Thethys in Carboniferous – Mid- to Late Triassic (Early-Cimmerian) event (Paul et al., 2003; Ramezani and Tucker, 2003; Sheikholeslami et al., 2008; Bagheri and Stampfli, 2008), and 2) of Neo-Tethys in Cretaceous–Eocene (Late-Cimmerian–Early Alpine) event (Ramezani and Tucker, 2003; Bagheri and Stampfli, 2008). However, new geochronological data of Jurassic age in this region (Khalatbari-Jafari, 2003; Rachidnejad-Omran et al., 2002; Sheikholeslami et al., 2003, 2008; Falznia et al., 2007; Bagheri and Stampfli, 2008; Rahmati-Ilkhchi et al. in press) led to consideration of an older concept of Mid-Cimmerian event of Aghanabati (1992) and several other evolutionary scenarios. For example, the Ar-Ar ages spanning between 187–156 Ma from the Anarak-Jandaq terrane of the Yazd block have been interpreted as a cooling subsequent to the Late Triassic (Early-Cimmerian) or even older metamorphic phase (Bagheri and Stampfli, 2008). In contrast, the zircon SHRIMP U-Pb (187±2.6 Ma) and monazite CHIME U-Th-Pb (180±21 Ma) ages from partial melts within the Qori complex in the Sanadaj-Sirjan zone have been interpreted as an extended phase of the Early-Cimmerian metamorphism (Falznia et al., 2007; 2009). According to Falznia et al. (2009), this metamorphism relates to collision between the Central Iranian domain and Arabian plates prior to opening of the Neo-Tethys Ocean, marked by intracontinental rifting and related an orogenic magmatism in Middle Jurassic (173±1.6 Ma). In this concept, the Upper Jurassic (147±0.76 Ma) arc-related metamorphism documents the beginning of a young and buoyant Neo-Tethys subduction. On the other hand, recent paleogeographic reconstructions assume either an independent Jurassic–Cretaceous drift of Sanandaj-Sirjan zone within the Neo-Tethys realm (Golonka, 2004) or a drift of the whole Cimmerian block within the frame of closing Paleo-Tethys in the north and simultaneous opening of Neo-Tethys in the south (Stampfli and Borel, 2004; Bagheri and Stampfli, 2008). Both these scenarios impose relatively long-term (Triassic–Cretaceous) existence of the Neo-Tethys Ocean that during its northward subduction facilitated formation of several back-arc basins (Bagheri and Stampfli, 2008).

Despite temporal proximity of Lower/Middle Jurassic metamorphism in the Qori and in the Shotur Kuh complexes, the burial and exhumation of the Shotur Kuh

complex cannot be related to an extended period of Early-Cimmerian event. This is because the D1 and D2 deformation and metamorphism in the Shotur Kuh affected both basement and Permian–Lower Jurassic sediments including the Shemshak Formation, which represents mollasic/forland deposition post-dating the Early-Cimmerian event (Assereto, 1966; Stocklin, 1968; Alavi 1996). Following Alavi (1992), who established the Middle Jurassic orogenic event in the Alborz region on the basis of tectono-metamorphic overprint of the Shemshak Formation, we attribute the metamorphism in the Shotur Kuh complex to the Mid-Cimmerian orogeny. The question remains, whether the Mid-Cimmerian event represents a broader orogenic process or it related to a series of Middle Jurassic–Cretaceous back-arc extensional events and compressional cycles controlled by northward subduction of the Neo-Tethys Ocean (Bagheri and Stampfli, 2008). Indeed, some mafic and ultramafic rocks near Kuh Siah Poshteh in Moalleman and small remnant of ophiolite near the Khondar anticline in Meyamey occur about 100 km to the SW and 95 km to the NE from the Shotur Kuh complex, respectively. The age data from these complexes are not available, but they are considered to represent remnants of ophiolites of pre-Cretaceous time (Jafariyan, 2000, Amini Chehragh, 1999). On the other hand, the Lower/Middle Jurassic extension/exhumation in the Shotur Kuh complex overlaps with the intracontinental rifting within the Cimmerian block (e.g. Falznia et al., 2009) and thus suggests an independent Mid-Cimmerian orogenic event prior to the major extensional process in the back-arc domain.

The Cretaceous to lower Eocene Sabzevar and Nain ophiolite complexes (Rossetti et al., 2009; Davoudzadeh, 1972) occurring to the NE and SW from the Shotur Kuh, respectively, are roughly NW–SE trending. Their alignment reflects the Late-Cimmerian – Early Alpine, probably NE–SW directed (cf. Sheikholeslami et al., 2008) closing of several back-arc basins across the Cimmerian domain at the late stages of Neo-Tethys closure. These directions are in perfect agreement with the observed Late Cretaceous NE–SW shortening D3 in the Shotur Kuh complex and imply a propagation of the deformation front inland.

The Late Miocene NW–SE shortening D4 in the Shotur Kuh complex is associated with the Alborz and Zagros phase of the Late Alpine collision between the Arabian and Eurasian plates (e.g. Alavi, 2004; Guest et al., 2006). Although our D4 compressional stress deviates from the roughly N–S directed convergence of the two plates, local stress field deviations are expected in case of a complex geometry of

interacting crustal segments with different rheological properties (Soukotis et al., 2000).

3.7. Conclusions

On the basis of structural, metamorphic and stratigraphic record, we distinguish following stages of tectonometamorphic evolution of the Shotur Kuh complex:

1) Lower/Middle Jurassic collisional crustal thickening led to Barrovian metamorphism with field metamorphic gradient of 20–22 °C km^{-1} that affected Neoproterozoic–Cambrian basement granitoids as well as Permian–Lower Jurassic cover rocks including the Shemshak Formation.

2) Subsequent exhumation of the Shotur Kuh complex marked by the deposition of Middle Jurassic conglomerates with pebbles of basement orthogneiss and Permian–Lower Jurassic cover, is associated with an upflow of lower crust resulting in updoming of the basement core and its top-to-the-Northwest unroofing along a low angle detachment shear zone at the basement/cover boundary. Both processes are affiliated to the Mid-Cimmerian event, which in turn might be associated with a series of Jurassic–Cretaceous collisional and extensional processes in the back-arc domain controlled by the Neo-Tethyan subduction.

3) Upper Cretaceous folding event is probably related to the Late-Cimmerian–Early Alpine orogeny which resulted from the convergence of Arabian and Eurasian plates, and the Cenozoic closure of the Neo-Tethys oceanic tract(s) by subduction.

4) Late Miocene to post-Miocene folding event is probably associated with Late Miocene Zagros and Alborz phase of N–S convergence between Arabian and Eurasian plates. This shortening event could be also combined with a left-lateral activity along the Great Kavir fault bounding system.

3.8. References

Aghanabati, A., 1992. Representing the Mid-Cimmerian tectonic event in Iran. Scientific Quarterly Journal, Geosciences, Vol. 6. Geological Survey of Iran.

Alavi M., l992 Thrust tectonics of the Binalood region. NE Iran: Tectonics I.I 360-370.

Alavi M., l996 Tectonostratigraphic Synthesis and Structural style of the Alborz Mountain System in northern Iran. J. Geodynamics Vol. 21, No. 1, pp. l-33.

Alavi, M., 2004. Regional stratigraphy of the Zagros fold-thrust belt of Iran, and its proforeland evolution. American Journal of Science 304, 1–20.

Árkai, P., Faryad, S.W., Vidal, O., Balogh, K. (2003): Very low-grade metamorphism of sedimentary rocks of the Meliata unit, Western Carpathians, Slovakia: implications of phyllosilicate characteristics - International Journal of Earth Sciences, 92, 68-85.

Assereto, R., 1966 The Jurassic Shemshak Formation in central Elburz (Iran). Riv Ital Paleont Stratigr 72:1133–1182

Amini Chehragh,1999. Geological map of Meyamey (scale 1:100,000). Geological Survey of Iran Tehran Iran.

Bagheri, H., Moore, F., Alderton D.H.M 2007. Cu–Ni–Co–As (U) mineralization in the Anarak area of central Iran. Journal of Asian Earth Sciences 29, 651–665.

Bagheri, S., Stampfli, G.M., 2008 The Anarak, Jandaq and Posht-e-Badam metamorphic complexes in central Iran: New geological data, relationships and tectonic implications. Tectonophysics 451:123–155

Baharifar,A. Moinevaziri, H., Bellon, H., Piqué, A,. 2004. The crystalline complexes of Hamadan (Sanandaj–Sirjan zone, western Iran): metasedimentary Mesozoic sequences affected by Late Cretaceous tectono-metamorphic and plutonic events. C. R. Geoscience 336, 1443–1452.

Berberian, F., Berberian, M., 1981 Tectono-plutonic episodes in Iran. In: Gupta HK and Delany FM (eds) Zagros-Hindu Kush-Himalaya Geodynamic Evolution. American Geophysical Union, Geodynamics Series 3, pp 5-32

Berberian, M., King, G.C.P., 1981. Towards a Paleogeography and Tectonic Evolution of Iran. Can J Earth Sci 8:210–265

Berman R. G., 1990. Mixing properties of Ca–Mg–Fe–Mn garnets. American Mineralogist 75:328–344.

Connolly, J.A.D., 2005. Computation of phase equilibria by linear programming: a tool for geodynamic modeling and its application to subduction zone decarbonation. Earth Planet Sci Lett 236:524–541

Crawford, A.R., 1977 A summary of isotopic age data for Iran, Pakistan and India: Memoire Societe Geologique de France 8:251–260

Davoudzadeh, M., 1972. Geology and petrography of the area north of Nain, Central Iran. Geol. Surv. Iran Rep., 14: 89 pp.

Fazlnia, A.N., Moradian, A., Rezaei, K., Moazzen, M., Alipour, S., 2007. Synchronous activity of anorthositic and S-type granitic magmas in the Chah Dozdan batholith, Neyriz, Iran: evidence of zircon SHRIMP and monazite CHIME dating. Journal of Sciences, Islamic Republic of Iran 18, 221-237.

Fazlnia, A.N., Schenk, V., Straaten, F. V. D., Mirmohammadi, M., 2009 Petrology, Geochemistry, and Geochronology of Trondhjemites from the Qori Complex, Neyriz, Iran. *LITHOS* doi: 10.1016/j.lithos.2009.03.047.

Franceschelli, M., Mellini, M., Turbanti Memmi, I. Ricci, C.A.,. 1986 - Fine-scale chlorite muscovite association in low-grade metapelites from Nurra (NW Sardinia) and the possible misidentification of metamorphic vermiculite. Contr. Miner. Petr., 93, 137-143.

Ganguly, J., Cheng, W., Tirone, M., 1996 Thermodynamics of alumosilicate garnet solid solution: new experimental data, an optimized model, and thermodynamic application. Contrib Mineral Petrol 126:137–151.

Gansser, A., Gupta, H.K., Delany, F.M., 1981. The geodynamic history of the Himalaya, Zagros, Hindu Kush, Himalaya; geodynamic evolution. Geodynamics Series 3, 111–121.

Golonka, J., 2004. Plate tectonic evolution of the southern margin of Eurasia in the Mesozoic and Cenozoic. Tectonophysics 381, 235-273.

Guest, B., Stockli, D., Grove, M., Axen, G.J., Lam, P.S., Hassanzadeh, J., 2006 Thermal histories from the central Alborz Mountains, northern Iran: Implications for the spatial and temporal distribution of deformation in northern Iran. Geological Society of America v. 118; no. 11/12; p. 1507–1521.

Holland, T.J.B., Powell, R., 1998. An internally consistent thermodynamic data set for phases of petrological interest. J Metam Geol 16:309–343.

Holland, T.J.B, Powell, R., 2003. Activity-composition relations for phases in petrological calculations: an asymmetric multicomponent formulation. Contrib Mineral Petrol 145:492–501

Holdaway, M.J., 2000 Application of new experimental and garnet Margules data to the garnet-biotite geothermometer. Am Mineral 85:881-892

Jafarian, M.B., 2000. Geological map of Kalateh-Reshm (scale 1:100,000)sheet No 6860. Geological Survey of Iran Tehran Iran.

Khalatbari-Jafari, M., Juteau, T., Bellon, H., Emami, H. 2003 Discovery of two ophiolite complexes of different ages in the Khoy area (NW Iran) C. R. Geoscience 335 917–929.

Kretz, R., 1983. Symbols For Rock-Forming Minerals. American Mineralogist, 68(1-2), 277-279.

Likhanov, I.I., Reverdatto, V.V., Sheplev, V.S., Verschinin, A.E. and Kozlov, P.S. 2001. Contact metamorphism of Fe- and Al-rich graphitic metapelites in the Transangarian region of the Yenisei Ridge, eastern Siberia, Russia. Lithos 58, 55–80

Newton, R.C., Charlu, T.V., Kleppa, O.J., 1980. Thermochemistry of the high structural state plagioclases. Geochim Cosmochim Acta 44:933-941

Paul, A., Kaviani, A., Hatzfeld, D., Mokhtari, M., 2003 Lithospheric structure of central Zagros from seismological Tomography. Four International Conferences of Earthquake Engineering and Seismology 12–14 May, Tehran Iran

Poirier, J. P. & Guillope, M. 1979. Deformation induced recrystallization of minerals. In: Mecanismes de deformation des mineraux et des roches (edited by Nicolas, A., Darot, M. & Willaime, C.). Bulletin de Mineralogie 102; 2-3. Masson, Paris, France, 67-74.

Rachidnejad-Omran N., Emami, M.H., Sabzehei, M., Rastad, E., Bellon, H., and Piqué, A., 2002 Lithostratigraphie et histoire paléozoïque à paléocène des complexes métamorphiques de la région de Muteh, zone de Sanandaj- Sirjan (Iran éridional): Comptes rendus Geoscience, v. 334, p. 1185–1191.

Rahmati Ilkhchi, M., 2002 Geological map of Razveh (scale 1:100,000).Geological Survey of Iran, Tehran Iran

Ramezani, J., Tucker, R.D., 2003 The Saghand Region, Central Iran: U–Pb geochronology, petrogenesis and implications for Gondwana tectonics. Am J Sci 303: 622–665.

Rossetti, F., Nasrabady, M. Vignaroli, G., Theye, T., Gerdes, A. Razavi, M.H. and Vaziri. H.M. 2009. Early Cretaceous migmatitic mafic granulites from the Sabzevar Range (NE Iran): implications for the closure of the Mesozoic peri-Tethyan oceans in central Iran. Tectonics (in press).

Sengör, A.M.C., 1990, Plate tectonics and orogenic research after 25 years; a Tethyan perspective: Earth Science Reviews, Elsevier Science Publishers, v. 27, p. 1–201.

Sengör, A.M.C., Altiner, D., Cin, A., Ustaomer, T., and Hsu, K.J., 1988, Origin and assembly of the Tethyside orogenic collage at the expense of Gondwana Land, in Audley-Charles, M.G., and Hallman, A., eds., Gondwana and Tethys: Geological Society [London] Special Publication 37, p. 119–181.

Sengör, A.M.C., and Natal'in, B.A., 1996a, Paleotectonics of Asia; fragments of a synthesis, in Yin, An, and Harrison, Mark, eds., The tectonic evolution of Asia: Cambridge, U.K., Cambridge University Press, p. 486–640.

Sheikholeslami, R., Bellon, H., Emami, H., Sabzehei, M., Piqué, A., 2003. Nouvelles données structurales et datations 40K-40Ar surles roches métamorphiques de la region de Neyriz (zone de Sanandaj-Sirjan, Iran méridional). Leur intérêt dans le cadre du domaine néo-tethysien du Moyen-Orient. Compates Rendus Geoscience 335, 981-991.

Sheikholeslami, MR., Pique, A., Mobayen, P., Sabzehei, M., Bellon, H., Emami, M.H., 2008 Tectono-metamorphic evolution of the Neyriz metamorphic complex, Quri-Kor-e-Sefid area (Sanandaj-Sirjan Zone, SW Iran) J Asian Earth Sci 31:504–521

Sokoutis, D., Bonini, M., Medvedev, S., Boccaletti, M., Talbot, C.J., Koyi, H., 2000 Indentation of a continent with a built-in thickness change: experiment and nature. Tectonophysics 320, 243–270

Stampfli, G.M., 1978 Etude géologique générale de l'Elburz oriental au S de Gonbad-e-Qabus, Iran N-E. Fac Sci Univ Genève Thesis No 1868 pp 329

Stampfli, G.M., Borel, G.D., 2002. A plate tectonic model for the Paleozoic and Mesozoic constrained by dynamic plate boundaries and restored synthetic oceanic isochrons. Earth and Planetary Science Letters 196, 17–33.

Stampfli, G., Marcoux, J., and Baud, A., 1991, Tethyan margins in space and time: Palaeogeography, Palaeoclimatology, Palaeoecology, v. 87, p. 374–409.

Stipp, M., Stünitz, H., Heilbronner, R. & Schmid, S. M. 2002a. Dynamic recrystallization of quartz: correlation between natural and experimental

conditions. In: Deformation mechanisms, rheology and tectonics: current status and future perspectives. (edited by de Meer, S., Drury, M.R., de Bresser, J. H. P. & Pennock, G. M.). Geological Society Special Publications 200.Geological Society, London, 171-190.

Stipp, M., Stünitz, H., Heilbronner, R. & Schmid, S. M. 2002b. The eastern Tonale fault zone: a 'natural laboratory' for crystal plastic deformation of quartz over a temperature range from 250 to 700 degrees C. Journal of Structural Geology 24(12), 1861-1884.

Stöcklin, J., 1968 Structural history and tectonics of Iran: a review. Amer Assoc Petroleum Geol Bull 52 (7): 1229–1258

Stocklin, J., 1974. Possible Ancient Continental Margins in Iran. In: Burke, C.A., Drake, C.L. (Eds.), The Geology of Continental Margins. Springer Verlag, New-York, pp. 873–887.

Takin M (1972) Iranian geology and continental drift in the Middle East: Nature 235:147–150.

Tinkham, D. K., Zuluaga, C. A. & Stowell, H. H., 2001. Metapelite phase equilibria modeling in MnNCKFMASH: The effect of variable Al_2O_3 and MgO/(MgO + FeO) on mineral stability. Geological Materials Research, 3, 1-42

Urai, J. L., Means, W. D. & Lister, G. S. 1986. Dynamic recrystallization of minerals. In: Mineral and Rock Deformation: Laboratory Studies; the Paterson Volume. (edited by Hobbs, B. E. & Heard, H. C.). Geophysical Monograph 36. American Geophysical Union, Washington, DC, UnitedStates, 161-199.

White, S. 1979. Grain and sub-grain size variations across a mylonite zone. Contributions to Mineralogy and Petrology 70(2), 193-202

White, R. W., Powell, R. & Holland, T. J. B., 2001. Calculation of partial melting equilibria in the system Na_2O- CaO-K_2O-FeO-MgO-Al_2O_3-SiO_2-H_2O (NCKFMASH). Journal of Metamorphic Geology, 19(2), 139-153.

Wu, CM., Cheng, B.H., 2006. Valid garnet-biotite (GB) geothermometry and garnet-aluminum silicate-plagioclase-quartz (GASP) geobarometry in metapelitic rocks. Lithos 89:1-23

CHAPTER 4

4.1. Summary and further research directions

Geochemical and geochronological data from igneous and metaigneous rocks in Iran show that the Neoproterozoic arc magmatism significantly contributed to the formation and consolidation of the Central Iran microplate (Ramezani and Tucker, 2003). This is confirmed also by our research results, indicating that the arc-related igneous rocks are present not only along the boundaries of the Central Iran block but also in all parts of this microplate. Because most of the Iran territory is represented by the Mesozoic sedimentary sequences, which form either thrust belts or covers of the basement blocks, it is difficult to obtain data about metamorphism and deformation of the Neoproterozoic crust and to reconstruct its pre-Mesozoic metamorphic history. Recent advances in getting various geochronological data (Table 1, Fig. 7, Chapter 1) from different geological units in Iran confirmed that the Central Iran basement units not only were affected by the Upper Cretaceous metamorphism and deformation but also experienced older (Lower, Middle, Late Cimmerian and Variscan) metamorphic processes. Most crystalline complexes, simply referred to as the pre-Cambrian basement units in Iran (Berberian et al., 1981), therefore need reinterpretation and modification in order to clear their tectono-metamorphic history and their relations to individual crustal blocks or metamorphic belts.

Metamorphic petrology from the Shotur Kuh complex showed a Middle-Jurassic amphibolite facies metamorphism that affected both the Neoproterozoic igneous rocks and adjacent sedimentary sequences. Based on their metamorphic mineral assemblages, estimated PT conditions, and structural analyses, at least three metamorphic and four deformation events can be recognized in the basement rocks. Evidence for the first two metamorphic events (low-pressure/medium-temperature and medium-pressure epidote amphibolite facies metamorphism) were recognized only in the metapelitic rocks (micaschists) adjacent to the orthogneisses and amphibolite. Based on the microfabrics (inclusions pattern of graphite and quartz) in muscovite porphyroblasts (pseudomorph after andalusite?), the first event related to a local thermal (contact) metamorphism. The second epidote-amphibolite facies event was recognized by the presence of two garnet generations (I and II) that are separated by a compositional gap. This metamorphism had prograde character with a temperature/pressure range from 525 °C/ 4.4 kbar to 585 °C / 5.4 kbar. The second

garnet started to grow at 560 °C/ 4.9 kbar and reached 600 °C/ 7.3 kbar, which corresponds well with PT conditions of the Middle-Jurassic amphibolite-facies metamorphism established in the adjacent metaigneous rocks.

Regarding two (thermal and epidote-amphibolite facies) metamorphic events on the one hand and lithological similarity between the micaschists and the Pre-Middle-Triassic phyllites on the other hand, two alternative interpretations can be considered for metamorphic evolution of the Shotur Kuh complex. The first interpretation assumes a Pre-Cambrian low- to very-low-grade metamorphic basement into which the igneous rocks were intruded and which resulted in only a thermal overprint in the micaschists. The epidote-amphibolite facies metamorphism, separated by pressure and temperature discontinuity from the Middle-Jurassic amphibolite-facies metamorphism, could relate to the Variscan event that is known from the Anarak area (Baghari and Stampfli, 2008). The whole complex, including Pre-Middle Triassic cover rocks, was later (during the Middle Jurassic) metamorphosed in amphibolite facies conditions. Preservation of prograde zoning in both garnet generations from the micaschist suggests that both metamorphic events were relatively short in order to totally equilibrate the mineral assemblages and to homogenize garnet zoning. As we could not recognize textural evidence for the epidote amphibolite facies events in the metaigneous rocks, the occurrence and age relations of this event in the Shotur Kuh complex need further investigation.

The second interpretation is based on lithological parallelization of the micaschists with the Permian-Triassic cover sequence. In this case, the two garnets should have formed during a single (Middle-Jurassic) metamorphism. If this is true, large-scale burial tectonic processes, which resulted in the formation and tectonic juxtaposition of amphibolite and greenschist facies rocks in the same stratigraphic unit, can be assumed. In addition to the difference in metamorphic grade (amphibolite facies micaschists and greenschist facies phyllite), the weakness of this interpretation is in the lack of arguments to explain the compositional gap between garnets I and II that gives higher PT conditions for garnet I rim and lower for garnet II core. If the chaistolic-like structures are after andalusite or cordierite, their formation also needs a thermal event prior to amphibolite facies metamorphism.

The Barrovian-type Middle-Jurassic metamorphism in the metaigneous and sedimentary rocks suggests crustal thickening, which is a typical feature in collision for orogenic belt. This metamorphism was associated with D1 and D2 deformations,

which resulted in a high-grade metamorphic foliation S1 and vertical shortening of S1 fabric with axial planar cleavages S2, respectively, in the basement and overlaying Permian-Lower Jurassic metasediments. Because the Paleotethys-related orogenic processes ended in the Early to Middle Triassic (Bagheri and Stampfli, 2008), formation of amphibolite facies metamorphism in the Shotur Kuh complex could relate to closure of the Neotethys. This oceanic basin started to close by northward subduction beneath the Iranian Microplate already in the Upper Triassic and resulted in the formation of a series of back-arc basins. Recent geochronological data from the Sabzevar area (Rossiti et al., 2009) show that the opening of the Sabzevar back-arc basin should have occurred prior to the Upper Cretaceous (Bagheri and Stampfli, 2008), while some of these rocks suffered by Lower Cretaceous metamorphism. It is not clear whether the Middle-Jurassic metamorphism in the Shotur Kuh complex related to closure of the Sabzevar back-arc basin or possibly to another back-arc basin, which could produce the Kuh Siah Poshteh mafic and ultramafic rocks (100 km WSW from the Shotur Kuh complex). In both cases, the geochronological data from the Shotur Kuh and other metamorphic units in Central suggest that the collisional tectonics processes that were related to closures of the Neotethys and their back-arc basin, started already in the Middle Jurassic.

In summary, the new data on timing of magmatism, metamorphism, and deformation of the Shotur Kuh complex open several significant questions with regard to the geodynamic evolution of the Great Kavir block in Central Iran. Parts of this block were affected by metamorphism and deformation related to closure of the Neotethyan ocean and its associated back-arc basins. One important question that should be solved is the possible existence of Pre-Middle-Jurassic metamorphism in the Shotur Kuh complex and its relation to other units in Central Iran. Although some Jurassic ages of metamorphism are present in the Snandaj-Shirjan zone, the Middle-Jurassic metamorphism in the Shotur-Kuh complex should be verified also in relation to closure of the Sabzevar or possibly other back-arc basins.

4.2.References:

Bagheri, S., Stampfli, G.M., 2008. The Anarak, Jandaq and Posht-e-Badam metamorphic complexes in central Iran: New geological data, relationships and tectonic implications. Tectonophysics 451:123–155.

Berberian, M., King, G.C.P., 1981. Towards a Paleogeography and Tectonic Evolution of Iran. Can J Earth Sci 8:210–265.

Ramezani J, Tucker RD, 2003. The Saghand Region, Central Iran: U–Pb geochronology, petrogenesis and implications for Gondwana tectonics. Am J Sci 303: 622–665

Rossetti, F., Nasrabady, M. Vignaroli, G., Theye, T., Gerdes, A. Razavi, M.H. and Vaziri. H.M. 2009. Early Cretaceous migmatitic mafic granulites from the Sabzevar Range (NE Iran): implications for the closure of the Mesozoic peri-Tethyan oceans in central Iran. Tectonics (in press).

Institute of Petrology and Structural Geology
Faculty of Science
Charles University
Prague, Czech Republic

METAMORPHISM AND GEOTECTONIC POSITION OF THE SHOTUR KUH COMPLEX, CENTRAL IRANIAN BLOCK

DISSERTATION

2009-09-09   **Mahmoud Rahmati Ilkhchi**

Institute of Petrology and Structural Geology
Faculty of Science
Charles University
Prague, Czech Republic

METAMORPHISM AND GEOTECTONIC POSITION OF THE SHOTUR KUH COMPLEX, CENTRAL IRANIAN BLOCK

PhD thesis by

Mahmoud Rahmati Ilkhchi

Supervised by
Prof. Ing. Shah Wali Faryad, CSc.
and
Co-supervised by
RNDr. Petr Jerábek, PhD.

A thesis submitted to the
Faculty of Science, Charles University
of the requirements for the degree of
Doctor of Philosophy
Institute of Petrology and Structural Geology
2009

Jury   **Prague, 2009**

Statement of originality

The results presented in this dissertation are outcome of my original scientific work in collaboration with my supervisors and other colleagues. To the best of my knowledge and belief, I declare that the results presented in my dissertation have not been published or presented by someone else. This dissertation has not been submitted for any other academic degrees at other university or educational institution.

Prague 2009

Mahmoud rahmati Ilkhchi

Statement of co-authors

On behalf of the co-authors, I declare that Mahmoud Rahmati Ilkhchi was the principle investigator of the scientific study presented in this dissertation and performed majority of the work. The contribution of the co-authors was mainly supplying of the analytical data and critical comments on the final versions of the manuscripts.

Prague, September 2009

Prof. Ing. Shah Wali Faryad, CSc.

Acknowledgements

This work is dedicated to my wife and my sons.

Mahmoud

Publications:

1. Mahmoud Rahmati-Ilkhchi, Shah Wali Faryad, František V. Holub, Jan Košler, and Wolfgang Frank. Magmatic and metamorphic evolution of the Shotur Kuh Metamorphic Complex (Central Iran). International Journal of Earth Sciences (in print)

2. Mahmoud Rahmati-Ilkhchi, Petr Jeřábek, Shah Wali Faryad and Hemin A. Koyi. Jurassic–Pliocene tectono-metamorphic history of the Shotur Kuh metamorphic complex in the Great Kavir Block (NE Iran). (in preparation)

3. Rahmati Ilkhchi M, 2002. Geological map of Razveh (scale 1:100,000).Geological Survey of Iran, Tehran Iran

3. Zahedi, M., Rahmati Ilkhchi M, Vaezipour, J., 1994. Geological map of Shahrekord (scale 1:250,000).Geological Survey of Iran, Tehran Iran

4. Rahmati Ilkhchi M, 2004. Geological map of Langerud (scale 1:100,000). Geological Survey of Iran, Tehran Iran

5. Rahmati Ilkhchi M, Babakhani, A.R., Sahandi, M.R., Khan Nazer, N.H., 2005. Geological map of Joghatay (scale 1:100,000).Geological Survey of Iran, Tehran Iran

Conference abstracts:

1. Mahmoud Rahmati Ilkhchi, Shah Wali Faryad, Karel Schulmann, Jan Kosler. 2006. Metamorphism and exhumation processes of the Shotur Kuh Metamorphic Complex, Semnan Province (Central Iran Zone). Geoline, 20, 55

2. Mahmoud Rahmati Ilkhchi, Shah Wali Faryad, Petr Jerabek, Jan Kosler. 2007. Origin and Exhumation of the Shotur Kuh Core Complex. 5th Meeting of the central European Tectonic Studies Group (CETeG),Tepla, Czech republic

3. Mahmoud Rahmati Ilkhchi, Shah Wali Faryad. 2008 Petrology and metamorphic evolution of the Shotur Kuh Complex in Central Iran. Geosciences Conference, Tehran

4. Mahmoud Rahmati Ilkhchi, Petr Jeřábek, Shah Wali Faryad, Jan Košler. 2008. Tectono-metamorphic evolution of the Shotur Kuh Metamorphic Core Complex in the Central Iranian Block. 6th Meeting of the Central European Tectonic Studies Group "CETeG", Upohlav, Slovakia

5. Mahmoud Rahmati Ilkhchi, Shah Wali Faryad, Jan Košler.
   Metamorphism of the Shotur Kuh Complex, Central Iran. 2008.
   86th Annual Meeting of the Deutsche Mineralogische Gesellschaft, Berlin

6. Mahmoud Rahmati-Ilkhchi, Shah Wali Faryad, Peter Jeřábek, František V. Holub, Jan Košler and Wolfgang Frank. 2009.
   Magmatic and tectonometamorphic history of the Shotur Kuh Metamorphic Complex, Rezveh area (Central Iran). 7th Meeting of the Central European Tectonic Studies Group "CETeG", Pécs, Hungary.

7. Mahmoud Rahmati-Ilkhchi, Shah Wali Faryad, Peter Jeřábek, František V. Holub, Jan Košler, and Wolfgang Frank. 2009.
   Magmatism and metamorphic evolution of the Great Kavir Block (Central Iran). Second Hindu Kush Conference, Kabul.

Table of Contents